A HYBRID FINITE ELEMENT PROCEDURE FOR SOIL-STRUCTURE INTERACTION INCLUDING CONSTRUCTION SEQUENCES

by

Shad Muhammad Sargand

Dissertation submitted to the Graduate Faculty of the
Virginia Polytechnic Institute and State University
in partial fulfillment of the requirements or the degree of
DOCTOR OF PHILOSOPHY
in
Civil Engineering

APPROVED:

C. S. Desai, Chairman

L. J. Johnson

T. Kuppusamy

M. Singh

A. E. Somers

March, 1981

Blacksburg, Virginia

ACKNOWLEDGMENTS

I wish to express my deepest appreciation to my advisor, C. S. Desai for his guidance, encouragement, and continuous support throughout this investigation and my studies at Virginia Tech.

I am grateful to my committee members, L. Johnson, T. Kuppusamy, M. P. Singh, and A. E. Somers, for their review of this dissertation and their many suggestions.

I am very indebted to , University of Nebraska, for his guidance during my education in the U.S.

Thanks are also due to my colleagues, for helping me in computer programming and for useful discussion in some aspects of this study.

I would like to thank and for the excellent typing of this dissertation.

I am greatly indebted to my parents for their encouragement, enthusiasm, and continuous support during all my education, to whom this work is dedicated.

Financial support for this investigation was provided by the Grant No. DAR77-20500, "Development of Improved Procedures for Simulation of Excavation and Application" by the National Science Foundation. This support is gratefully acknowledged.

TABLE OF CONTENTS

TABLE OF CONTENTS (cont.)

LIST OF FIGURES

LIST OF FIGURES (cont.)

LIST OF FIGURES (cont.)

LIST OF FIGURES (cont.)

LIST OF TABLES

CHAPTER 1

INTRODUCTION

The finite element method has been well established as a numerical tool and has been used successfully for solving many engineering problems. In this method, a region is discretized into a finite number of subregions which are called finite elements. The elements are connected by a finite number of nodes which are situated on their boundaries. An approximate solution is formulated for each subregion and then these are combined by a suitable procedure to obtain the solution for the entire region. There are various types of finite element models. Among them are displacement models, equilibrium models, hybrid models, and mixed models [1].

The displacement model can be derived from the principle of stationary (minimum) potential energy. In this model, the displacements are assumed within a finite element such that they satisfy continuity conditions within an element and along the inter-element boundaries; the stresses are computed from the gradient of displacement functions. In this model, the boundary traction and the equilibrium equations within an element are not exactly satisfied. As a result, the predicted stresses may not be accurate. A model that can predict stresses with greater accuracy than those from the displacement method is the equilibrium model. This model can be derived from the principle of stationary (minimum) complementary

energy. However, the finite element equilibrium model may not be practical because it is usually difficult to derive a stress field that satisfies the prescribed tractions and equilibrium equations. Also the predicted displacements by this model may not be accurate [1].

Alternatives to the displacement or equilibrium formulations are mixed and hybrid methods. The mixed method is often derived from the Hellinger-Reissner variational principle. In this method, the stress and displacement fields are assumed separately for each element. The hybrid methods are derived from modified potential or modified complementary energy principles. The model which is derived from modified potential energy principles is called the hybrid displacement model; in this model, the displacement field is assumed within the element and independent displacement and/or stress fields are assumed on the element boundaries. The model which is formulated from the modified complementary energy principle is called the hybrid stress model; in this model, an equilibrium stress field is assumed within each element and an independent displacement field is assumed on the element boundaries.

In geomechanics, the most commonly used finite element procedure is based on the displacement model [2]. Geotechnical engineers have used this method to solve problems involving such complexities as material nonlinearity, geometric nonlinearity, and boundary nonlinearity. But some problems such as underground and open excavations are highly complicated; the complexity is due to factors such as

unloading, singularities (such as corners), change of geometry and the existence of structures before or after excavation. In order to realistically simulate such problems and to include the above factors, there is need for a finite element model which will predict both stresses and displacements with greater accuracy than the finite element displacement method. The hybrid stress model is considered for soil-structure interaction problems including simulation of excavation.

The objectives of this study are:

(1) To develop a procedure based on the finite element hybrid stress method for simulation of underground and surface excavations. The proposed procedure will include the consideration of material nonlinearity and soil-structure interaction.

(2) To solve some practical problems with the new procedure and then to compare the results with those for the displacement model and observed (field) data.

In Chapter 2, basic formulations for the hybrid stress model for elastic and elastic-plastic solids are presented, and element equations for a four-node and for an eight-node isoparametric element are derived. Also, in this chapter an interface element is formulated.

Chapter 3 gives a brief review of the theories of elasticity and plasticity, then describes the constitutive laws which are used in this study.

In Chapter 4, the computer procedure is verified by solving a few available problems and by comparing predictions with the exact solutions or the solutions obtained by other investigators. Also, here the implementation and the accuracy of the hybrid stress model are discussed.

Chapter 5 gives a review of the current procedure of simulation of the excavation by displacement finite element model. In this chapter, the new procedure for simulation of the excavation based on the hybrid stress model are proposed and its convergence and uniqueness is investigated.

Chapter 6 presents the application of the new procedure to some practical problems and the comparison of its results with those from displacement model and observed (field) data.

Chapter 7 in devoted to summary and conclusions in this investigation along with the recommendation for further studies.

CHAPTER 2

HYBRID STRESS MODEL

2.1 Introduction

The hybrid stress model was first introduced by Pian [3]. In this model, he assumed an equilibrium stress field within the element in terms of undetermined coefficients and expressed the displacement on the boundary of the element in terms of the element nodal displacements. Subsequently, Pian and Tong [4] formulated the hybrid stress model based on a modified stationary complementary energy principle, and they also considered the topics of convergence and bounds [5,6]. This model is attractive because the unknowns of the final matrix equations can be expressed in terms of the element nodal displacements, and it is easier to construct compatible interpolation functions for displacements at interelement boundaries. Several investigators have applied the hybrid stress model to the analysis of structures, and have shown that this model predicts stresses and displacement with greater accuracy than those by the finite element displacement method [4,6,7,8]. By using a special eigenvalue technique Ahmad and Irons [7] proved that the hybrid stress model is superior to the displacement model.

2.2 Hybrid Stress Model for Elastic Analysis

The modified complementary energy functional Π_{mc} which has been used for the derivation of the hybrid stress model for an elastic solid is expressed as [4]

$$\Pi_{mc} = \sum_{n} \left[\int_{V_n} \frac{1}{2} D_{ijkl} \sigma_{ij} \sigma_{kl} \, dV - \int_{\partial V_n} T_i u_i \, dS + \int_{S_{\sigma_n}} \bar{T}_i u_i dS \right] \tag{2.1}$$

where

D_{ijkl} = elastic complaince tensor,

σ_{ij} = stress tensor,

T_i = surface tractions,

$\bar{T}_i$ = prescribed boundary tractions along the boundary S_{σ_n},

u_i = boundary displacement, and

∂V_n = entire boundary of subregion V_n.

The stress distribution in an element can be expressed in terms of undetermined parameters $\{\beta\}$ as,

$$\{\sigma\} = [P] \{\beta\} + [P_B] \{\beta_B\} \tag{2.2}$$

The matrices $[P]$ and $[P_B]$ are functions of the coordinates and the values of $\{\beta_B\}$ are known. The stresses consist of two parts. The first part $[P] \{\beta\}$ must satisfy the homogeneous part of the equations of equilibrium, and the second part $[P_B] \{\beta_B\}$ is a particular solution of the equilibrium equation:

$$\sigma_{ij,j} + \bar{F}_i = 0 \tag{2.3}$$

where $\bar{F}_i$ are the prescribed body forces.

The surface tractions due to the assumed stress fields can be expressed as

$$T_i = \sigma_{ij} n_j \tag{2.4}$$

where n_i denotes the direction cosine of the normal to the boundary.

The interelement boundary displacement functions can be expressed in terms of an interpolation function [L] and the generalized displacements {q} as

$$\{u\} = [L]\ \{q\} \tag{2.5}$$

substituting Eqs. (2.2) and (2.5) into Eq. (2.1) gives

$$\Pi_{mc} = \sum_n \left(\frac{1}{2}\{\beta\}^T [H]\ \{\beta\} + \{\beta\}^T [H_B]\ \{\beta_B\} - \{\beta\}^T [G]\ \{q\} + \{\bar{Q}\}^T \{q\} + C_n\right) \tag{2.6}$$

where

$$[H] = \int_{V_n} [P]^T [D]\ [P]\ dV \tag{2.7}$$

$$[H_B] = \int_{V_n} [P]^T [D]\ [P_B]\ dV \tag{2.8}$$

$$[G] = \int_{\partial V_n} [R]^T [L]\ dS \tag{2.9}$$

$$[G_B] = \int_{\partial V_n} [R_B]^T [L]\ dS \tag{2.10}$$

$$\{\bar{Q}\}^T = -\{\beta_B\}\ [G_B] + \int_{S_{\sigma_n}} [\bar{T}]^T [L]\ dS \tag{2.11}$$

$$C_n = \frac{1}{2}\{\beta_B\}^T \left(\int_{V_n} [P_B]^T [D]\ [P_B]\ dV\right) \{\beta_B\} \tag{2.12}$$

Here C_n is a scalar-constant.

The matrices [R] and $[R_B]$ can be computed simply by using Eq. (2.4) and by substituting the coordinates of the element boundaries into the matrices [P] and $[P_B]$, respectively.

By taking the variation of Π_{mc} with respect to $\{\beta\}$ and setting the resulting expressions to zero, the vector $\{\beta\}$ can be expressed in terms of $\{q\}$ as

$$\{\beta\} = [H]^{-1} ([G] \{q\} - [H_B] \{\beta_B\}) \tag{2.13}$$

By substituting Eq. (2.13) into Eq. (2.6), the modified complementary energy functional Π_{mc} can be expressed only in terms of the generalized displacements $\{q\}$ as

$$\Pi_{mc} = - \sum_n (\frac{1}{2} \{q\}^T [k] \{q\} - \{Q\}^T \{q\} + B_n) \tag{2.14}$$

where

$$[k] = [G]^T [H]^{-1} [G], \tag{2.15}$$

$$\{Q\} = [G]^T [H]^{-1} [H_B] \{\beta_B\} + \{\bar{Q}\}, \tag{2.16}$$

$$B_n = \frac{1}{2} \{\beta_B\}^T [H_B]^T [H]^{-1} [H_B] \{\beta_B\} - C_n \tag{2.17}$$

Here [k] and $\{Q\}$ are element stiffness matrix, and equivalent nodal force vector, respectively, and B_n is a scalar constant.

The knowledge of the stiffness matrix and equivalent nodal forces of each element permits assembly of the overall stiffness matrix and the load vector of the system. After applying the prescribed boundary constraints, the system can be solved by any standard technique to obtain the nodal displacements.

In this study, the hybrid stress approach is used for complex problems in geomechanics involving soil-structure interaction, nonlinear material behavior, insitu stress conditions and simulation of construction sequences such as embankment, dewatering, and excavation.

Most previous works on this approach have used linear elastic material behavior. Hence, the present formulation incorporates linear elastic behavior, particularly to verify the formulation and code developed herein. However, since most geologic media, under the influence of the foregoing factors, exhibit nonlinear response, this study also involves formulation and incorporation of an elastic-plastic model. Descriptions of these constitutive laws are given in a subsequent chapter. A brief description of the technique of nonlinear analysis used is presented below.

2.3 Elastic-Plastic Analysis

The most widely used methods for analysis of elastic-plastic problems are the tangent stiffness method, the initial strain method, and initial stress method. In the tangent method, for each increment of load, a new constitutive relation is computed and the stiffness matrix is updated, Fig. (2.1). In the initial strain method, the coefficients of the stiffness matrix are kept constant, and the effect of plasticity is included by introducing

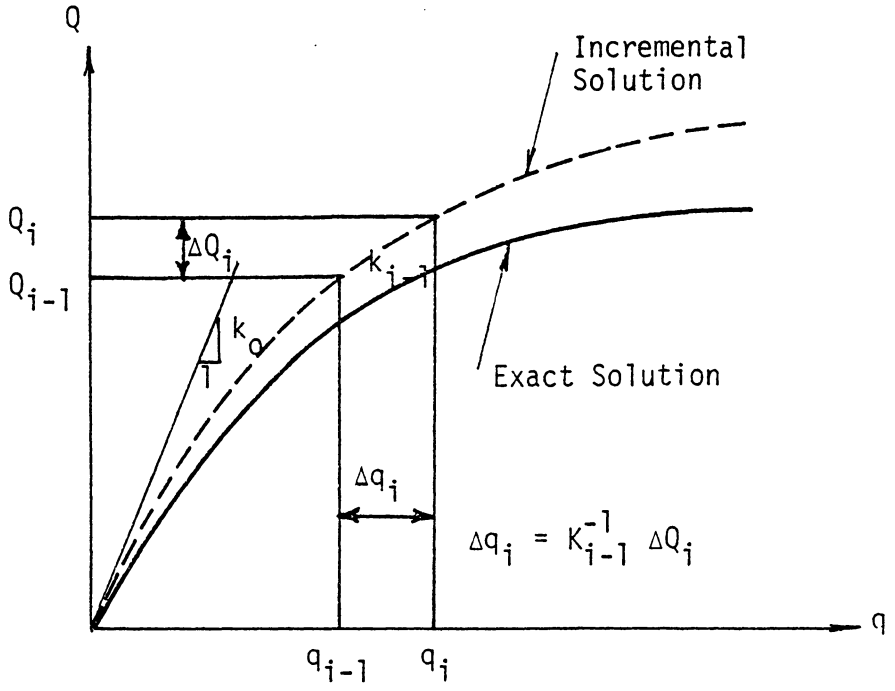

Figure 2.1 Incremental Procedure

equivalent nodal forces which are computed based on the plastic strains. In the initial stress method, the elastic stiffness is used throughout the analysis. However in the plastic region, the predicted stresses will be higher than the correct equilibrium state of stress. The equivalent nodal forces are computed from the difference of predicted stresses and correct state of stresses at the same level of strain Fig. (2.2).

There are various techniques used to accelerate the convergence of the foregoing methods. The detailed description of these methods and their merits and demerits are discussed in Refs. [9, 10]. The application of these techniques in the hybrid stress model has been reviewed in Ref. [11]. Several versions of initial stress method in the hybrid stress model are presented in Refs. [11, 12, 13]. Only one of these approaches is used in this study and its formulation is given next.

2.4 Initial Stress Procedure in the Hybrid Stress Model

The functional Π_{mc} in the incremental form for an elastic-plastic problems is expressed as [11]

$$\Pi_{mc} = \sum_{n} \Big[\int_{V_n} \frac{1}{2} D_{ijkl} \, (\Delta\sigma_{ij} + \sigma^{o}_{ij}) \, (\Delta\sigma_{kl} + \sigma^{o}_{kl}) \, dV - \int_{\partial V_n} \Delta T_i \, \Delta u_i \, dS + \int_{S_{\sigma_n}} \Delta \bar{T}_i \, \Delta u_i \, dS \Big] \qquad (2.18)$$

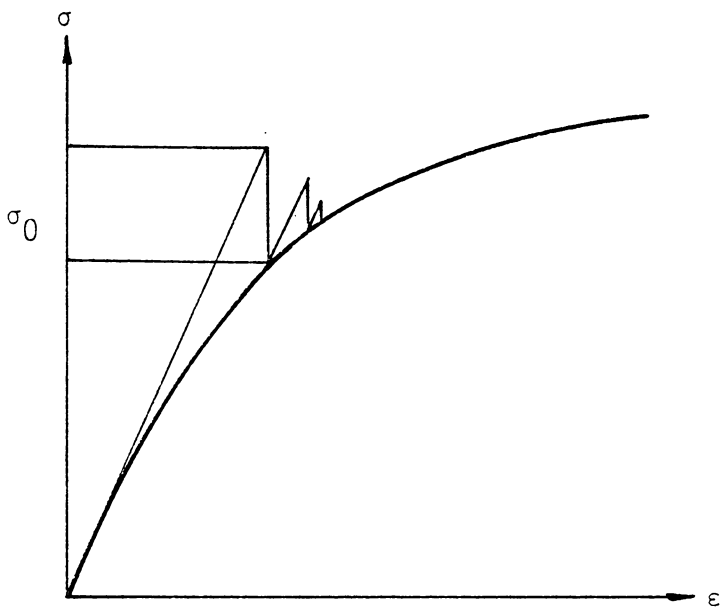

Figure 2.2 Initial Stress Procedure

where σ^{o}_{ij} is the difference between predicted increments of stresses and the correct increments of stresses at the same level of strain.

Similar to the Eqs. (2.2) and (2.5), the stress and the displacement increments can be assumed as

$$\{\Delta\sigma\} = [P]\ \{\Delta\beta\} \text{ and} \tag{2.19}$$

$$\{\Delta u\} = [L]\ \{\Delta q\} \tag{2.20}$$

Substitution of Eqs. (2.19) and (2.20) into Eq. (2.18) gives

$$\Pi_{mc} = \sum_{n} [\tfrac{1}{2}\ \{\Delta\beta\}^{T}[H]\ \{\Delta\beta\} + \{\Delta\beta\}^{T}\ \{Z\} - \{\Delta\beta\}^{T}\ [G]\ \{\Delta q\} + \{\Delta q\}^{T}\ \{\Delta\overline{Q}_{n}\} + C] \tag{2.21}$$

where

$$\{\Delta\overline{Q}_{n}\} = \int_{S_{\sigma_n}} [L]^{T}\ \{\Delta\overline{T}\}\ dS \tag{2.22}$$

$$\{Z\} = \int_{V_n} [P]^{T}\ [D]\ \{\sigma^{o}\}\ dV \tag{2.23}$$

Matrices [H] and [G] are defined in section 2.2 and C is a scalar constant.

By taking the variation of functional Eq. (2.21), with respect to $\{\Delta\beta\}$ and setting the result equal to zero, leads to

$$\{\Delta\beta\} = [H]^{-1}\ ([G]\ \{\Delta q\} - \{Z\}) \tag{2.24}$$

Substituting Eq. (2.24) into Eq. (2.21) yields

$$\Pi_{mc} = \sum_n \frac{1}{2} \{\Delta q\}^T [K_n] \{\Delta q\} - \{\Delta q\}^T (\{\Delta \bar{Q}_n\} + \{Q_n^o\})] \qquad (2.25)$$

where

$$[K_n] = [G]^T [H]^{-1} [G] \quad \text{and} \qquad (2.26)$$

$$\{Q_n^o\} = [G]^T [H]^{-1} \{Z\} \qquad (2.27)$$

The element sitffness $[K_n]$ is the same as in Eq. (2.15), but the load vector $\{Q_n\}$ consists of two parts, external loading increments $\{\Delta \bar{Q}_n\}$ and equivalent nodal loads due to initial or residual stress $\{Q_n^o\}$.

$$\{Q_n\} = \{\Delta \bar{Q}_n\} + \{Q_n^o\} \qquad (2.28)$$

2.4.1 Computational Procedure

The algorithm for the elastic-plastic analysis is given here. This procedure is based on the assumption that the load is applied in small increments such the initial stress for a given increment can be approximated by the values of the initial stress from the previous increment [11]. In this algorithm, the terms of Gaussian integration points are denoted by 'gp' and yield function by f. They will be explained in Section 2.5.1 and Section 3.3, respectively.

Steps in Algorithm

The algorithm for the ith increment can be summarized as follows:

1. Solve $[K]\ \{\Delta q_i\} = \{\Delta \bar{Q}_i\} + \{Q^o_{i-1}\}$ (2.29)

2. The vector $\{\Delta\beta\}$ is determined from the increment of nodal displacements by using Eq. (2.24) and the vector $\{Z_{i-1}\}$ of the previous increment; $\{A_o\} = 0$ for the first increment.

3. Compute the increments of the stresses for a Gaussian integration point, Eq. (2.19).

4. Calculate the total increments in the stresses as

$$\{\Delta\sigma'^{gp}\} = \{\Delta\sigma^{gp}\} + \{\sigma^{ogp}_{i-1}\} \quad (2.30)$$

Here $\{\sigma^{ogp}_{i-1}\}$ is initial stress vector from previous increment and $\{\sigma^o_o\} = 0$.

5. Evaluate the increment in the strain using the elastic constitutive relations

$$\{\Delta\varepsilon^{gp}_i\} = [D]\ \{\Delta\sigma'^{gp}\} \quad (2.31)$$

6. Calculate a trial vector of total stresses

$$\{\Delta^{gp}_t\} = \{\sigma^{gp}_{i-1}\} + \{\Delta\sigma'^{gp}\} \quad (2.32)$$

Here $\{\sigma^{gp}_{i-1}\}$ = total stresses at the end of previous increment.

7. Compute yield function f,

   a. if $f < 0$, then compute total stresses and total strains as

$$\{\sigma_i^{gp}\} = \{\sigma_t^{gp}\} \text{ and}$$

$$\{\varepsilon_i^{gp}\} = \{\varepsilon_{i-1}^{gp}\} + \{\Delta\varepsilon_i^{gp}\} \qquad (2.33)$$

   and return to step 3 and continue for other Gaussian integration point.

   b. If $f \geq 0$ preform the following steps:

   Compute the correct increments in stresses $\{\Delta\sigma_{c_i}^{gp}\}$ by using elastic-plastic constitutive law $[C]^{ep}$ as

$$\{\Delta\sigma_{c_i}^{gp}\} = [C]^{ep} \{\Delta\varepsilon_i^{gp}\} \qquad (2.34)$$

   Here $[C]^{ep}$ can be determined based on the state of stress at the end of previous increment [13]. The matrix $[C]^{e-p}$ is described in Section

9. Calculate the initial stress vector as

$$\{\sigma^{ogp}\} = \{\Delta\sigma'^{gp}\} - \{\Delta\sigma_{c_i}^{gp}\} \qquad (2.35)$$

10. Compute the total stresses and strains as

$$\{\sigma_i^{gp}\} = \{\sigma_{i-1}^{gp}\} + \{\Delta\sigma_{c_i}^{gp}\} \qquad (2.36)$$

$$\{\varepsilon_i^{gp}\} = \{\varepsilon_{i-1}^{gp}\} + \{\Delta\varepsilon_i^{gp}\} \qquad (2.37)$$

Repeat steps 2 to 9 for all Gaussian integration points.

11. Evaluate the vector $\{Z_i\}$ numerically by using Eq. (2.23).

12. Compute the vector $\{Q_n^o\}$ by using Eq. (2.27).

If the load is applied in small increments, the results of the analysis will be satisfactory. The solution can be improved by using an iterative scheme [14].

In the hybrid stress model, the inversion of the matrix [H] is one of the most time consuming parts of the computation. The two basic features of using the initial stress approach in hybrid stress model are, there is no need to invert the matrix [H] more than once for each element during all analysis, and there is no need to give any special consideration to the elements which may unload during the analysis. The latter feature is due to the fact that the elastic stiffness is used during all steps and it is assumed that the unloading is purely an elastic phenomenon.

2.5 Hybrid Stress Element Equations

In the context of finite element analysis, it is more convenient in computation to use non-dimensional local coordinate systems than to use a global coordinate system. In the finite element displacement methods, interpolation functions are used to relate the displacements of any point within an element to the nodal displacements. If the same interpolation functions are used for transformation of coordinates of the element, then this element is called an isoparametric element as shown in Figures (2.3a) and (2.3b), the details of this concept appear in Refs. [9, 10].

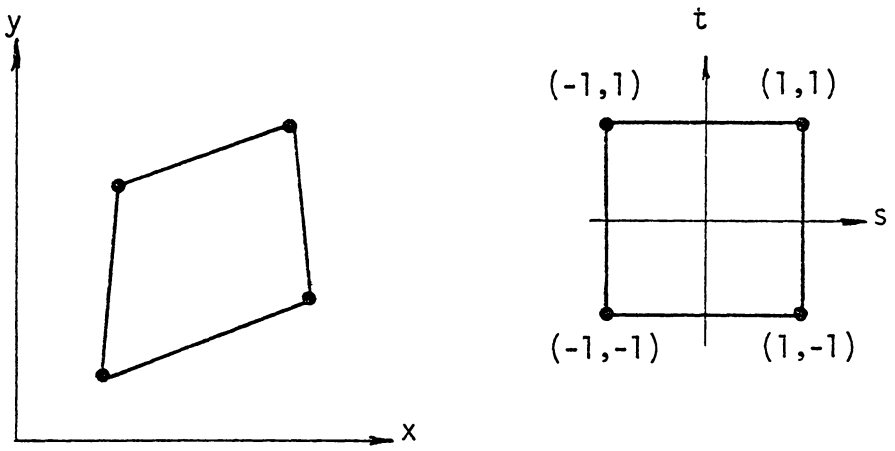

Figure 2.3a Mapping for 4-Node Element

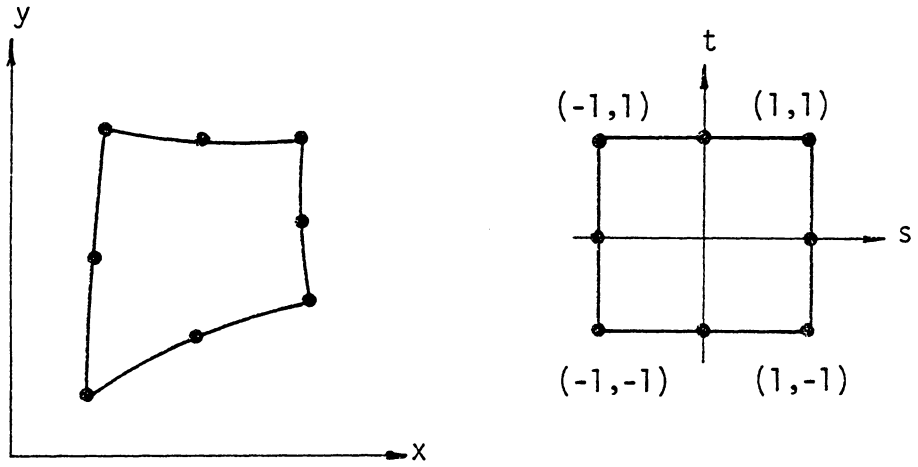

Figure 2.3b Mapping for 8-Node Element

Details of Element Formulation

A relation between the global and local coordinates for two-dimensional elements is expressed as

$$x = \sum_{i=1}^{n} N_i X_i \tag{2.38}$$

$$y = \sum_{i=1}^{n} N_i Y_i \tag{2.39}$$

where

n = 4 for four-node element,

n = 8 for eight-node element, and

N_i = interpolation functions.

There is one-to-one correspondence between the global coordinates (x,y) and the local coordinates (s,t).

By using the chain rule of differentiation the following relation between local and global coordinates can be written as

$$\begin{Bmatrix} \frac{\partial}{\partial s} \\ \\ \frac{\partial}{\partial t} \end{Bmatrix} = J(s,t) \begin{Bmatrix} \frac{\partial}{\partial x} \\ \\ \frac{\partial}{\partial y} \end{Bmatrix} \tag{2.40}$$

where J is the Jacobian matrix

$$[J] = \begin{bmatrix} \frac{\partial x}{\partial s} & \frac{\partial y}{\partial s} \\ \frac{\partial x}{\partial t} & \frac{\partial y}{\partial t} \end{bmatrix}$$

$$= \sum_{i=1}^{n} \begin{bmatrix} \frac{\partial N_i}{\partial s} X_i & \frac{\partial N_i}{\partial s} Y_i \\ \frac{\partial N_i}{\partial t} X_i & \frac{\partial N_i}{\partial t} Y_i \end{bmatrix} \qquad (2.41)$$

In addition, it is noted that dxdy = det [J] dsdt

The above ideas are used to formulate four-node and eight-node isoparametric quadrilateral elements based on the hybrid stress model.

2.5.1 Four-Node Isoparametric Quadrilateral Element

The following stress field is used to derive the element equations:

$$\begin{Bmatrix} \sigma_x \\ \sigma_y \\ \sigma_{xy} \end{Bmatrix} = \begin{bmatrix} 1 & x & y & 0 & 0 & 0 & 0 \\ 0 & 0 & 0 & 1 & x & y & 0 \\ 0 & -y & 0 & 0 & 0 & -x & 1 \end{bmatrix} \begin{Bmatrix} \beta_1 \\ \beta_2 \\ \beta_3 \\ \beta_4 \\ \beta_5 \\ \beta_6 \\ \beta_7 \end{Bmatrix} \qquad (2.42)$$

Throughout this dissertation in the case of two-dimensional problems, x, y, and xy are used in place of x_{11}, x_{22}, and x_{12}.

For the four-node element, the body force is not considered

because this element formulation is used essentially for a comparison purpose, and it is not applied in the analysis of the geomechanics problems.

The coordinates are transformed by using the following interpolation functions.

$$N_i = \frac{1}{4} (1 + ss_i) (1 + tt_i) \tag{2.43}$$

where the subscript i denotes the values of s and t at node i.

The displacements on the boundary of the element are assumed to vary linearly as

$$\{u\} = [L] \{q\} \tag{2.44}$$

where

$$\{u\}^T = [u^1, v^1, u^2, v^2, u^3, v^3, u^4, v^4] \tag{2.45}$$

$$\{q\}^T = [q_1, q_2, q_3, q_4, q_5, q_6, q_7, q_8] \tag{2.46}$$

$$[L] = \begin{bmatrix} L_1 & 0 & L_2 & 0 & 0 & 0 & 0 & 0 \\ 0 & L_1 & 0 & L_2 & 0 & 0 & 0 & 0 \\ 0 & 0 & L_1 & 0 & L_2 & 0 & 0 & 0 \\ 0 & 0 & 0 & L_1 & 0 & L_2 & 0 & 0 \\ 0 & 0 & 0 & 0 & L_2 & 0 & L_1 & 0 \\ 0 & 0 & 0 & 0 & 0 & L_2 & 0 & L_1 \\ L_1 & 0 & 0 & 0 & 0 & 0 & L_2 & 0 \\ 0 & L_1 & 0 & 0 & 0 & 0 & 0 & L_2 \end{bmatrix} \tag{2.47}$$

$$L_1 = \frac{1}{2}(1 - s)$$

$$L_2 = \frac{1}{2}(1 + s)$$

The superscripts in Eq. (2.45) denote the sides, s corresponds to the local coordinate for each side of an element which varies from - 1 to +1, Fig. (2.4a), and {q} is the vector of nodal displacements Fig. (2.4b).

The matrices [H] and [G] are evaluated numerically by using Gaussian integration technique. In the case of four-node quadrilateral element, 2 by 2 integration is used. Subroutine LINV2P from International Mathematical and Statistical Libraries [15] is utilized to invert the matrix [H] in the formulation of the four-node and eight node elements. By using the matrices $[H]^{-1}$ and [G] the element stiffnesses are computed from Eq. (2.15).

Since the body force is not considered in the four-node formulation, the element load vector can be computed in the same manner as displacement model. The load vector due to the linear distributed prescribed surface tractions Fig. (2.5) are given as

$$\{\bar{Q}\} = \begin{Bmatrix} \ell/6\ (2\bar{T}_{x_1} + \bar{T}_{x_2}) \\ \ell/6\ (\bar{T}_{x_1} + 2\bar{T}_{x_2}) \\ \ell/6\ (2\bar{T}_{y_1} + \bar{T}_{y_2}) \\ \ell/6\ (\bar{T}_{y_1} + 2\bar{T}_{y_2}) \end{Bmatrix} \qquad (2.48)$$

where ℓ = length of the side

Figure 2.4a Linear Interpolation Function for One-Dimensional Element

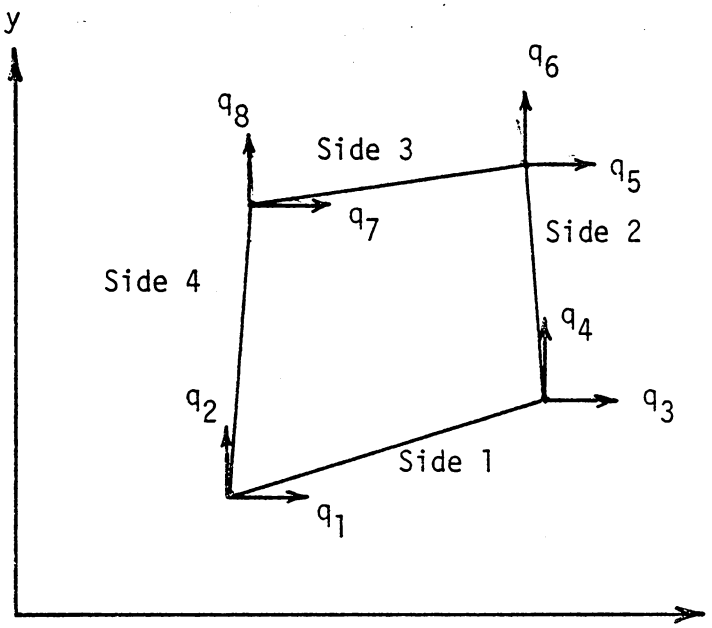

Figure 2.4b Node Quadrilateral Element with Sign Convention

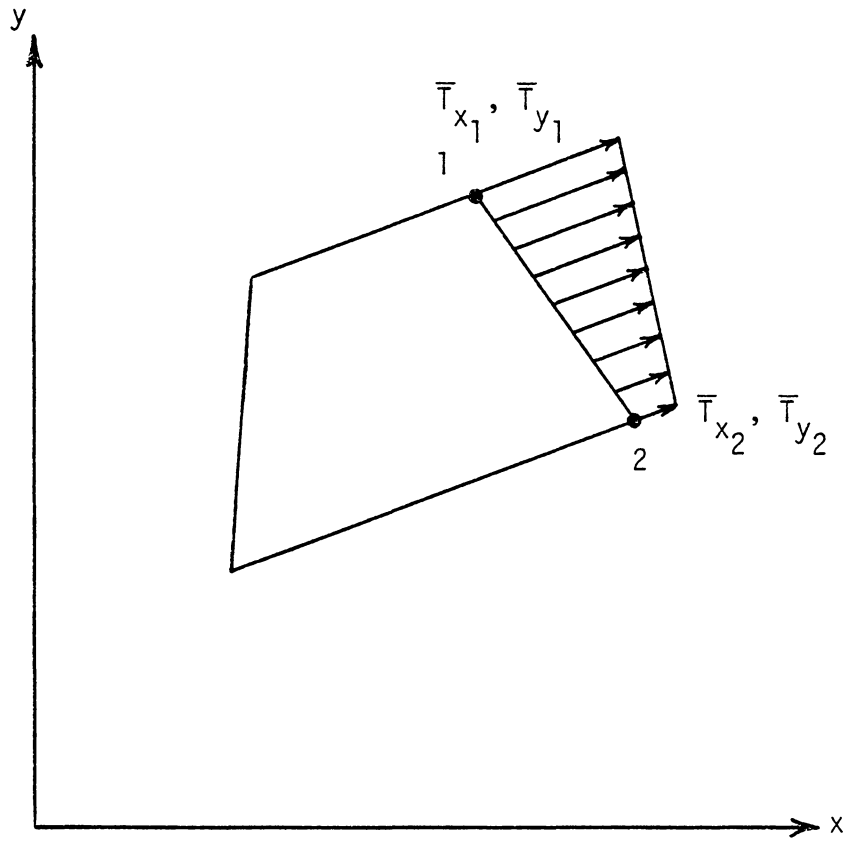

Figure 2.5 Surface Tractions on 4-Node Quadrilateral Element

After the evaluation of the stiffness matrices and load vectors for all elements, the overall stiffness matrix and load vector are assembled. By imposing the boundary conditions, the system equations are solved to obtain the nodal displacements using Gaussian elimination technique. In order to evaluate the stresses, first the vector $\{\beta\}$ should be computed for each element by using Eq. (2.13). Then the stresses at any point within the element can be determined by Eq. (2.2).

2.5.2 Eight-Node Quadrilateral Element

The distribution of the stresses within a element are computed from the following assumed Airy stress function:

$$\begin{aligned}\phi = {} & \beta_1 s^2 + \beta_2 t^2 + \beta_3 st + \beta_4 s^3 + \beta_5 t^3 + \beta_6 s^2 t + \beta_7 st^2 \\ & + \beta_8 s^4 + \beta_9 t^4 + \beta_{10} st^3 + \beta_{11} s^2 t^2 + \beta_{12} s^3 t + \beta_{13} s^5 \\ & + \beta_{14} t^5 + \beta_{15} s^4 t + \beta_{16} st^4 + \beta_{17} s^3 t^2 + \beta_{18} s^2 t^3 \end{aligned} \tag{2.49}$$

The reason why the Airy stress function is assumed based on the local coordinates is discussed in Chapter 4.

The stress components can be computed by taking the second derivatives of function ϕ with respect to x and y. This approach insures the satisfaction of the homogeneous part of the equilibrium Eq. (2.3). The stresses due to the uniform prescribed body forces can be included such that $[P_B]$ $\{\beta_B\}$ will be the particular solution of the equilibrium equation. Hence,

$$\begin{Bmatrix} \sigma_x \\ \sigma_y \\ \tau_{xy} \end{Bmatrix} = \begin{Bmatrix} \frac{\partial^2 \phi}{\partial y^2} \\ \frac{\partial^2 \phi}{\partial x^2} \\ -\frac{\partial^2 \phi}{\partial x \partial y} \end{Bmatrix} + \begin{Bmatrix} 0 \\ y\rho \\ 0 \end{Bmatrix} \tag{2.50}$$

where ρ is the unit weight of the solid.

Applying the chain rule, one can determine the second derivatives of the stress function with respect to x and y as

$$[B] = [J]^{-1} \times (A_1 - A_2 - A_3) \times [[J]^T]^{-1} \tag{2.51}$$

where

$$[B] = \begin{bmatrix} \frac{\partial^2 \phi}{\partial x^2} & \frac{\partial^2 \phi}{\partial x \partial y} \\ \frac{\partial^2 \phi}{\partial x \partial y} & \frac{\partial^2 \phi}{\partial y^2} \end{bmatrix} \tag{2.52}$$

$$[A_1] = \begin{bmatrix} \frac{\partial^2 \phi}{\partial x^2} & \frac{\partial^2 \phi}{\partial s \partial t} \\ \frac{\partial^2 \phi}{\partial s \partial t} & \frac{\partial^2 \phi}{\partial t^2} \end{bmatrix} \tag{2.53}$$

$$[A_2] = \frac{\partial \phi}{\partial x} \begin{bmatrix} \frac{\partial^2 x}{\partial s^2} & \frac{\partial^2 x}{\partial s \partial t} \\ \frac{\partial^2 x}{\partial s \partial t} & \frac{\partial^2 x}{\partial t^2} \end{bmatrix} \tag{2.54}$$

$$[A_3] = \frac{\partial \phi}{\partial y} \begin{bmatrix} \frac{\partial^2 y}{\partial s^2} & \frac{\partial^2 y}{\partial s \partial t} \\ \frac{\partial^2 y}{\partial s \partial t} & \frac{\partial^2 y}{\partial t^2} \end{bmatrix} \tag{2.55}$$

For transformation of coordinates, the following interpolation functions are used:

$$N_i = \frac{1}{4}(1 + ss_i)(1 + tt_i)(ss_i + tt_i - 1) \quad \text{for } i = 1,3,5,7$$

$$N_i = \frac{1}{2}(1 - s^2)(1 + tt_i) \quad \text{for } i = 2,6 \tag{2.56}$$

$$N_i = \frac{1}{2}(1 + ss_i)(1 - t^2) \quad \text{for } i = 4,8$$

where the subscript i denotes the values of s and t at node i.

The displacement components on each side of an element in the x and y directions are expressed as

$$\{u\} = [L]\{q\} \tag{2.57}$$

where

$$\{u\}^T = [u^1, v^1, u^2, v^2, u^3, v^3, u^4, v^4] \tag{2.58}$$

$$\{q\}^T = [q_1, q_2, q_3, q_4, q_5, q_6, q_7, q_8, q_9, q_{10}, q_{11}, q_{12}, q_{13}, q_{14}, q_{15}, q_{16}], \tag{2.59}$$

and

$$[L] = \begin{bmatrix}
L_1 & 0 & L_2 & 0 & L_3 & 0 & 0 & 0 & 0 & 0 & 0 & 0 & 0 & 0 & 0 & 0 \\
0 & L_1 & 0 & L_2 & 0 & L_3 & 0 & 0 & 0 & 0 & 0 & 0 & 0 & 0 & 0 & 0 \\
0 & 0 & 0 & 0 & L_1 & 0 & L_2 & 0 & L_3 & 0 & 0 & 0 & 0 & 0 & 0 & 0 \\
0 & 0 & 0 & 0 & 0 & L_1 & 0 & L_2 & 0 & L_3 & 0 & 0 & 0 & 0 & 0 & 0 \\
0 & 0 & 0 & 0 & 0 & 0 & 0 & 0 & L_3 & 0 & L_2 & 0 & L_1 & 0 & 0 & 0 \\
0 & 0 & 0 & 0 & 0 & 0 & 0 & 0 & 0 & L_3 & 0 & L_2 & 0 & L_1 & 0 & 0 \\
L_1 & 0 & 0 & 0 & 0 & 0 & 0 & 0 & 0 & 0 & 0 & 0 & L_3 & 0 & L_2 & 0 \\
0 & L_1 & 0 & 0 & 0 & 0 & 0 & 0 & 0 & 0 & 0 & 0 & 0 & L_3 & 0 & L_2
\end{bmatrix} \qquad (2.60)$$

$$L_1 = \frac{1}{2} s\,(s - 1)$$

$$L_2 = (1 - s^2)$$

$$L_3 = \frac{1}{2} s\,(s + 1)$$

"s" denotes the local coordinate of each side of an element which varies from - 1 to + 1, Fig. (2.6a), and $\{q\}$ is the vector of nodal displacements, Fig. (2.6b).

Due to the complex coefficients in the matrix [P], the integration of matrixes [H] and [G] are carried numerically. In the case of the eight-node element, because of the appearance of higher order terms in matrix [P], a 4 by 4 Gaussian integration is used. The stiffness matrix is in the same computer manner as that of the four-node element. Here the load vector for an element requires more computational work; this is due to the inclusion of body force. In Eq. (2.16), the first part of the right hand side contains the equivalent nodal forces due to the prescribed body force where it can be calculated during the computation of the stiffness matrix for the element; and the second part is the result of the prescribed surface tractions, where for uniformly distributed surface tractions, that part of the load vector can be evaluated as, Fig. (2.7):

$$\{\bar{Q}\} = \begin{Bmatrix} \ell/6\ \bar{T}_{x_1} \\ \ell/6\ \bar{T}_{x_2} \\ \ell/3(\bar{T}_{x_1} + \bar{T}_{x_2}) \\ \ell/6\ \bar{T}_{y_1} \\ \ell/6\ \bar{T}_{y_2} \\ \ell/3\ (\bar{T}_{y_1} + \bar{T}_{y_2}) \end{Bmatrix} \tag{2.61}$$

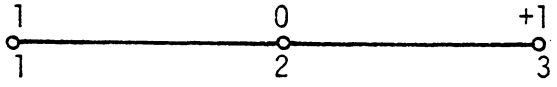

Figure 2.6a Quadratic Interpolation Functions in One Dimensional Element

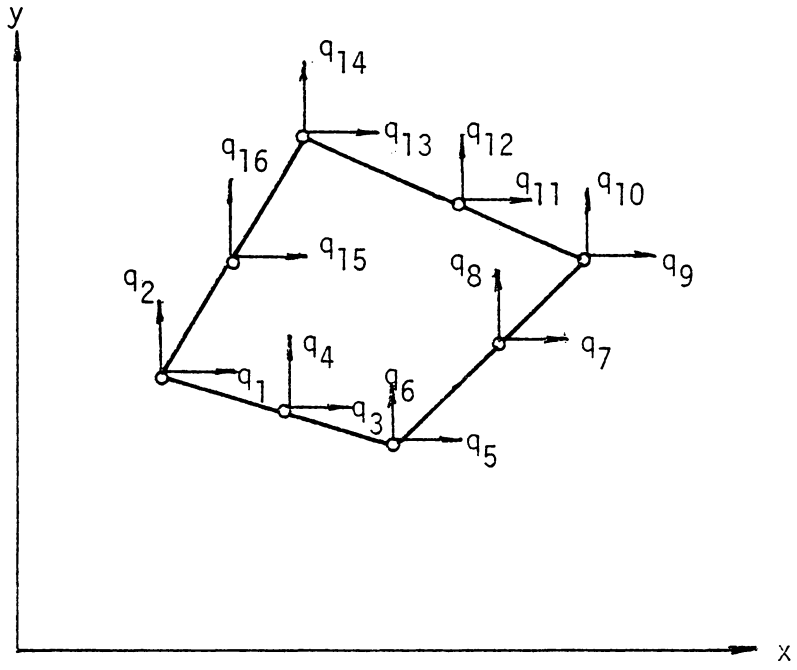

Figure 2.6b 8-Node Quadrilateral Element with Sign Convention

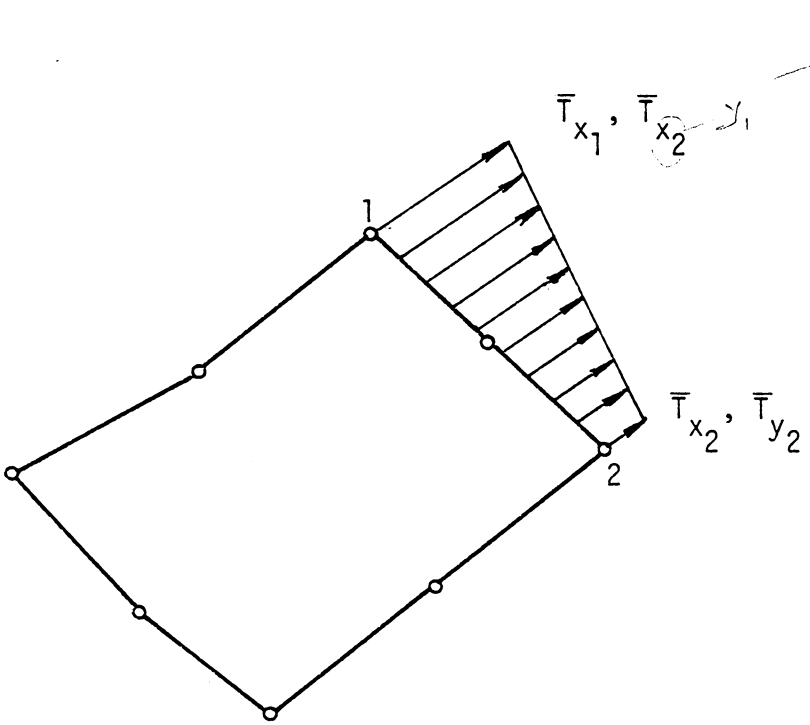

Figure 2.7 Surface Tractions on 8-Node Quadrilateral Element

Here the overall stiffness matrix and load vector are assembled and then solved by using the frontal technique; the detailed description of the technique along with the subroutine adopted in this study are given in Ref. [16].

2.6 Interface Element

In many geomechanics problems dissimilar materials are in contact, e.g., a soil-footing, soil-retaining wall, and a soil-tunnel lining. The load transfer mechanism between two unlike materials is affected by the behavior at the mating surface. Thus during loading, special consideration should be given to the modes of deformation such as non-slip, slip, opening, and closing of contact surfaces. In the conventional finite element models, where interelement compatibility is required, the soil-structure interaction is modeled by a special interface or joint element, which should permit relative movement, separation, and closing of the contact surfaces.

A number of interface elements have been proposed [17, 18, 19, 20] and applied with some success. Most of them are usually adequate for predicting the behavior prior to debonding or separation of the contact surfaces. Most interface elements are not capable of simulating adequate debonding, loss of contact and rebonding. Research for development of better interface elements is continuing.

In this study, a thin regular isoparametric eight-node element is used as an interface element (see Fig. (2.8)). The idea of 'thin' soil or structural elements as interface elements has been the subject of an investigation in the Geomechanics group at Virginia Tech for the last few years [21, 22]. The element is formulated using the conventional displacement method. The slip mode of deformation is included by introducing shear modulus in the constitutive matrix. Other coefficients in the constitutive matrix are computed based on linear or nonlinear (elastic) behavior of the thin interface, which is essentially a soil element. An average value of Young's modulus E and Poisson's ratio ν of the material are used. The constitutive matrix (in the case of plane strain) can be written as

$$[C] = \begin{bmatrix} \frac{E(1-\nu)}{(1+\nu)(1-2\nu)} & \frac{\nu E}{(1+\nu)(1-2\nu)} & 0 \\ \frac{\nu E}{(1+\nu)(1-2\nu)} & \frac{E(1-\nu)}{(1+\nu)(1-2\nu)} & 0 \\ 0 & 0 & G \end{bmatrix} \quad (2.62)$$

The strength of the interface is governed by

$$\tau_{max} = c_a + \sigma_n \tan\bar{\phi} \quad (2.63)$$

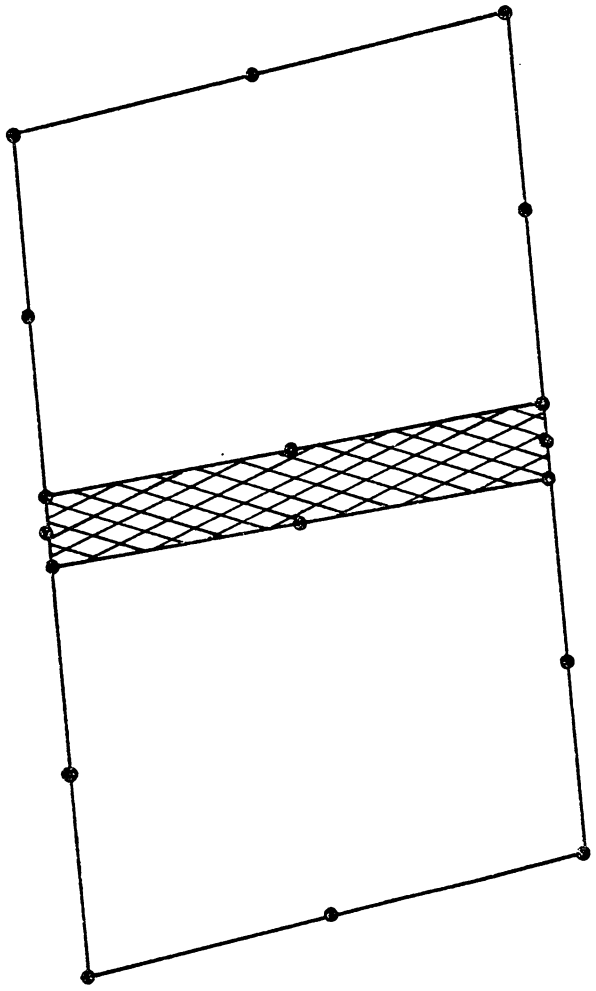

Figure 2.8 Interface Element

where

$\bar{\tau}_{max}$ = maximum bond strength,

c_a = adhesion on the interface,

σ_n = normal stress on the interface, and

$\bar{\phi}$ = friction angle of the interface

The values of the shear modulus G, the angle of friction $\bar{\phi}$, and adhesion c_a can be determined by using a direct shear test.

Based on the assumption that there is a linear relationship between the shear force F_s and lateral displacement u, as shown in Figs. (2.9a) and (2.9b), the shear modulus for an interface can be computed as [21, 23]

$$G = \tau/G \tag{2.64}$$

where

$$\tau = F_s/A \tag{2.65}$$

$$\theta \approx \frac{\Delta u}{t} \tag{2.66}$$

t = thickness of the interface element

A = area of the contact

For the thickness of an interface element, a small finite value can be assigned. Failure of the interface can be caused by the shear stress on the interface exceeding τ_{max} or by opening of the contact surface.

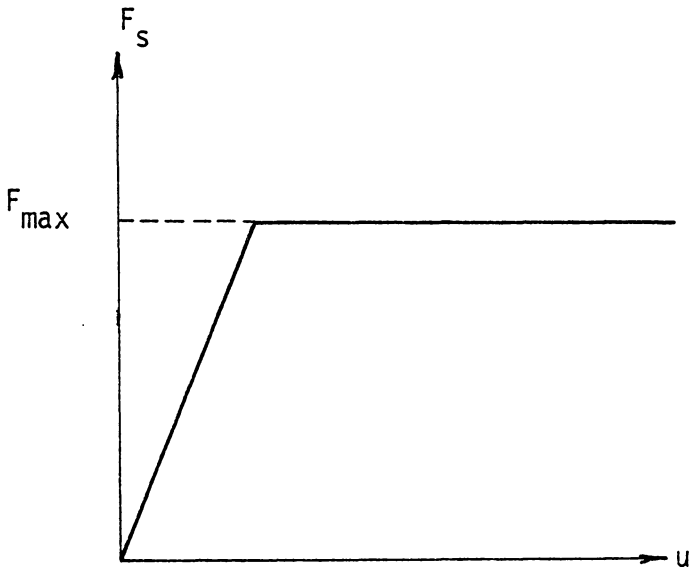

Figure 2.9a Stress-Displacement Relationship at the Interface

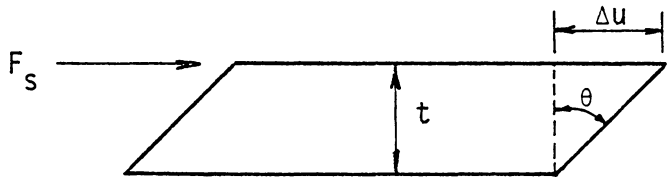

Figure 2.9b Deformation at the Interface

The present form of the interface element used in this investigation is not capable of simulating the opening mode of deformation adequately. However, to improve the capability of this class of interface elements, further research is in progress [21, 22].

Despite the fact that the interface elements are derived from the displacement method, the assembling of interface elements with the hybrid stress elements does not cause any problem because the variation of the displacements on the boundaries of both types of elements are identical.

CHAPTER 3

CONSTITUTIVE LAWS

3.1 Introduction

The success of the application of any numerical method such as the finite element, finite difference, and boundary integral methods in geomechanics, is not only dependent upon the accuracy of the methods, but also upon how well and realistically the behaviour of the geologic media is simulated under multiaxial stresses.

Generally, there are three categories of schemes for the modeling of the constitutive behaviour of soils and of rocks [2]: 1) the curve-fitting methods, where a curve (or curves) represent the stress-strain relations of a material; 2) elasticity theories (linear and nonlinear), and plasticity theories. Desai and Christian [2] have reviewed various schemes; only models that are used in this study are described here.

3.2 Elastic Models

When a body is subjected to external forces or displacements, it experiences change in its size and shape. Upon removal of these forces or displacements if the body recovers its original size and shape, the phenomenon is called elastic behavior. The material which deforms elastically with a linear stress-strain relationship is represented by the generalized Hooke's law as [24]

$$\sigma_{ij} = C_{ijkl}\varepsilon_{kl} \tag{3.1}$$

where C_{ijkl} are constants. The specialization of Eq. (3.1) for an isotropic homogeneous material is [24]

$$\sigma_{ij} = \frac{E}{1+\nu} \left[\varepsilon_{ij} + \frac{\nu}{1-2\nu} \varepsilon_{kk}\delta_{ij}\right] \tag{3.2}$$

where

E = Young's modulus,

ν = Poisson's ratio, and

δ_{ij} = Kronecker delta.

The inverse relationship of the Eq. (3.2) can be written as

$$\varepsilon_{ij} = \frac{1+\nu}{E} \sigma_{ij} - \frac{\nu}{E} \sigma_{kk}\delta_{ij} \tag{3.3}$$

In the cases of plane strain and plane stress idealizations, Eq. (3.3) can be simplified as [9]

Plane Strain

$$\begin{Bmatrix} \varepsilon_x \\ \varepsilon_y \\ \gamma_{xy} \end{Bmatrix} = \frac{1+\nu}{E} \begin{bmatrix} 1-\nu & -\nu & 0 \\ -\nu & 1-\nu & 0 \\ 0 & 0 & 2 \end{bmatrix} \begin{Bmatrix} \sigma_x \\ \sigma_y \\ \tau_{xy} \end{Bmatrix} \tag{3.4}$$

Plane Stress

$$\begin{Bmatrix} \varepsilon_x \\ \varepsilon_y \\ \gamma_{xy} \end{Bmatrix} = \frac{1}{E} \begin{bmatrix} 1 & -\nu & 0 \\ -\nu & 1 & 0 \\ 0 & 0 & 2(1+\nu) \end{bmatrix} \begin{Bmatrix} \sigma_x \\ \sigma_y \\ \tau_{xy} \end{Bmatrix} \tag{3.5}$$

where

$$\gamma_{xy} = 2\varepsilon_{xy}$$

Throughout this study the constitutive matrix is expressed as

$$\{\sigma\} = [C]\{\varepsilon\} \tag{3.6}$$

$$\{\varepsilon\} = [D]\{\sigma\} \tag{3.7}$$

where

$$[D] = [C]^{-1}$$

Most geologic media do not exhibit linear elastic behavior. A number of nonlinear models are used for geomechanics problems to simulate approximately the actual behavior of soils and rocks. The plasticity theory play a very significant role in the formulation of some of these nonlinear models. In the next section, a brief description of a few basic theories in plasticity are given and then a nonlinear model which is used in this study is explained.

3.3 Theory of Plasticity

When a solid body is loaded beyond its elastic limit, there will be a permanent deformation upon unloading. The theory of plasticity deals with such behavior, and is a broad subject. Here a brief review of some of the basic theories in plasticity used in this study are given.

There are two theories in plasticity--the deformation theory and the flow theory [25]. The deformation theory is based on the assumption that there are unique constitutive relations between the

total strain and the current state of stress and these relations are independent of the stress path. In the flow theory, relations are expressed between stress and strain increments. These constitutive relations are affected by the stress path. Since behavior of soils and some rocks are generally dependent on the stress path, the flow theory has been widely used in geomechanics.

When the plastic deformation occurs, the material flows under continuing application of stress. Similar to fluid flow, there is a potential function with some other criteria to describe the material behavior. These criteria are adequately explained in the literature on the subject. However, here a brief description is given.

Yield Surface. It is defined in terms of the state of stress, σ_{ij}, plastic strain, ε^p_{ij}, and material parameter κ, Fig. (3.1) as

$$f(\sigma_{ij}, \varepsilon^p_{ij}, \kappa) = 0 \tag{3.8}$$

where

$f < 0$, the solid deforms elastically,

$f = 0$, the solid deforms plastically, and

$f > 0$, impossible state of stress.

Flow Rule - The flow rule defines the relation between plastic strain increments, $d\varepsilon^p_{ij}$, and the potential surface as [10]

$$d\varepsilon^p_{ij} = \lambda \frac{\partial Q}{\partial \sigma_{ij}} \tag{3.9}$$

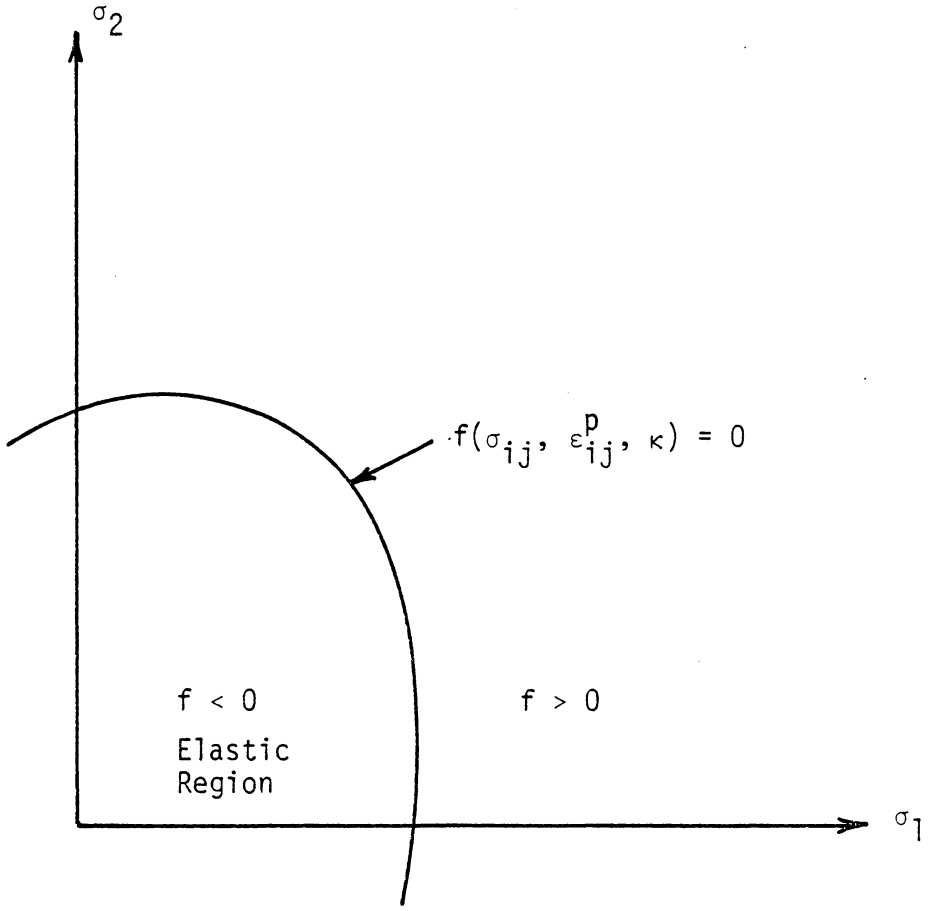

Figure 3.1 Yield Surface in Two-Dimensional Stress Space

where λ is a positive scalar factor of proportionality and the potential surface, Q, is a surface which is normal to the plastic strain increments and is a function of the state of stress and the plastic strain increments. When $F = Q$, it is known as associated plasticity, and if $F \neq Q$, it is referred to as nonassociated plasticity. In this study, the associated plasticity is considered.

Hardening (Softening) Theories - The yield surface for some materials grows or undergoes a rigid body motion during the plastic deformation. This phenomenon is due to the hardening (softening). When the yield surface grows uniformly in all directions without any translation, it is called isotropic hardening, Fig. (3.2a). If the yield surface translates without any change in its shape and size, it is called kinematic hardening, Fig. (3.2b). The combination of isotropic hardening and kinematic hardening is called anisotropic hardening.

There are two commonly used hypotheses to measure the degree of hardening [25], work hardening and strain hardening. In the work hardening hypotheses the degree of hardening is a function of the total dissipated plastic work, whereas in the strain hardening, the degree of hardening is related to the total plastic deformation.

Incremental Relations

In this section, incremental relations between stresses and strains for associated plasticity ($f \equiv Q$) are derived. It is assumed that the total strain increments consist of elastic and plastic increments as

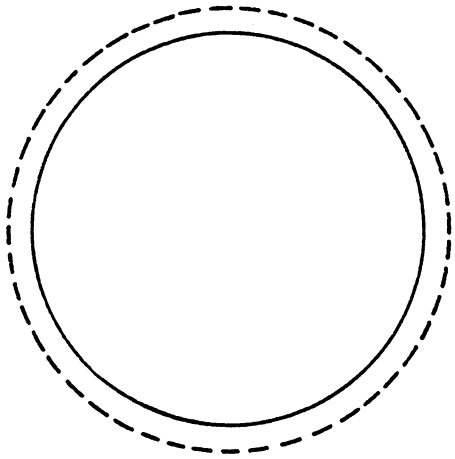

Figure 3.2a Isotropic Hardening

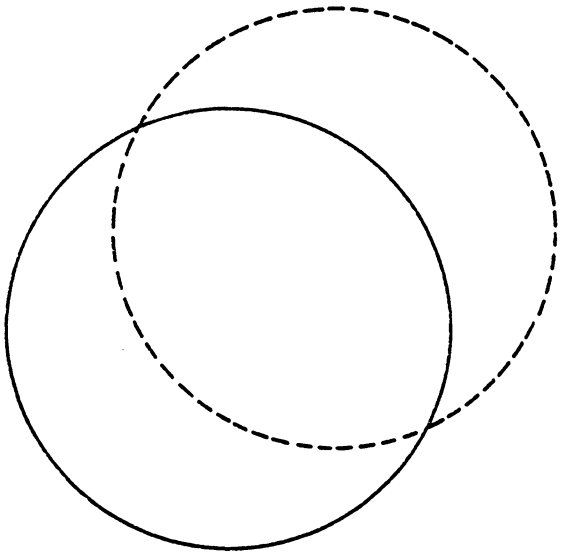

Figure 3.2b Kinematic Hardening

$$d\varepsilon_{ij} = d\varepsilon^{e}_{ij} + d\varepsilon^{p}_{ij} \tag{3.10}$$

or $$d\varepsilon^{e}_{ij} = d\varepsilon_{ij} - d\varepsilon^{p}_{ij} \tag{3.11}$$

where the superscript e and p denote the elastic strain increment and the plastic strain increment, respectively.

The stress increments can be computed as

$$d\sigma_{ij} = C^{e}_{ijkl}\, d\varepsilon^{e}_{kl} \tag{3.12}$$

where

C^{e}_{ijkl} = elastic constitutive tensor

Substitution of Eq. (3.12) and (3.9) in Eq. (3.11) gives

$$d\varepsilon^{e}_{ij} = d\varepsilon_{ij} - \lambda\frac{\partial f}{\partial \sigma_{ij}} \tag{3.13}$$

Differentiation of Eq. (3.8) yields

$$df = \frac{\partial f}{\partial \sigma_{ij}}\, d\sigma_{ij} + \frac{\partial f}{\partial \varepsilon^{p}_{ij}}\, d\varepsilon^{p}_{ij} + \frac{\partial f}{\partial \kappa}\, d\kappa = 0 \tag{3.14}$$

Substitution of Eqs. (3.1), (3.12) and (3.13) in Eq. (3.14) leads to

$$\frac{\partial f}{\partial \sigma_{ij}}\, C^{e}_{ijkl}\, (d\varepsilon_{kl} - \lambda\frac{\partial f}{\partial \sigma_{ij}}) + \frac{\partial f}{\partial \varepsilon^{p}_{ij}}\, \frac{\partial f}{\partial \sigma_{ij}}\, \lambda + \frac{\partial f}{\partial \kappa}\, d\kappa = 0 \tag{3.15}$$

Solution of Eq. (3.15) for λ gives

$$\lambda = \frac{\frac{\partial f}{\partial \sigma_{ij}} C^{e}_{ijkl}\, d\varepsilon_{kl} + \frac{\partial f}{\partial \kappa} d\kappa}{\frac{\partial f}{\partial \sigma_{ij}} C^{e}_{ijkl} \frac{\partial f}{\partial \sigma_{kl}} - \frac{\partial f}{\partial \varepsilon^{p}_{ij}} \frac{\partial f}{\partial \sigma_{ij}}} \tag{3.16}$$

By using Eqs. (3.9) and (3.16) the incremental plastic strains can be computed as

$$d\varepsilon^{p}_{ij} = \frac{\frac{\partial f}{\partial \sigma_{rs}} C^{e}_{rskl} \frac{\partial f}{\partial \sigma_{ij}} d\varepsilon_{kl} + \frac{\partial f}{\partial \kappa} d\kappa \frac{\partial f}{\partial \sigma_{ij}}}{\frac{\partial f}{\partial \sigma_{rs}} C^{e}_{rskl} \frac{\partial f}{\partial \sigma_{kl}} - \frac{\partial f}{\partial \varepsilon^{p}_{rs}} \frac{\partial f}{\partial \sigma_{rs}}} \tag{3.17}$$

Since $\kappa = \kappa(d\varepsilon^{p}_{ij})$, the term $\frac{\partial f}{\partial \kappa} d\kappa \frac{\partial f}{\partial \sigma_{ij}}$ from Eq. (3.17) can be neglected, then

$$d\varepsilon^{p}_{ij} = \frac{\frac{\partial f}{\partial \sigma_{rs}} C^{e}_{rskl} \frac{\partial f}{\partial \sigma_{ij}} d\varepsilon_{kl}}{\frac{\partial f}{\partial \sigma_{rs}} C^{e}_{rskl} \frac{\partial f}{\partial \sigma_{kl}} - \frac{\partial f}{\partial \varepsilon^{p}_{rs}} \frac{\partial f}{\partial \sigma_{rs}}} \tag{3.18}$$

By using Eqs. (3.11), (3.12), and (3.18), the incremental relations between stress and strain can be written as

$$d\sigma_{pq} = C^{ep}_{pqij}\, d\varepsilon_{ij} \tag{3.19}$$

where

$$C^{ep}_{pqij} = C^{e}_{pqij} - \frac{\frac{\partial f}{\partial \sigma_{rs}} C^{e}_{rsij} C^{e}_{pqkl} \frac{\partial f}{\partial \sigma_{kl}}}{\frac{\partial f}{\partial \sigma_{rs}} C^{e}_{rskl} \frac{\partial f}{\partial \sigma_{kl}} - \frac{\partial f}{\partial \varepsilon^{p}_{rs}} \frac{\partial f}{\partial \sigma_{rs}}} \tag{3.20}$$

Here C^{ep}_{pqij} is called elastic-plastic constitutive tensor. This is a general form of the incremental relations between stress and strain,

and a specialized form of this relation can be constructed for a material with a given yield function and hardening function using the above relationship. To utilize the elastic-plastic constitutive relations in connection with the finite element method, normally it is expressed in matrix form; the constitutive matrix is symmetric in associated plasticity [10]. The incremental relations between stress and strain for the constitutive model which is used in this study is represented next.

3.3.1 Drucker-Prager Model

For elastic-plastic analysis of frictional materials such as soils, Drucker-Prager [27] suggested the yield criterion where the effect of the first invariant of the stress tensor is included in the yield function, Figs. (3.3, 3.5), as

$$f = J_{2D}^{1/2} + \alpha J_1 - \kappa = 0 \tag{3.21}$$

where

$$J_1 = \sigma_{11} + \sigma_{22} + \sigma_{33} \tag{3.22}$$

J_1 is referred to as the first invariant of the stress tensor, and

$$J_{2D} = \frac{1}{6}\left[(\sigma_{11} - \sigma_{22})^2 + (\sigma_{22} - \sigma_{33})^2 + (\sigma_{33} - \sigma_{11})^2\right] + \sigma_{12}^2 + \sigma_{13}^2 + \sigma_{23}^2 \tag{3.23}$$

where J_{2D} is the second invariant of the deviatoric stress tensor. The constants α and κ are determined from the cohesion,

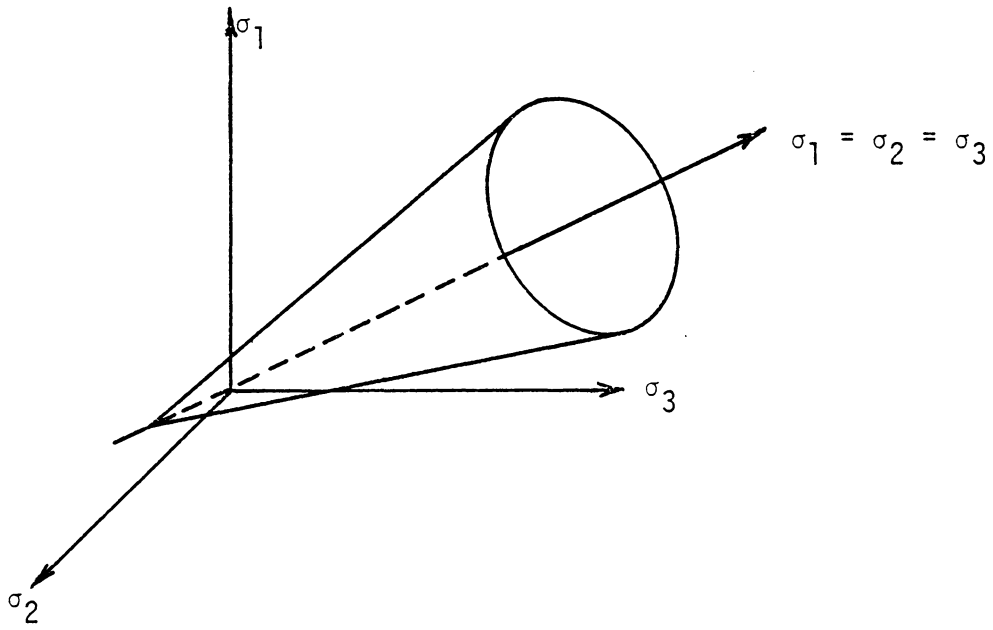

Failure 3.3 Drucker-Prager Failure Criterion

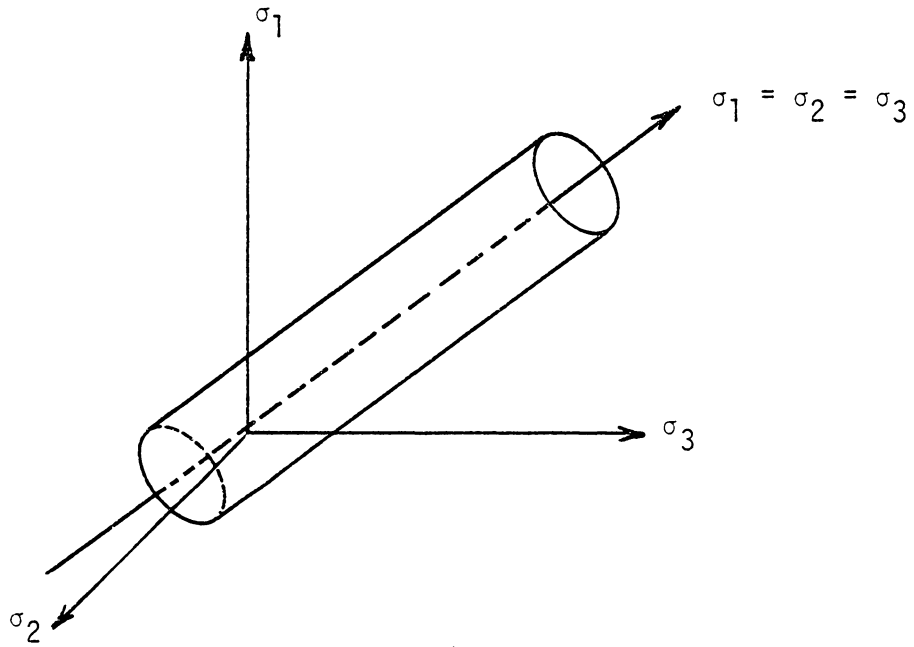

Figure 3.4 von Mises Failure Criterion

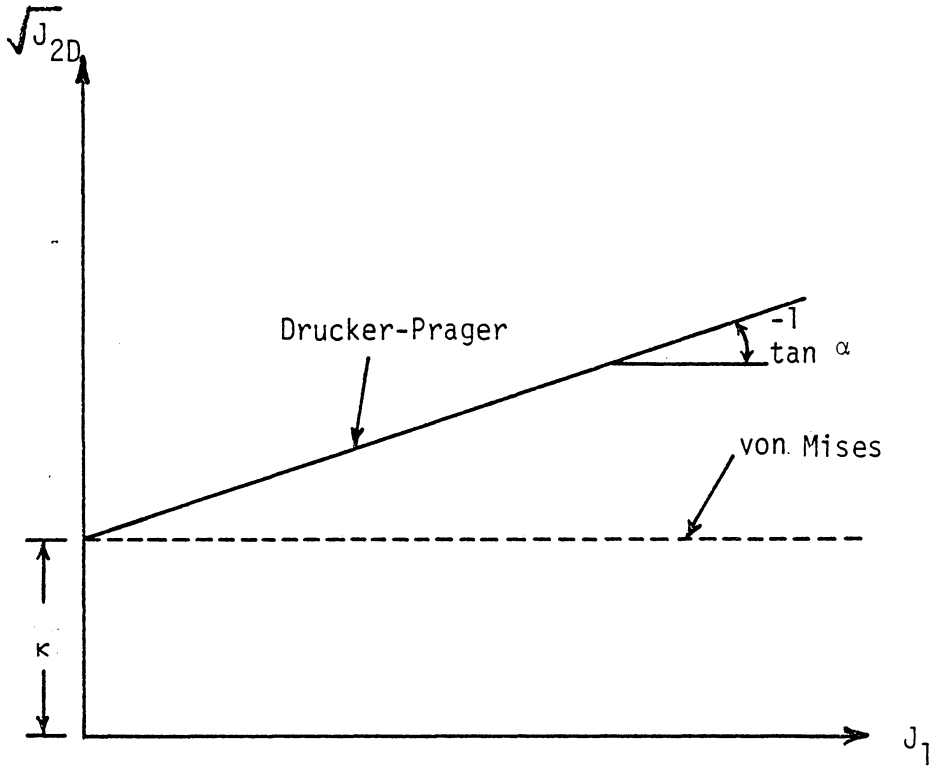

Figure 3.5 Drucker-Prager and von Mises Failure Surfaces in $J_1 - \sqrt{J_{2D}}$ Space

c, and the angle of internal friction, ϕ, of the material [2].

In case of a material with zero angle of internal friction, Eq. (3.21) reduces to the von Mises yield criterion, Figs. (3.4, 3.5) as

$$f = J_{2D}^{1/2} - \kappa = 0 \tag{3.24}$$

The vonMises criterion simulates the yielding behavior of metals and saturated clays under undrained loading condition reasonably well. The hardening can be incorporated in this model by changing the value of κ with strain history. In the von Mises criterion, the yield behavior is independent of the hydrostatic pressure, whereas this is not true in the case of frictional materials. On the other hand, the Drucker-Prager criterion can simulate the behavior of frictional materials fairly well. The limitations of the Drucker-Prager criterion are discussed in Ref. [2].

The incremental relations between stress and strain for conditions of plane strain based on the Drucker-Prager Model are written as [2]

$$\alpha = \frac{\tan \phi}{(9 + 12 \tan^2 \phi)^{1/2}} \tag{3.25}$$

$$\kappa = \frac{3c}{(9 + 12 \tan^2 \phi)^{1/2}} \tag{3.26}$$

$$\Delta\sigma_x = 2G\{(1 - 2A\sigma_x - B - C\sigma)\ \Delta\varepsilon_x + [(\sigma_x + \sigma_y)$$

$$A - B - C\ \sigma_x\sigma_y]\ \Delta\varepsilon_y + (-A\tau_{xy} - C\sigma_x\tau_{xy})\ \Delta\gamma_{xy}\}$$

$$\Delta\sigma_y = 2G\ \{[(\sigma_x + \sigma_y\ A - B - C\sigma_x\sigma_y]\ \Delta\varepsilon_x$$

$$+ (1 - 2A\sigma_y - B - C\sigma_y^2)\ \Delta\varepsilon_y \qquad (3.27)$$

$$+ (-A\tau_{xy} - C\sigma_y\tau_{xy})\ \Delta\gamma_{xy}\}$$

$$\Delta\tau_{xy} = 2G\ \{(-A\tau_{xy} - C\sigma_x\tau_{xy})\ \Delta\varepsilon_x + (-A\tau_{xy} - C\sigma_y\tau_{xy})\ \Delta\varepsilon_y$$

$$+ (1/2 - C\tau_{xy}^2)\ \Delta\gamma_{xy}\}$$

where

$$A = \frac{h}{P\kappa}$$

$$B = (\alpha - \frac{J_1}{6J_{2D}^{1/2}})\ \frac{2h}{1 + 9\alpha^2\ K/G} - \frac{3K\nu}{EP}$$

$$C = \frac{1}{2kPJ_{2D}^{1/2}}$$

$$P = \frac{J_{2D}^{1/2}}{k}\ (1 + \frac{9\alpha^2 K}{G})$$

$$h = \frac{3K}{2G}\ \alpha - \frac{J_1}{6J_{2D}^{1/2}}$$

$$G = \frac{E}{3\ (1 - 2\nu)}$$

$$K = \frac{E}{3(1 - 2v)}$$

The details of the derivation appear in Refs. [2,27].

The Drucker-Prager model along with linear elastic behavior are introduced in the computer program in this study.

CHAPTER 4

VERIFICATION

4.1 Introduction

The computer programs employing the hybrid stress model developed in this study are used to solve four preliminary problems. The predicted results are compared with the exact solutions or with solutions obtained by other investigators. In Chapter 6, verifications are presented with respect to two complex problems in geomechanics. The first two problems are analyzed by using linear elastic properties, and the second two problems are solved based on the elastic-plastic model. Also in this chapter, the numerical properties of the element stiffness matrices are investigated and evaluated.

4.2 Pure Beam Bending Problem

Consider a beam subjected to a loading that causes pure bending, Fig. (4.1). This problem can be idealized for plane stress, and due to the symmetries only one quarter of the beam is discretized. Desai and Abel [2] analyzed this problem by using four-node quadrilateral elements by utilizing the displacement method. The elements consist of four constant strain triangles. The material properties are given as

$$E = 30 \times 10^6 \text{ psi} \quad (1 \text{ psi} = 6.894 \text{ kN/m}^2)$$

$$\nu = 0.3$$

$$h \text{ (thickness)} = 1.0 \text{ inch} \quad (1 \text{ in.} = 2.54 \text{ cm})$$

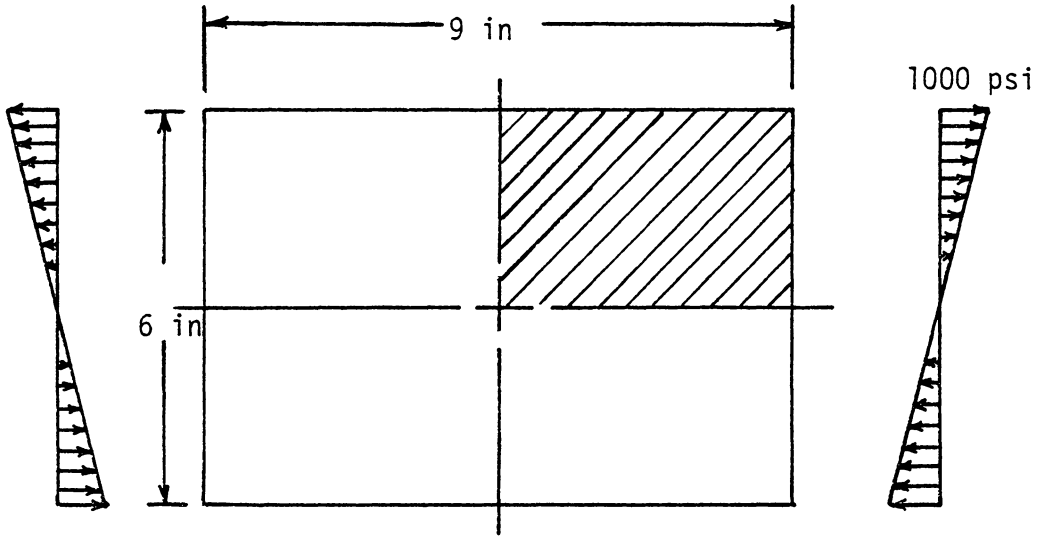

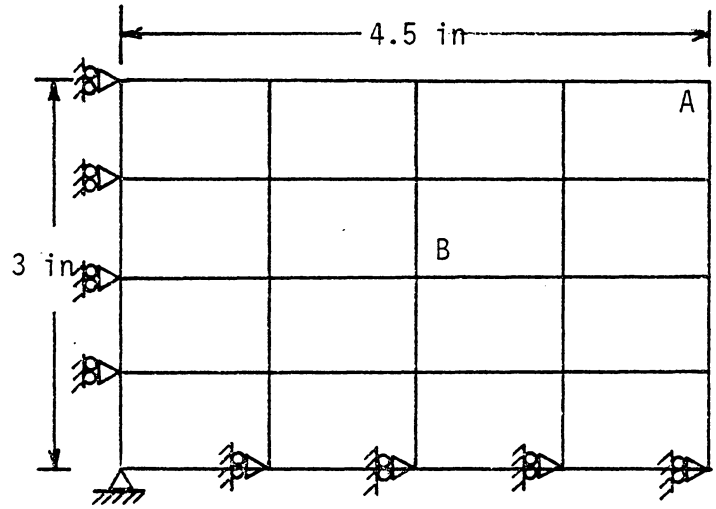

(1 in = 2.54 cm)

Figure 4.1 Pure-Bending Prcblem

This problem is solved first by using four-node quadrilateral-hybrid stress elements, where the stresses are assumed to vary linearly in the x and y directions as shown in Equation (2.42). The comparison of the results from the hybrid stress model and the displacement model with exact solution are shown in Table (4.1). The results from the two analyses show that the hybrid stress model with very simple assumed stress distribution and coarse mesh can predict displacements with a greater accuracy than the displacement method.

For a reliable and consistent solution, a minimum number of β's should be included in a stress field. In order to assure the existence of a solution for β's, one can include the number of β's based on the following criterion [4]:

$$n \geq (m-r) \tag{4.1}$$

where

n = total number of β's for an element,

m = total number of generalized displacement for an element, and

r = total number of rigid body degrees of freedom

The number of β's for a four-node quadrilateral element were increased from seven to eighteen, Table (4.2), and the same beam bending problem was solved. The results did not improve compared to the element with seven β's, and in fact, they started to get worse. This implies that the accuracy of the solution may

Table 4.1

Comparison of Displacement for Pure Beam Bending Problem

	Displacement at Point A (inches x 10^{-4})		Displacement at Point B (inches x 10^{-4})	
	u	v	u	v
4-Node Element				
Desai and Abel: [9] (25 nodes, 16 elements)	1.4552	-1.2399	0.3679	-0.3123
Hybrid Stress Model				
(25 nodes, 16 elements, 5β's)	1.5004	-1.2758	0.3751	-0.3192
(25 nodes, 16 elements, 7β's)	1.4803	-1.2597	0.3720	-0.3160
(25 nodes, 16 elements, 18β's)	1.4786	-1.2584	0.3718	-0.3159
8-Node Element				
Hybrid Stress Model (21 nodes, 4 elements, 18β's)	1.5000	-1.2750	0.3750	-0.3188
Exact	1.5000	-1.2750	0.3750	-0.31875

Table 4.2

[P] Matrix in Terms of Global Coordinates

$$[P] = \begin{bmatrix} 1 & y & 0 & 0 & 0 & x & 0 & y^2 & 0 & x^2 & xy & 0 & xy^2 & y^3 & 0 & x^2y & \frac{x^3}{3} & 0 \\ 0 & 0 & 1 & x & 0 & 0 & y & 0 & x^2 & y^2 & 0 & xy & 0 & 0 & x^3 & \frac{y^3}{3} & xy^2 & x^2y \\ 0 & 0 & 0 & 0 & 1 & -y & -x & 0 & 0 & -2xy & \frac{-y^2}{2} & \frac{-x^2}{2} & \frac{-y^3}{3} & 0 & 0 & -xy^2 & -x^2y & \frac{-x^3}{3} \end{bmatrix}$$

deteriorate if the number of β's are increased without using additional generalized boundary displacements q [4].

The matrix [H] Eq. (2.7) is positive definite. But when the stress vector $\{\sigma\}$, Eq. (2.2) is expressed in terms of polynomials of global coordinates (x,y) using eighteen β's, Table (4.2), due to computation errors, the matrix [H] may not remain positive definite for some elements located far away from the origin of global coordinate, Fig. (4.2). One of the approaches which can be used to overcome this difficulty is to assume a stress function in terms of local coordinates (s,t) and compute the stresses from the stress function. In this approach, a transformation of coordinates becomes necessary.

Thus, in the current study a stress function in terms of local coordinates (s,t) is assumed which contains eighteen β's, Eq. (2.49). The stiffness matrix of a square element with thickness t, Young's modulus E and Poisson's ratio 0.33, is computed by using Table (4.2) and Eq. (2.49). The results are identical, (see Table (4.3)). The results using Table (4.2) are also reported in Ref. [3].

The beam problem was also solved by using a four-node quadrilateral element, where the element stiffness matrix was formulated by using the following stress distribution:

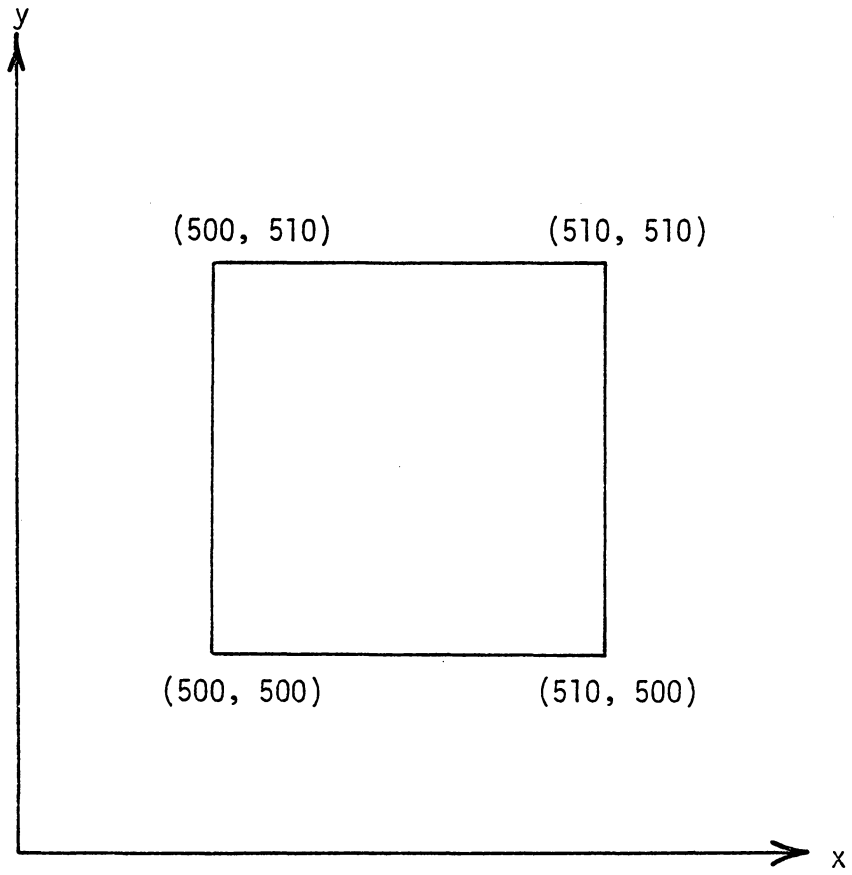

Figure 4.2 Four Node Element

Table 4.3

Stiffness Matrix

$$[K] = Et \begin{bmatrix} 0.47229 & 0.18750 & -0.28479 & -0.00 & -0.27771 & -0.18750 & 0.090205 & 0.00 \\ & 0.47229 & 0.00 & 0.090205 & -0.18750 & -0.27771 & 0.00 & -0.28479 \\ & & 0.47229 & -0.18750 & 0.090205 & 0.00 & -0.27771 & 0.18750 \\ & & & 0.47229 & 0.00 & -0.28479 & 0.18750 & -0.27771 \\ & & & & 0.47229 & 0.18750 & -0.28479 & 0.00 \\ & & & & & 0.47229 & 0.00 & 0.090205 \\ & & & & & & 0.47229 & -0.18750 \\ & & & & & & & 0.47229 \end{bmatrix}$$

SYM.

$$\begin{Bmatrix} \sigma_x \\ \sigma_y \\ \tau_{xy} \end{Bmatrix} = \begin{bmatrix} 1 & y & 0 & 0 & 0 \\ 0 & 0 & 1 & x & 0 \\ 0 & 0 & 0 & 0 & 1 \end{bmatrix} \begin{Bmatrix} \beta_1 \\ \beta_2 \\ \beta_3 \\ \beta_4 \\ \beta_5 \end{Bmatrix} \qquad (4.2)$$

Examination of Eq. (4.2) reveals that the distribution of horizontal stress σ_x is similar to the exact solution which can be computed from the beam theory. The predicted displacements using Equation (4.2) are very close to the exact solution, especially in the x direction as shown in Table (4.1). It can be deduced that if a knowledge of stress distribution is available for a given problem, for quicker convergence it may be beneficial to assume the stress field according to the known stress distribution. For example, an assumed stress function can be based on the solution of stresses (in polynomial form) from the theory of elasticity.

A noteworthy improvement occurs when the number of generalized boundary displacements q's are increased from eight to sixteen, and the number of β's are kept to eighteen. In other words, an eight-node quadrilateral element is developed. For the beam problem solved by using only four elements, the results are almost coincident with the exact solutions, Table (4.1). In the remaining part of this dissertation, the eight-node quadrilateral element with eighteen β's is used.

All computations are done by using double precision arithmetic and, as mentioned before, the subroutine LINV2P from IMSL library is used for the inversion of matrix [H] [15].

4.3 Plate with Circular Hole

This problem is chosen first to determine how accurate the hybrid stress model can predict stress distributions around a circular hole involving the stress concentration. Second, this problem is in some aspects similar to the excavation problem. The load condition and geometry are shown in Fig. (4.2); the material properties considered in the present analysis

$$E = 10000.0 \text{ kN/cm}^2$$

$$\nu = 0.25$$

$$h \text{ (thickness)} = 1.0 \text{ cm}$$

First, a convergence test was performed by using four different meshes, Figs. (4.3), (4.4), (4.5), and (4.6). Figure (4.7) shows the magnitude of horizontal stress σ_x at point A against the number of nodes using the eight-node hybrid stress element, and an eight-node displacement element. The agreement between the present model and the exact solution is excellent; the exact solution can be found in Ref. [29]. It can be seen that the hybrid stress model predicts the stresses more accurately with a course mesh, compared to the displacement model with a finer mesh.

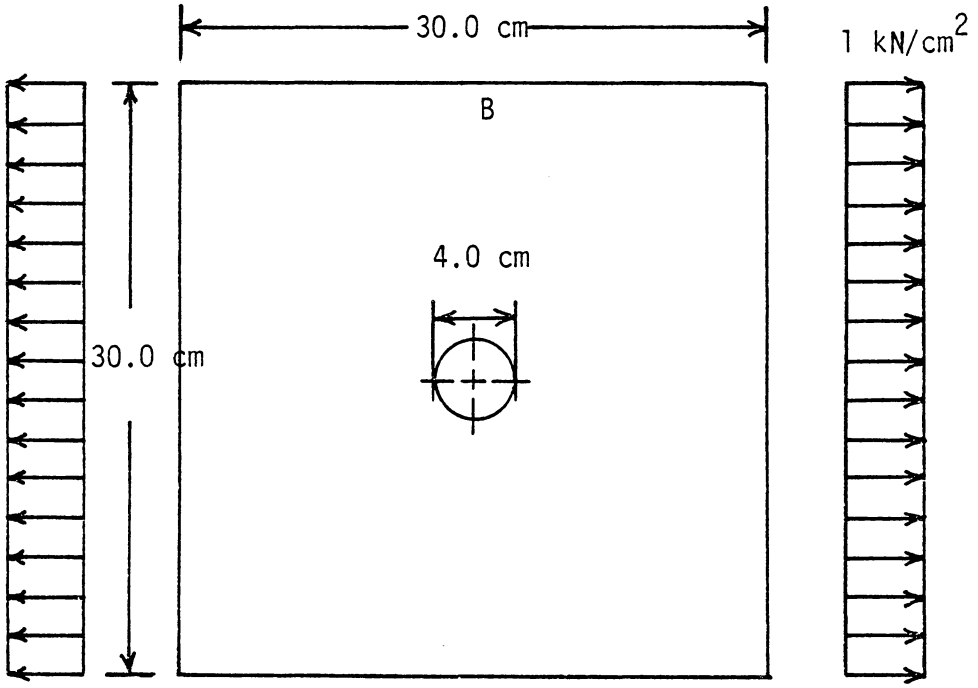

Figure 4.2 Square Plate with a Scale

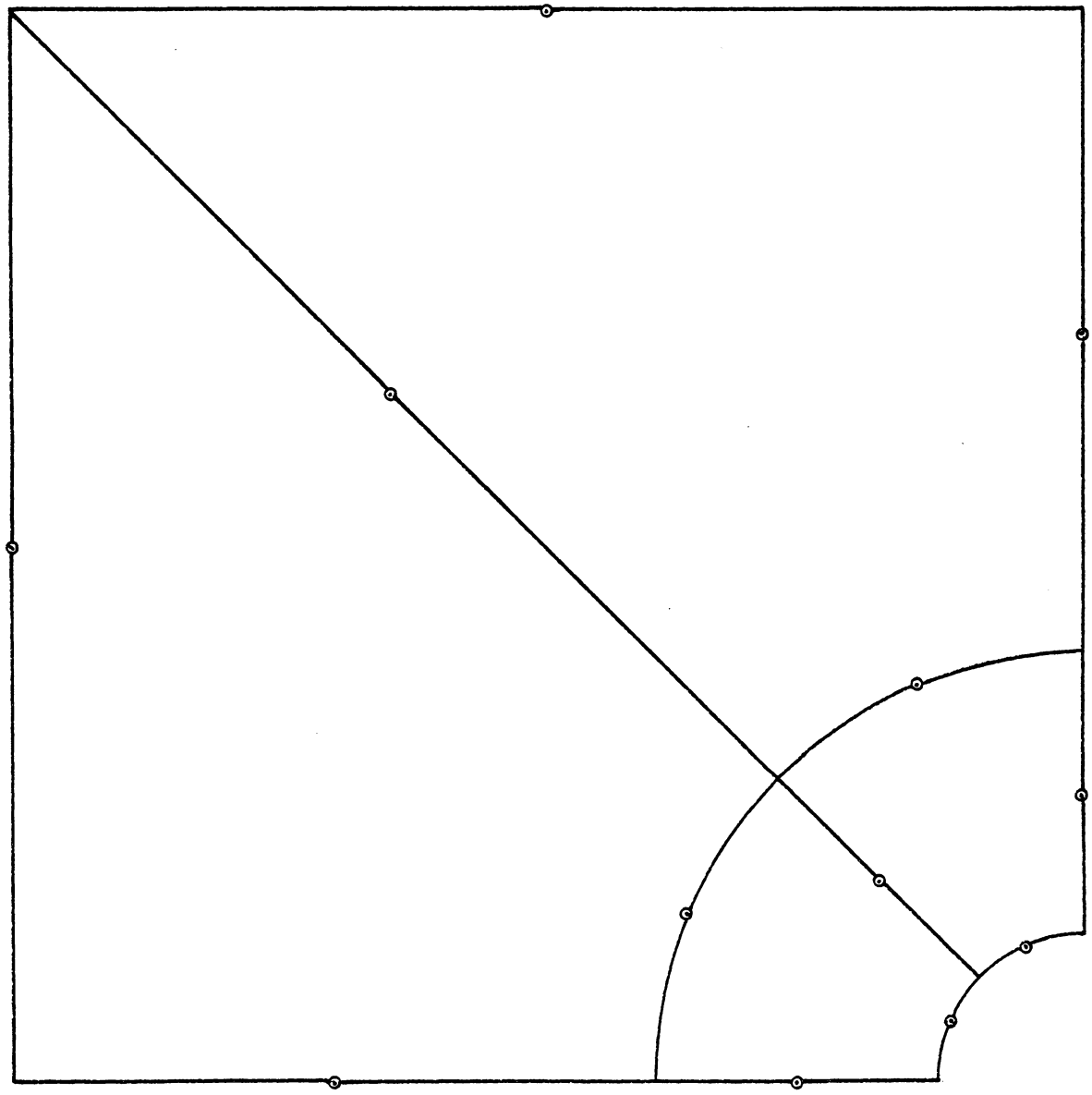

Figure 4.3 Finite Element Mesh with 4 Elements
(Plate with a hole)

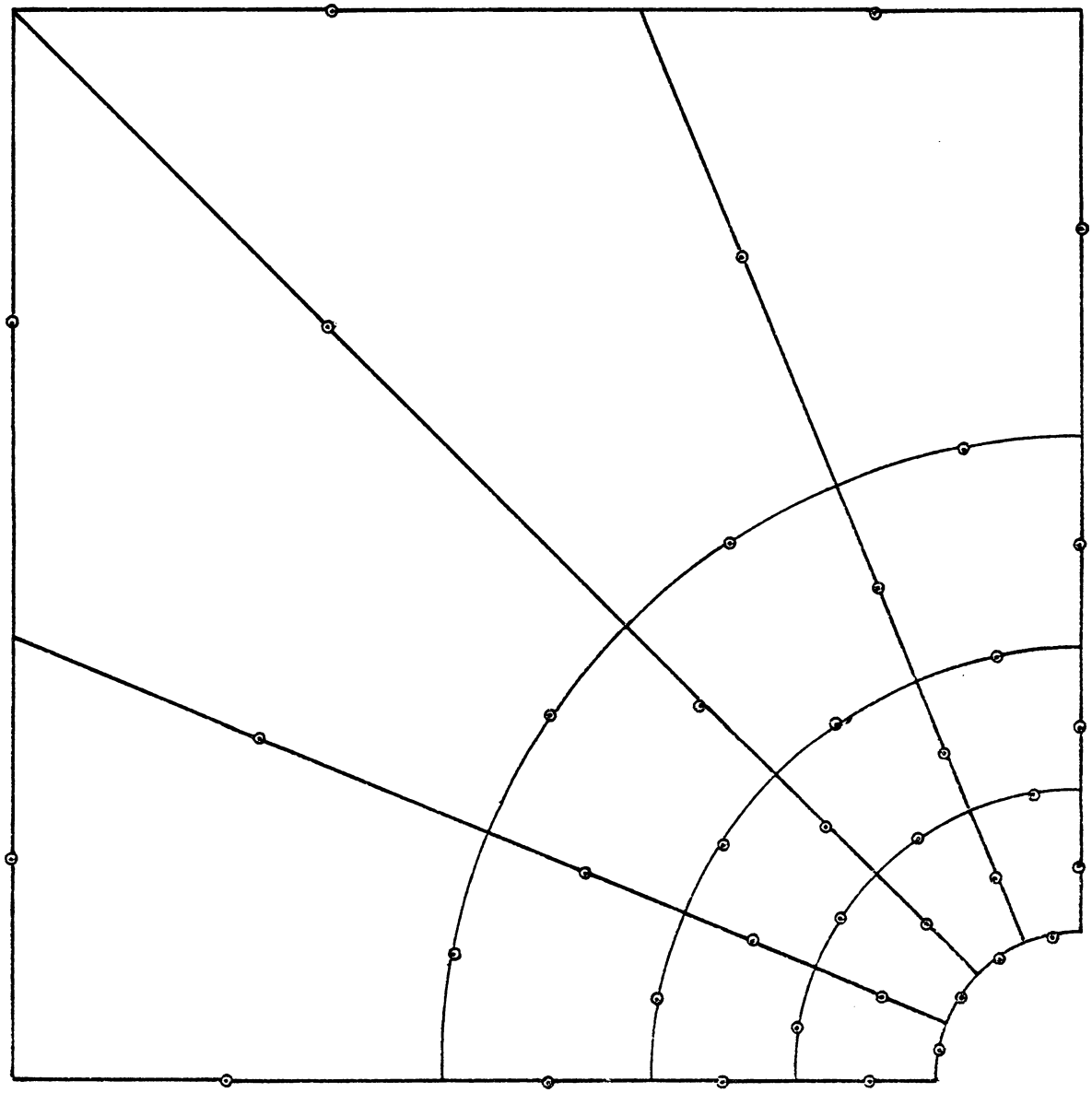

Figure 4.4 Finite Element Mesh with 16 Elements (Plate with a hole)

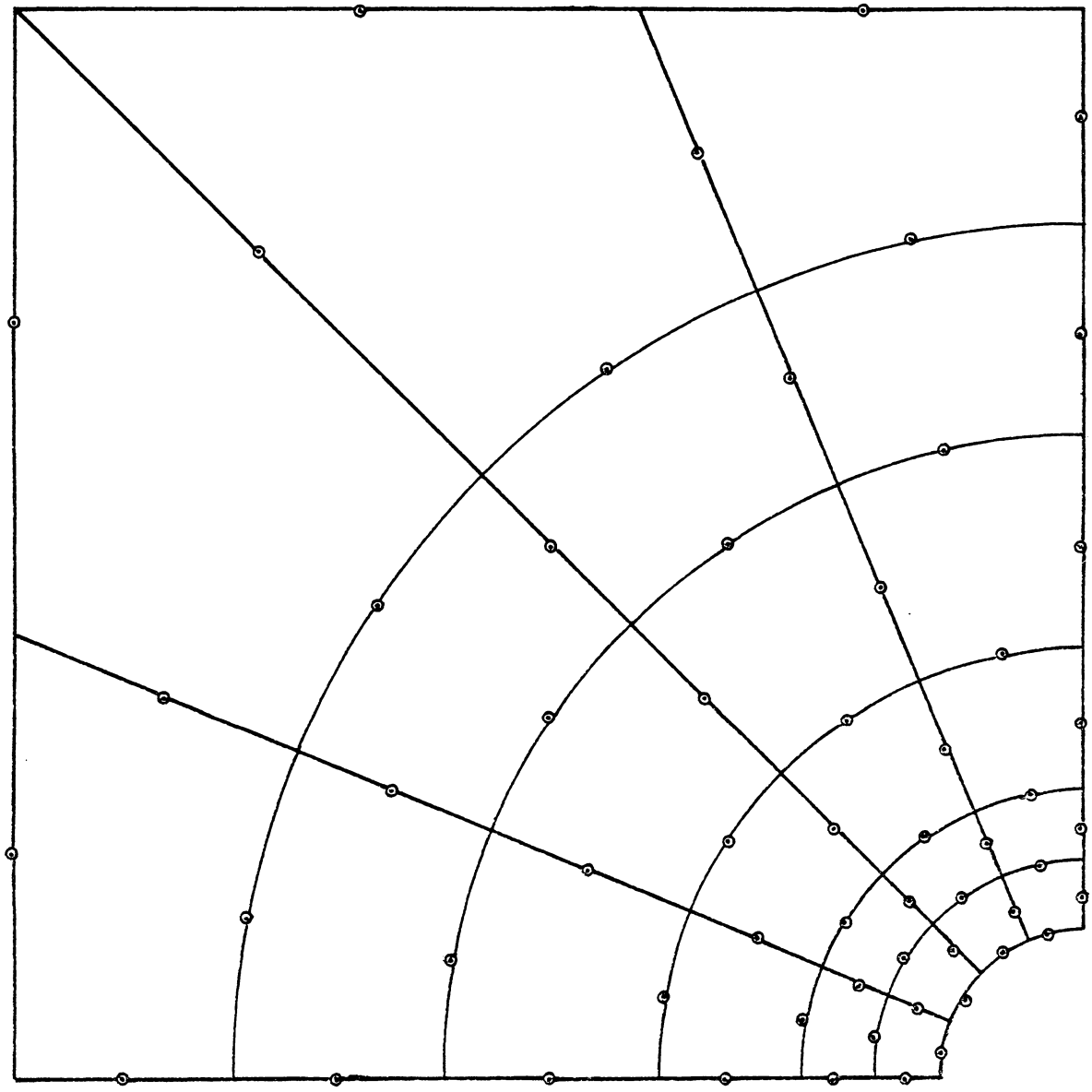

Figure 4.5 Finite Element Mesh with 24 Elements (Plate with a hole)

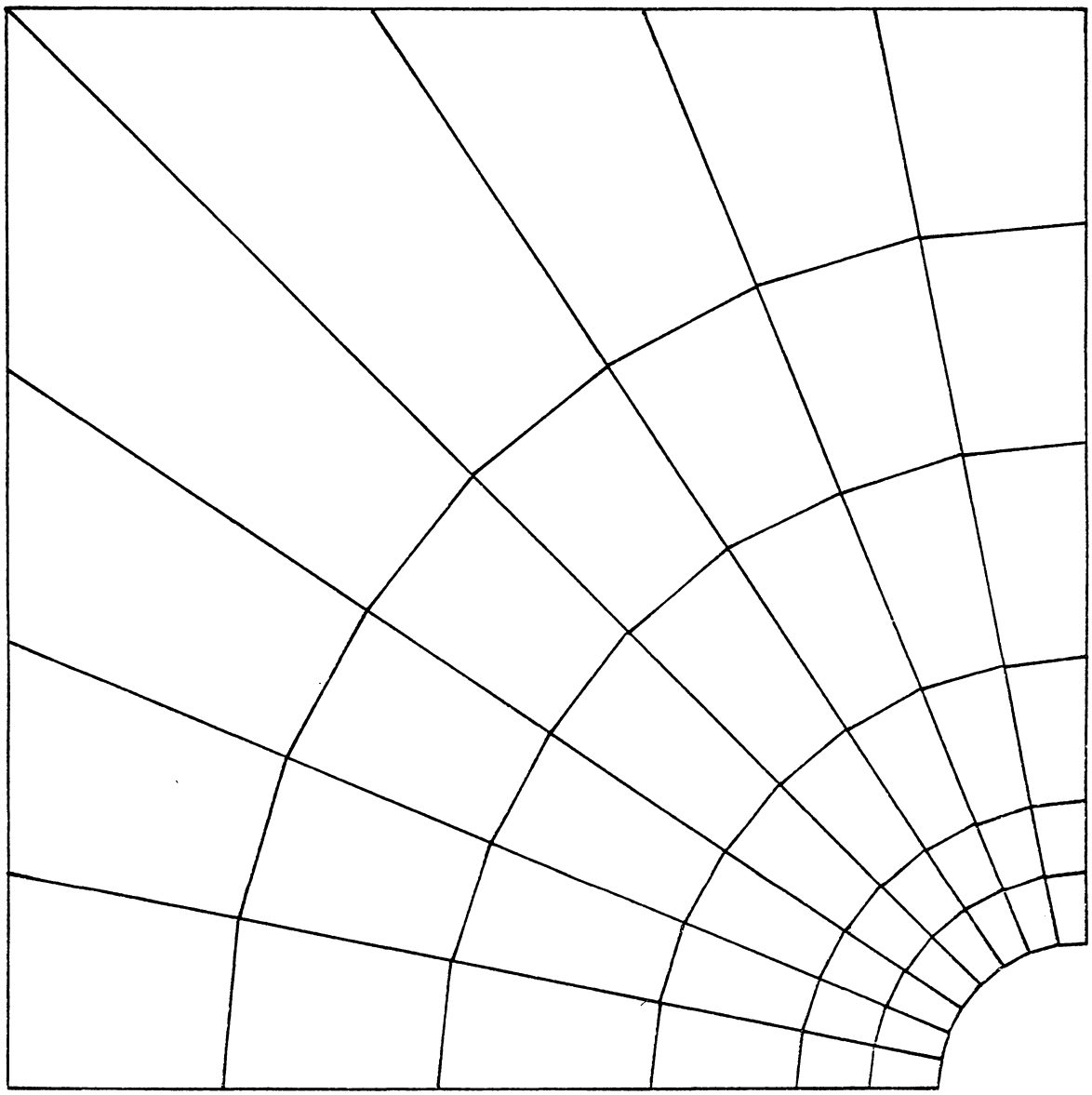

Figure 4.6 Finite Element Mesh with 48 Elements (Plate with a hole)

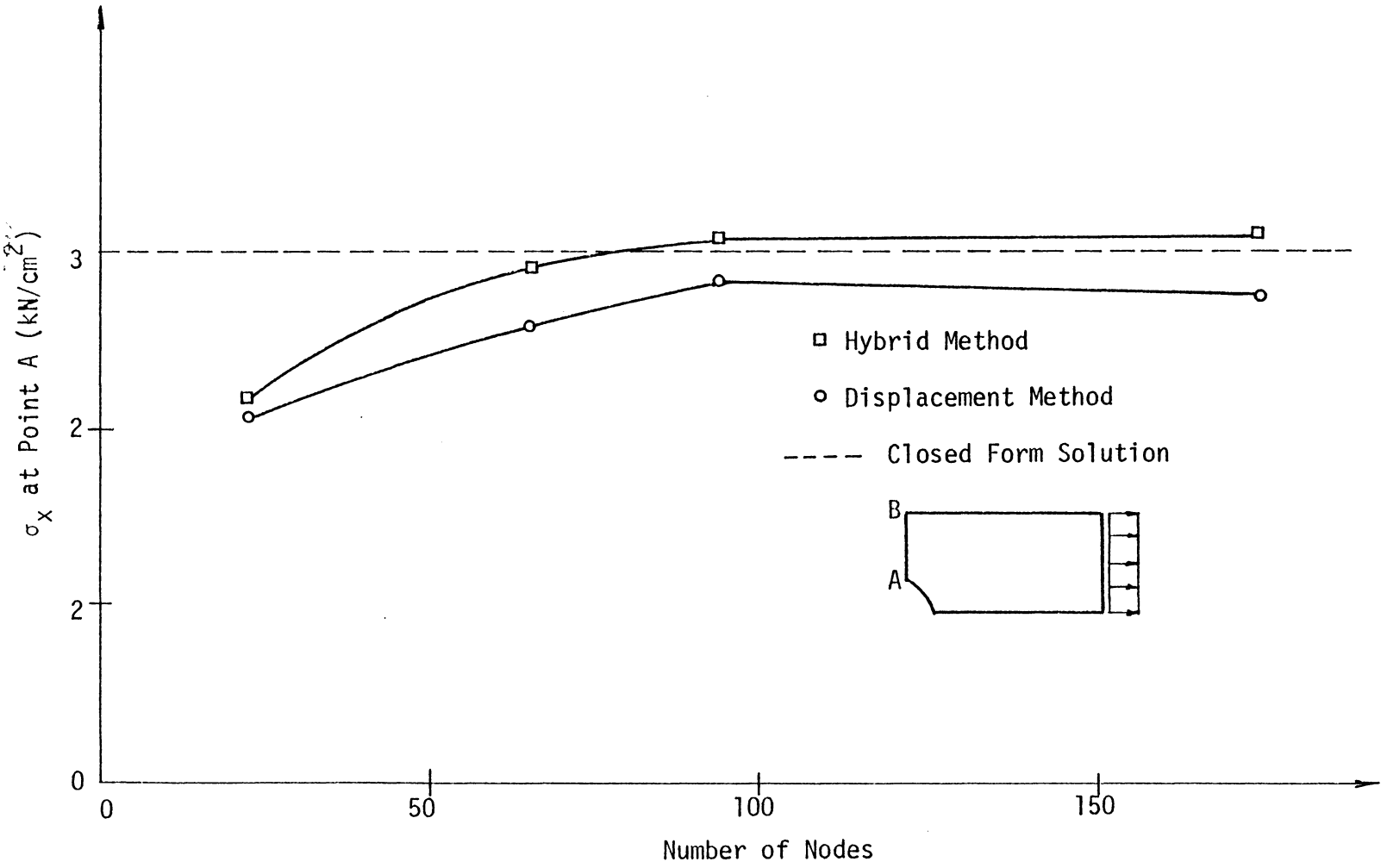

Figure 4.7 Variation of σ_x with Number of Nodes

In the displacement methods, the stresses are usually computed at integration points. The stress at point A,which is located on the boundary of an element, are obtained by using smoothing techniques [16]. In the case of the hybrid stress model, the stresses on the boundary are computed directly by substitution of the coordinates of the boundary into Eq. (2). Since the interelement continuity of stresses does not exist in the hybrid stress model, the average values of stresses on the interelement boundary are computed.

Figure (4.8) shows the variation of horizontal stress σ_x along AB. It can be noted that the displacement method and the hybrid method yield similar results, close to the exact solution at some distance away from the hole. But near the hole the hybrid stress model predicts improved stresses compared to those from the displacement method.

4.4 Strip Footing

In order to corroborate the nonlinear feature of the computer program by using the hybrid stress model, two strip footings are analyzed, and the results are compared with the solutions reported in the literature.

In the first case, a flexible strip footing supported on a homogeneous isotropic soil layer is considered. This problem has been solved by Lambe and Whitman [30] using the finite difference method, and by Boomlualohr et al. [31] using the displacement method utilizing the vonMises yield criterion.

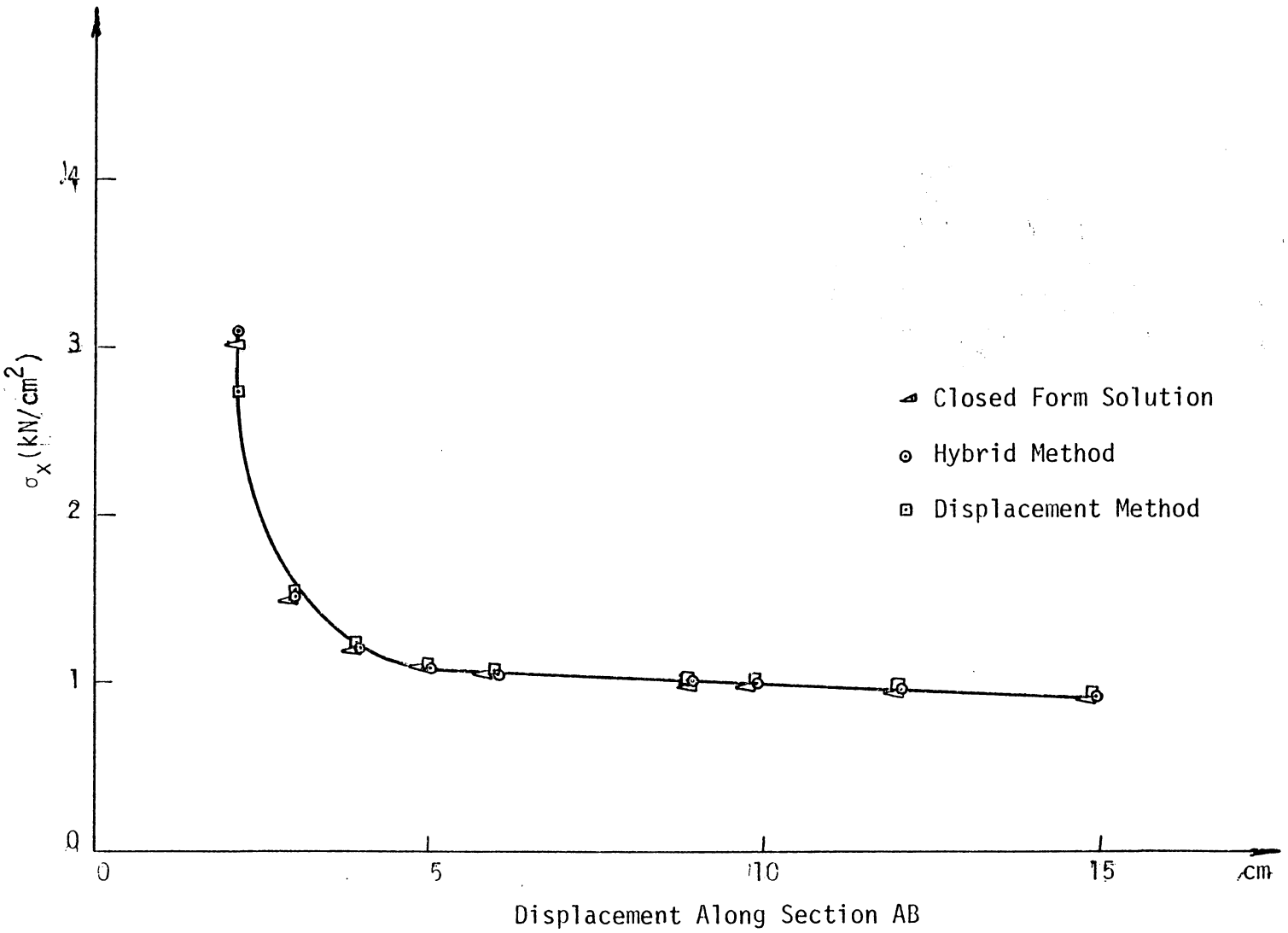

Figure 4.8 Variation of Stress Along the Section (48 Elements)

The dimensions for the problem are illustrated in Fig. (4.9), and the soil properties are

$$E = 720 \text{ ksf} \quad (3515.4 t/m^2)$$

$$c = 3.5 \text{ ksf} \quad (17.1 t/m^2)$$

$$\nu = 0.3$$

$$h \text{ (thickness)} = 1.0 \text{ ft}$$

The strip footing is analyzed as a plane strain problem. In the current study, the Drucker and Prager model is employed in the analysis. It can be observed from Fig. (4.10) that the present results of settlement agree well with the solutions given in Ref. [31]. It should be noted that for the soil with internal friction angle equal to zero that the Drucker and Prager model reduces to the vonMises yield criterion.

In the second case, a flexible strip footing supported on a frictional soil is analyzed. The problem is illustrated in Fig. (4.11) and the following values for the soil parameters are assumed throughout the analysis:

$$E = 30000 \text{ t/m}^2$$

$$\nu = 0.3$$

$$c = 0.0$$

$$h \text{ (thickness)} = 1.0 \text{ m}$$

Christian, et al. [32] have solved this problem by using the displacement method with the Mohr Coulomb yield criterion. In

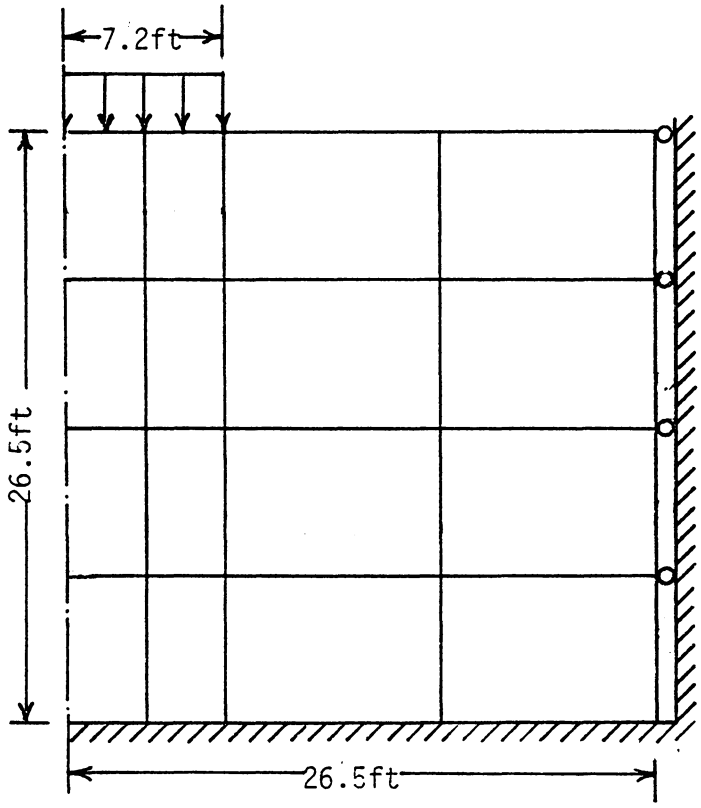

1 ft = 0.3048 m

Figure 4.9 Footing Problem

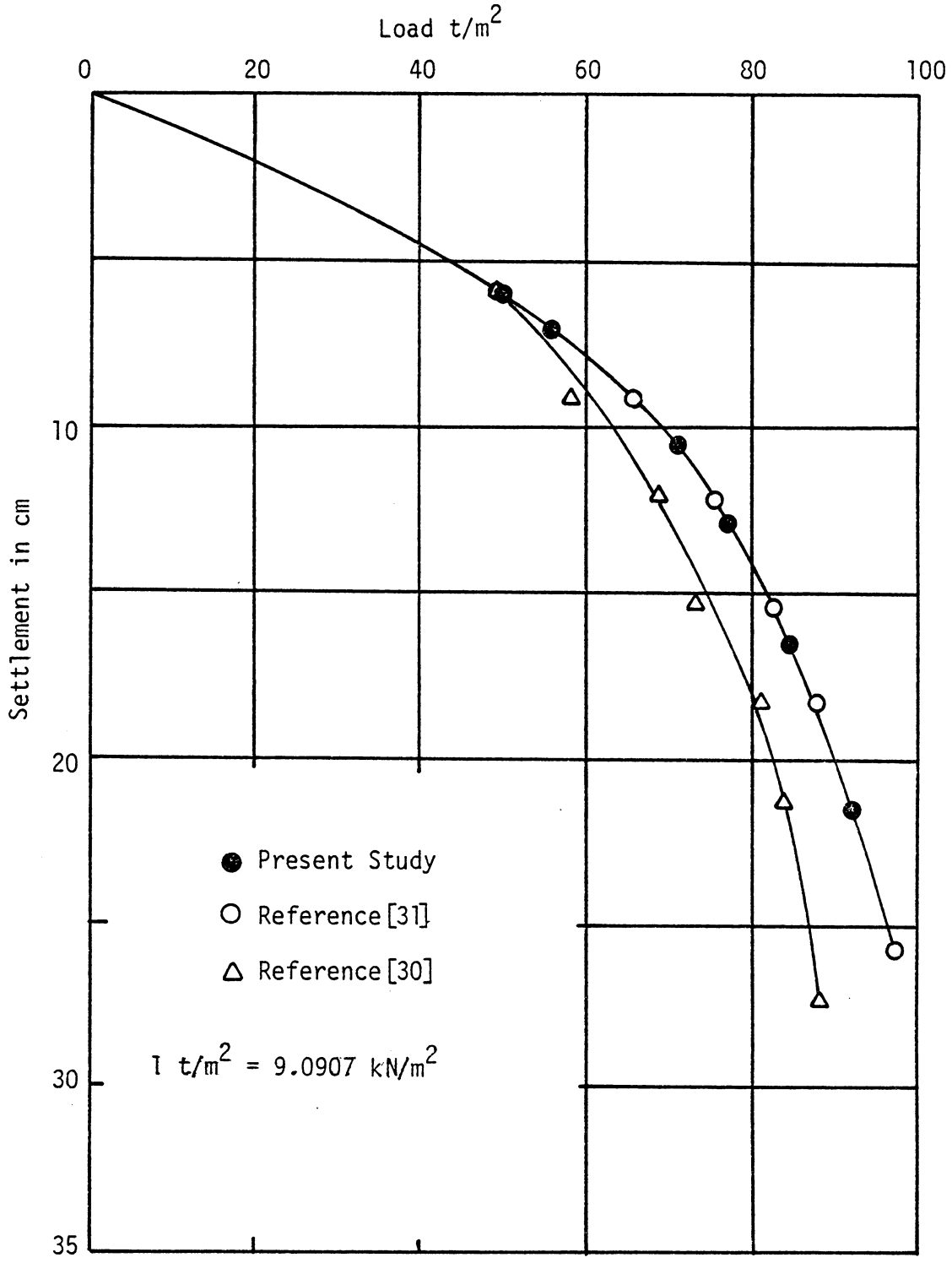

Figure 4.10 Comparison of Settlement Under the Load

the present study, the analysis is performed by using the hybrid stress method and the Drucker-Prager model.

The finite mesh shown in Fig. (4.11) consists of sixteen elements whereas Christian et al. [32] used thirty elements. The reason for designing such a coarse mesh is that in the previous problems, it has been seen that the hybrid stress model predicts accurate displacements and stresses with much coarser mesh.

A comparison of the settlements obtained from the present study and those from Ref. [32] are shown in Fig. (4.12). The agreement between the solutions for settlement under the load is good. However, the ultimate load predicted by the hybrid stress model was lower than that from Ref. [32]. This appears to be appropriate since the hybrid model contains certain stress distribution modes and can be considered nearer to complementary approach, which could predict improved failure or ultimate loads. Both methods, however, yield higher ultimate bearing capacity than is given by Terzaghi's formulae, Fig. (4.12).

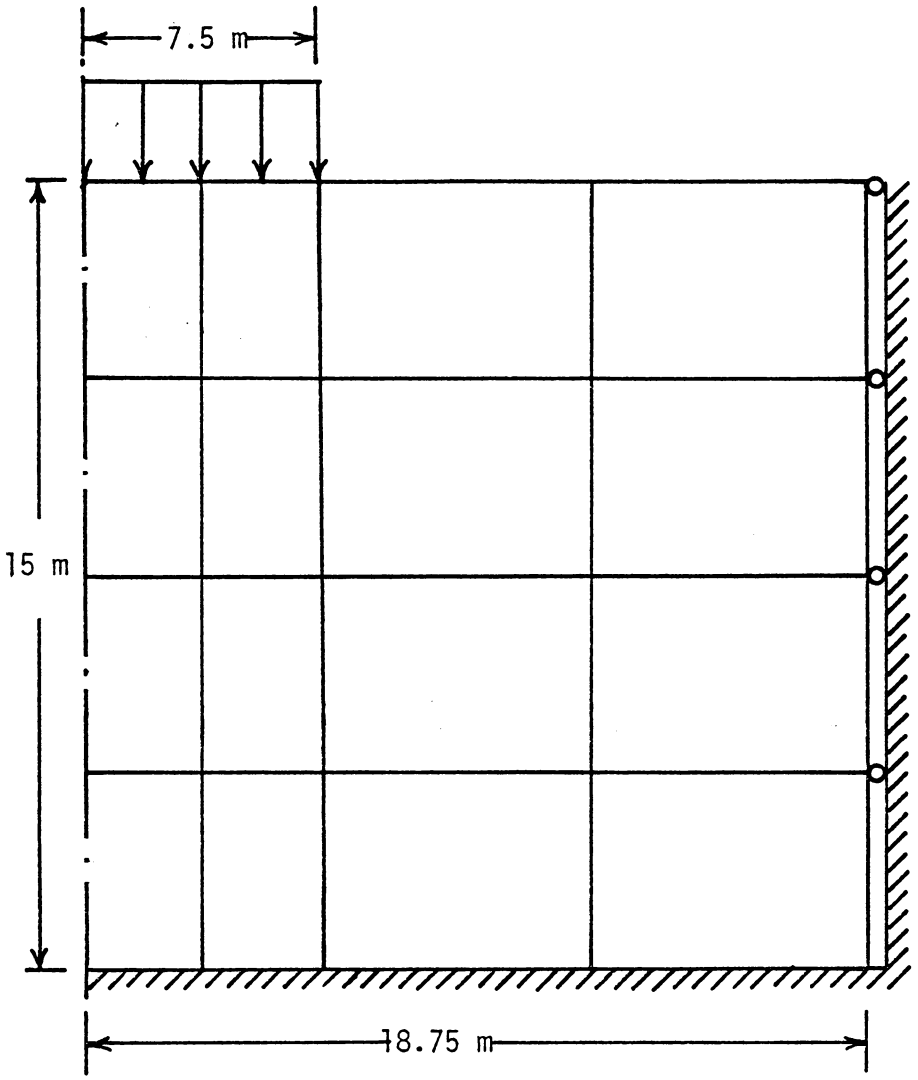

Figure 4.11 Footing Problem

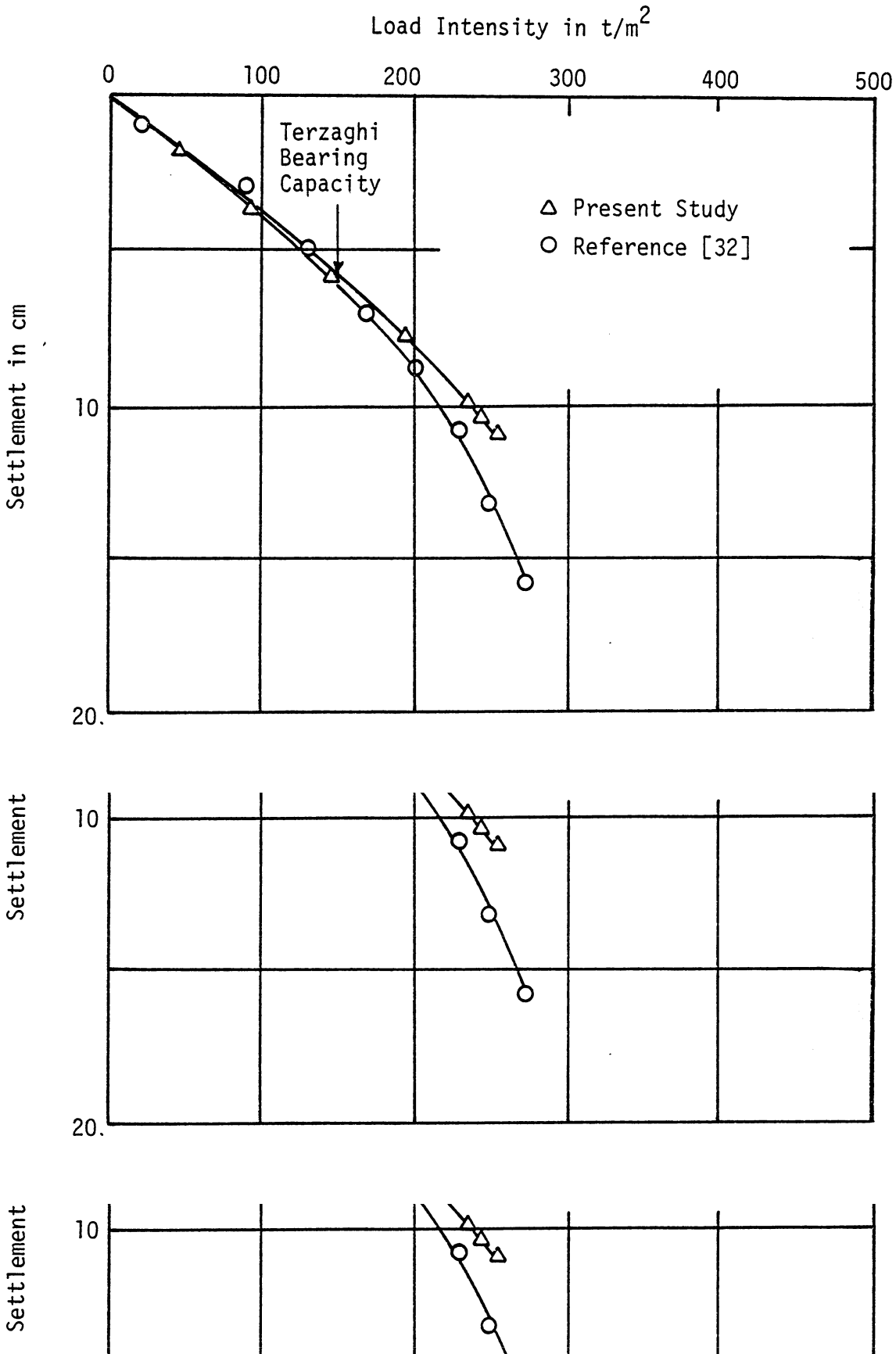
Load Intensity in t/m2
0
100
200
300
400
500
Terzaghi
Bearing
Capacity
Present Study
Reference [32]
Settlement in cm
10
20.
Settlement
10
20.
Settlement
10

CHAPTER 5

SIMULATION OF CONSTRUCTION SEQUENCES

5.1 Introduction

The demands for underground structures such as tunnels, underground storage, manufacturing facilities, and underground power plants, and for utilization of underground resources such as mine ores are rising. Construction sequences plays a significant role in the analysis and design of such structures.

The deformation behavior of geologic media is usually dependent on the history of loading and unloading, and, also, in each stage of construction, the state-of-stress in the surrounding material may change. Hence, it is more realistic to simulate the construction sequences in order to account for the stress history effects.

The construction sequences can involve excavation, dewatering, deposition, and installation of support systems. The computer program developed in this study incorporates these stages of construction, but here greater emphasis is given to the simulation of excavation.

5.2 Simulation of Excavation

When a layer of a geologic medium is excavated, the state of stress in the soil or rock changes. This alteration of the state of stress is associated with deformations in the surrounding material. The design of lining and other support systems in tunnels and in open excavation are influenced by the history of changes in stress and deformation.

Excavation is a complex problem and in some instances can be time dependent, but for simplicity, often the effect of time on the behavior of the surrounding material can be neglected. Initial attempts towards simulation of excavation involved the assumption of linear elastic behavior for the media [33]. Since soils and some rocks are nonlinear, it is more rational to treat these media as nonlinear. Due to the advancement in computer technology it is possible to solve such highly nonlinear problems by using the finite element methods.

In this chapter, a summary of the presently available models of simulation of excavation employing the displacement finite element methods is presented, and also a new method based on the hybrid stress model is proposed and discussed.

5.2.1 Available Models for Simulation of Excavation

Most available models for simulation of excavation utilizing the displacement methods are based on the model originally proposed by Goodman and Brown [34]. In this model, first the initial state of stress or geostatic stress, $(\sigma_x^0, \sigma_y^0, \sigma_{xy}^0)$, prior to the start of excavation, is determined. This can be done by using one cycle of the finite-element method; here the magnitude of the horizontal insitu stresses can be found from

$$\sigma_x = K_0 \sigma_y \tag{5.1}$$

where K_0 is referred to as the coefficient of lateral pressure (stress) at rest.

For the special situation when the ground surface is horizontal, the vertical stress can be obtained by means of the integral

$$\sigma_y = \int_0^z \gamma dz \tag{5.2}$$

where

γ = unit weight of the soil, and

z = the depth

Excavation is simulated in a number of increments. In each increment, a stress free surface is created by applying equivalent nodal forces on the excavation surface due to the increment of excavation, Fig. (5.1). The equivalent nodal forces are then computed from the existing state-of-stress and applied with opposite sign to the excavated surface. The displacements, stresses, and strains are calculated and added to the values for the previous step as

$$\{\sigma_i\} = \{\sigma_0\} - \sum_{j=1}^{i} \{\Delta\sigma_j\} \tag{5.3}$$

$$\{q_i\} = \{q_0\} - \sum_{j=1}^{i} \{\Delta q_i\} \tag{5.4}$$

$$\{\varepsilon_i\} = \{\varepsilon_0\} - \sum_{j=1}^{i} \{\Delta\varepsilon_i\} \tag{5.5}$$

The procedure of excavation is illustrated in Fig. (5.1).

Various techniques have been used to evaluate the stresses or equivalent nodal forces on the excavation boundary. Clough and

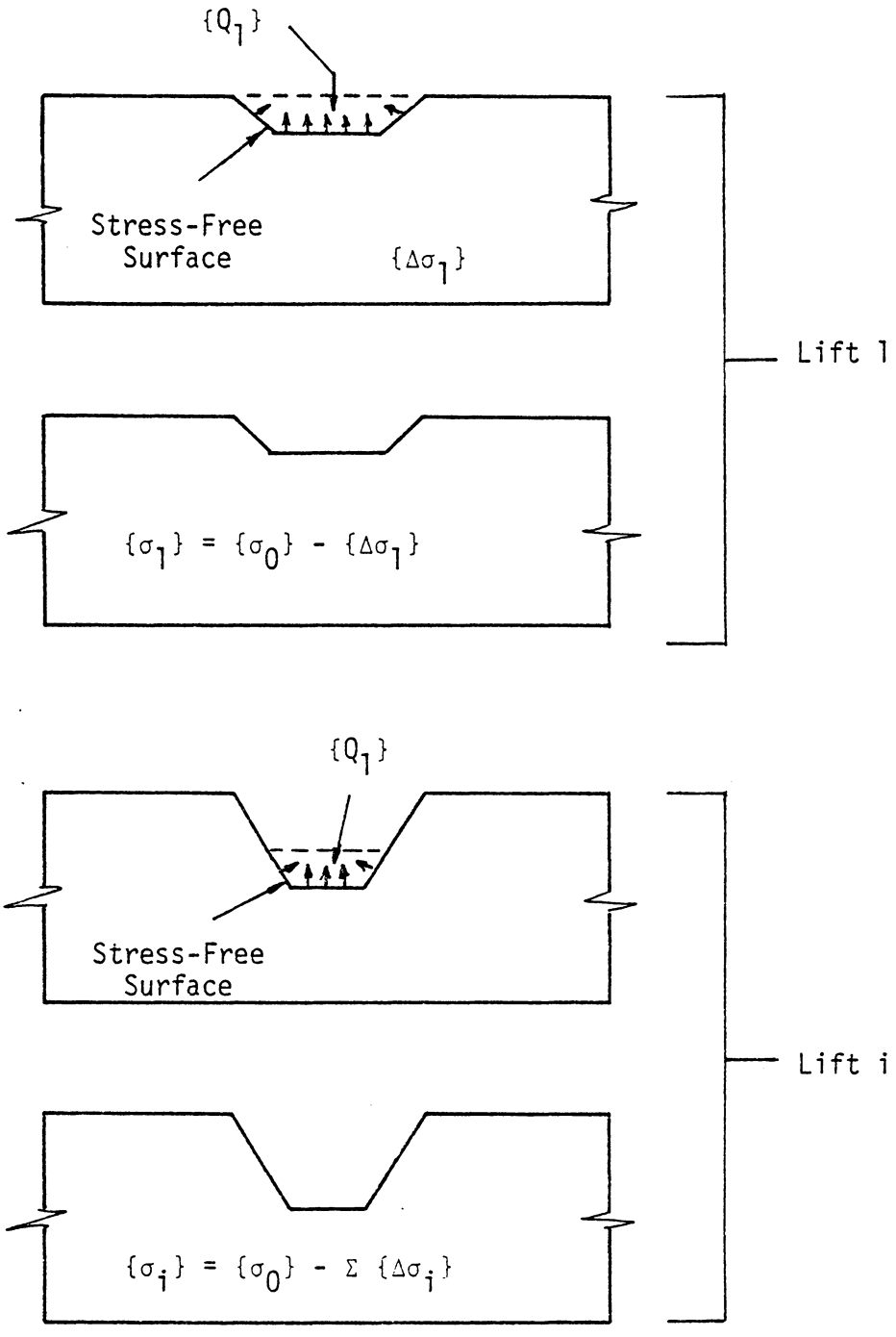

Figure 5.1 Simulation of Excavation [9]

Duncan [35] proposed a procedure for simulation of excavation using four node quadrilateral elements. Since, in these elements, the stresses are computed at the center of the elements, a nonlinear interpolation function was employed to compute the stresses on the excavation boundary from the state-of-stress of four elements which are located adjacent to the excavation boundary. The equivalent nodel forces were computed from the boundary stresses by assuming that the stresses vary linearly along the sides of the element. In this approach, the results for the problem with singularities, such as corners, may not be reliable because the displacement approach with the quadrilateral elements may not predict accurate stresses especially close to the point of singularity, and also the selection of the "best" four interpolation elements can influence the results [36].

Christian and Wong [37] investigated the use of lower order elements such as a linear triangle or four-node quadrilateral element in simulation of excavation in elastic media. It was pointed out that behavior under excavation in linearly elastic material should be independent of the number of cutting sequences, but for the lower order finite elements they used, this criterion did not hold. In other words, the problem can be dependent on the number of cutting sequences. This error can become more serious when one tries to simulate excavation in nonlinear materials because nonlinear problems are usually solved in a number of increments and the errors may be cumulative. Christian and Wong [37] indicated that the errors may be

caused by the fact that the lower-order elements are inadequate to provide accurate stress distributions near the corners of the excavation. Desai, Johnson, and Hargett [38] also discussed the limitations of the displacement approach with the foregoing procedure for computing equivalent equilibrating forces for creating a free surface in the simulation process. It was also proposed that an evaluation of the equivalent forces can be accomplished by using the following formula [39]:

$$\{F\} = \int_V [B]^T \{\sigma_0\} dV \tag{5.5}$$

where

$[B]$ = strain-displacement transformation matrix

$\{\sigma_0\}$ = equivalent stress vector

Mana [40] used eight-node isoparametric elements in the displacement model, where Eq. (5.5) was utilized for computing the equivalent forces for creating the stress-free surface. He simulated excavation in linear elastic material by using one step and then three steps, showing that the predicted behavior from both approaches was identical. He analyzed two cases of braced excavation constructed in soft clays, and compared the prediction with field observations.

Lightner [41] developed a procedure and program to simulate construction sequences by using eight-node elements and included a number of constitutive laws.

It has been mentioned before that all previous models are based on the displacement method, and that it may not predict accurate stress distributions especially in the analysis of problems involving singularities. In the current study, a program based on the hybrid stress model is developed and a number of components for this program are adapted from a code based on the displacement method developed by Lightner and Desai [42,43].

5.2.2 Simulation of Excavation by the Hybrid Stress Model

The hybrid finite element procedure developed here is based on eight-node isoparametric elements. The scheme of simulation in this model is similar to that illustrated in Fig. (5.1). There are a number of approaches which can be applied to determine the stresses or the equivalent nodal forces on the boundary of excavation. The simplest approach is to compute the stresses directly on the boundary of the excavation by substitution of the coordinates of the boundary in the assumed stress fields, Eq. (2.2), using the excavated elements which have a common boundary with the unexcavated elements. The equivalent nodal forces can be computed by using the magnitudes of the boundary stresses and the interpolation function used for the displacements of particular boundary, Eq. (2.5). After each step, the vector of $\{\beta\}$ is accumulated for use in the computation of the stresses on the boundary of the excavation in the next step. This approach can be used in a linear elastic analysis of excavation. However, a problem will arise when one wants to simulate excavation

in an elastic-plastic medium by using the initial stress method used in this study. This is due to the fact that in plastic regions the stresses are corrected at the integration points. In other words, the stresses are corrected without any correction in the magnitude of the vector $\{\Delta\beta\}$ Eq. (2.35). Thus, the vector $\{\Delta\beta\}$ cannot be used to compute the stresses on the boundary of the excavation.

The foregoing difficulty in using the initial stress method is explained in Chapter 2 and can be handled by: 1) computing the vector $\{\beta\}$ from the magnitudes of stresses at integration points using a least-squares procedure based on the assumed stress field, Eq. (2.2); 2) the equivalent nodal force vector $\{F\}$ can be computed by the means of equation

$$\{F\} = \sum_{m=1}^{M} \left([G]^T[H]^{-1} \int_V [P]^T[D]\{\sigma_0\}dV\right) \tag{5.6}$$

where $\{\sigma_0\}$ denotes the stress vector at the integration points. (The rest of the terms have been defined previously.)

The second approach is adapted in this study. The insitu stress must be treated differently in this approach because in Eq. (5.6) the vector $\{\sigma_0\}$ is just due to the homogeneous part of stresses, Eq. (2.2). One cycle of the stress hybrid model is used to compute the insitu stress. In this cycle, the Poisson's ratio ν is computed as

$$\nu = \frac{K_0}{K_0 + 1} \tag{5.7}$$

where K_o is the coefficient of lateral pressure (stress) at rest.

The stresses on the boundary of excavation due to the insitu stress are computed by substitution of the coordinates of the boundary into Eq. (2.2) using the excavated elements which have common boundary with the unexcavated elements. In each step of excavation, the equivalent nodal forces due to the homogeneous part of the stresses are computed by using Eq. (5.6) and then added to the equivalent nodal forces due to the insitu stress. The stresses and the displacements are accumulated after each increment.

Verification of Model

The validity of any model using finite element methods for simulation of excavation must be verified for two criteria [40], uniqueness and convergence.

In excavation, when a layer of geologic media with linear elastic properties is excavated in one step or several steps the behavior should be the same. This phenomenon is called uniqueness test.

The new approach based on the hybrid stress model is applied to simulate an excavation in linear elastic geologic media by using one step and three steps. The properties of material are

$$E = 10{,}000 \text{ t/m}^2$$

$$\nu = 0.3$$

$$\gamma = 1.8 \text{ t/m}^3$$

$$K_0 = 0.9$$

The finite element grid is shown in Fig. (5.2). The predictions of behavior from both analyses are identical as is shown in Tables (5.1) and (5.2). Thus, the new approach satisfies the uniqueness criterion.

To investigate the convergence of equivalent nodal forces, a one-dimensional problem for which the exact solution can be found by theory of elasticity [29] is analyzed. The dimensions of the problem are given in Fig. (5.2). This problem is idealized as plane strain and the material properties are

$$E = 10{,}000 \text{ t/m}^2$$

$$\nu = 0.2$$

$$\gamma = 1.0 \text{ t/m}^3$$

$$K_0 = 0.5$$

This problem was also solved by Mana [40]. A comparison of numerical results obtained from the hybrid stress model, the displacement method, and the exact solution are shown in Figs. (5.3) and (5.4). It can be seen that the equivalent nodal forces and the displacements computed from the present method using only one element yield exact solutions, whereas the displacement method using eight elements failed to do so [40]. The new procedure using the hybrid stress model satisfies both criteria of uniqueness and convergence.

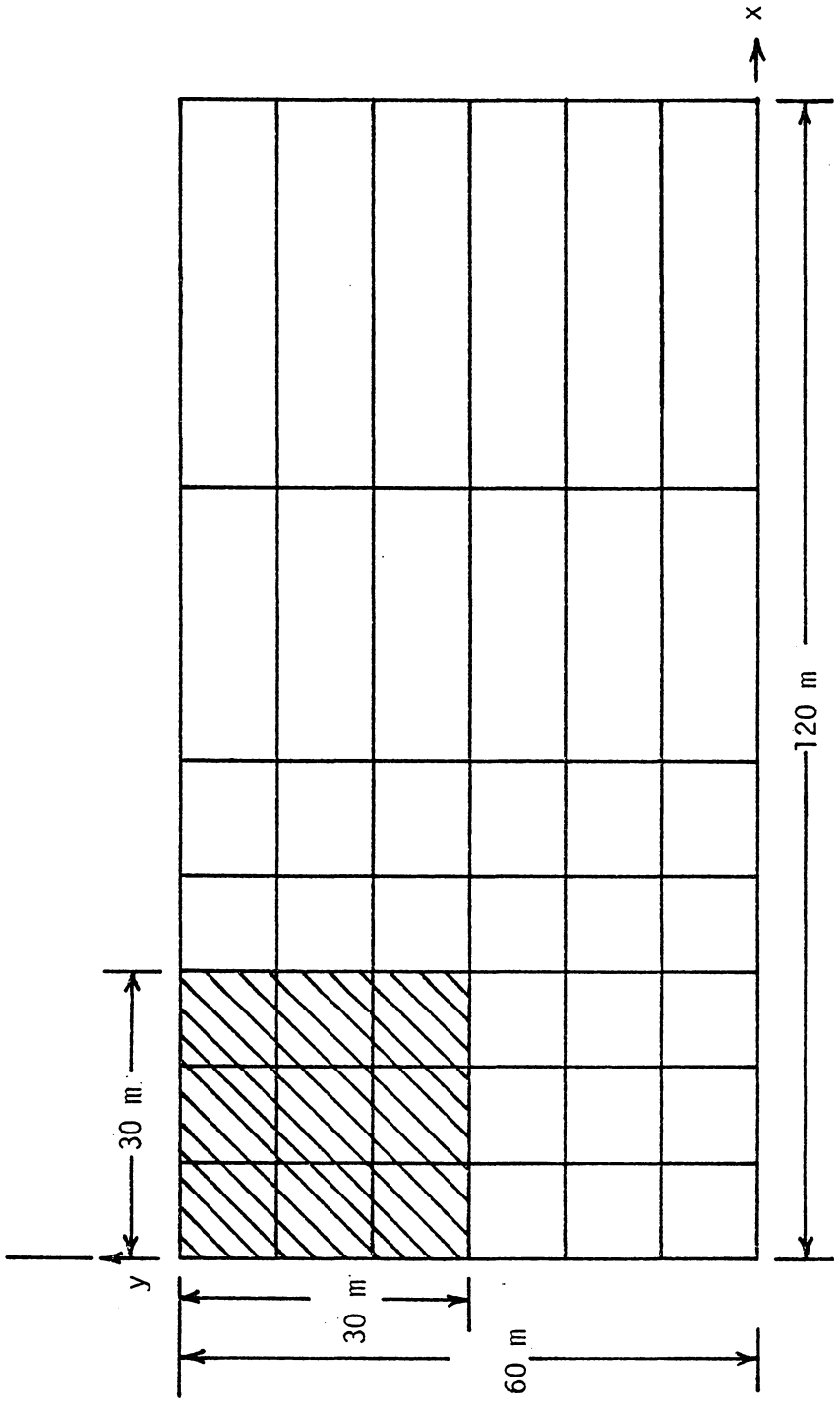

Figure 5.2 Finite Element Mesh for Excavation Problem

Table 5.1

Displacements of Selected Nodes (m)

Node Number	Node Coordinate		One Step		Three Steps	
	x	y	u	v	u	v
62	3.0	5.0	-0.014506	0.07740	-0.014506	0.00774
63	30.0	10.0	-0.025391	0.015189	-0.025391	0.015189
64	30.0	15.0	-0.033584	0.022581	-0.025391	0.022581
65	30.0	20.0	-0.039843	0.028103	-0.039843	0.02803
66	30.0	25.0	-0.042434	0.034489	-0.043434	0.034489
67	30.0	30.0	-0.047128	0.031933	-0.047128	0.031833
73	30.0	60.0	-0.062315	0.005897	-0.062315	0.005897
75	35.0	10.0	-0.024510	0.010460	-0.024510	0.010460
106	52.0	25.0	-0.036824	0.005958	-0.036824	0.005958
110	52.0	45.0	-0.053804	-0.001191	-0.053804	-0.001191
111	52.0	50.0	-0.054203	-0.004109	-0.054203	-0.004109

Table 5.2

Stresses at Selected Points (t/m^2)

Element Number	Point Coordinate		One Step			Three Steps		
	x	y	σ_x	σ_y	τ_{xy}	σ_x	σ_y	τ_{xy}
1	0.694	0.694	-77.9686	-61.6133	- 0.5339	-77.9686	-61.6133	- 0.5339
9	10.694	20.694	-57.7263	-18.9742	- 2.5814	-57.7263	-18.9742	- 2.5814
21	30.694	20.694	-58.4372	-54.4967	-16.3270	-58.4372	-54.4967	-16.3270
27	40.833	20.694	-57.2269	-64.7646	- 6.9043	-57.2269	-64.7646	- 6.9043
35	53.944	40.694	-19.0717	-35.3368	- 2.8935	-19.0717	-35.3368	- 2.8935
42	82.777	50.694	- 6.6134	-16.7099	- 0.4229	- 6.6134	-16.7099	- 0.4229

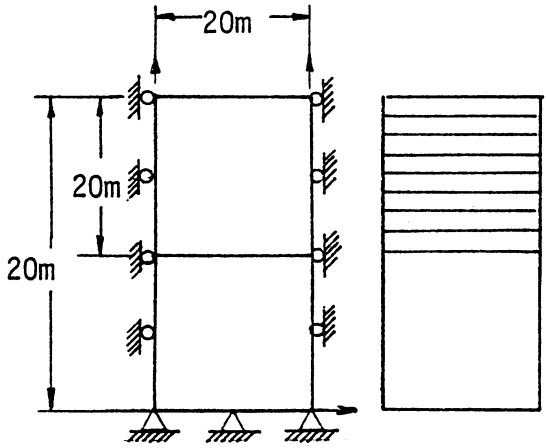

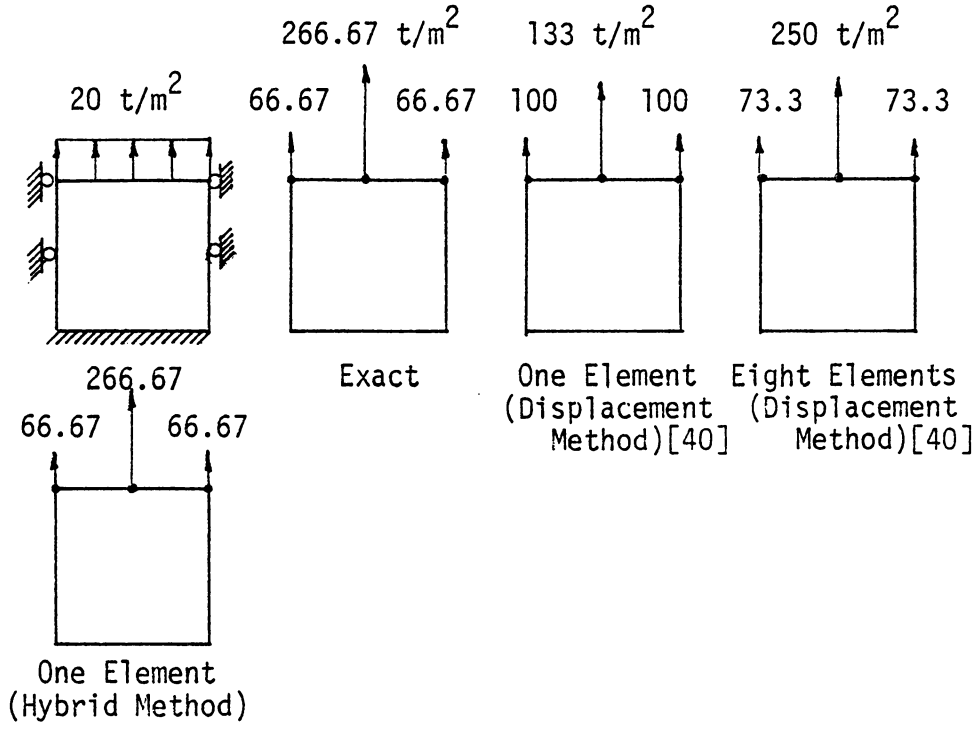

Figure 5.3 One-Dimensional Excavation

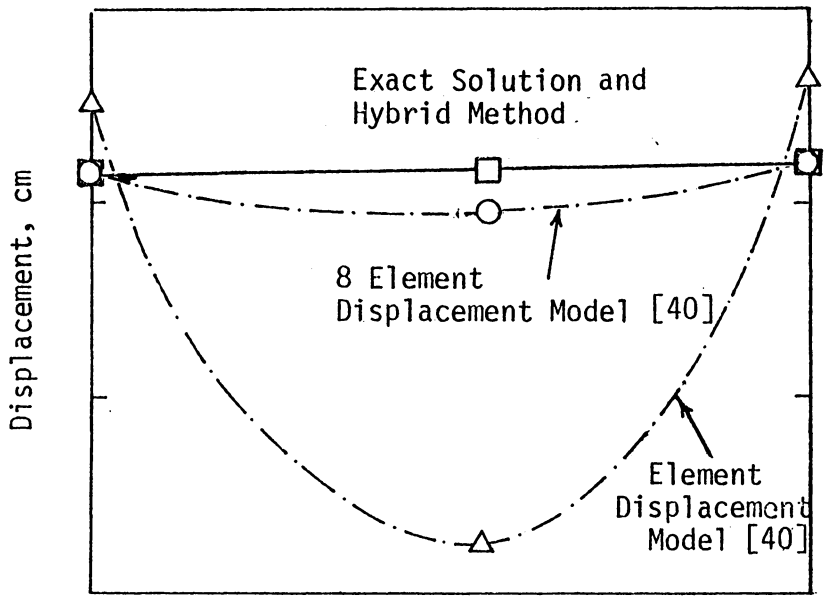

Figure 5.4 Comparison of Displacement for 1D Excavation
(Surface of Excavation)

CHAPTER 6

FIELD PROBLEMS

6.1 Introduction

In this chapter, two practical problems are solved to verify the proposed hybrid procedure for simulation of excavation. The problems are: 1) braced excavation in soft clay, and 2) excavation in a tunnel. The predictions from the present study are compared with the field observations and with those obtained by employing the displacement method. The material properties and the details of the field problems are adopted from other investigators [40,45].

6.2 Braced Excavation in Soft Clay

In this section, the proposed procedure is applied to a case of braced excavation in soft clay. The excavation site and a profile of soil is illustrated in Fig. (6.1). This is a test section (Vaterland 1) on the Oslo subway system which was instrumented and the field data were reported by the Norwegion Geotechnical Institute (1966). A finite element analysis of this case using the displacement method was reported by Mana [40].

The results from the present analysis are compared with those from Ref. [40] and the field observations. For a consistent comparison the same material properties [40] Table (6.1) are used, but in this study a much coarser finite element mesh is employed, Fig. (6.2).

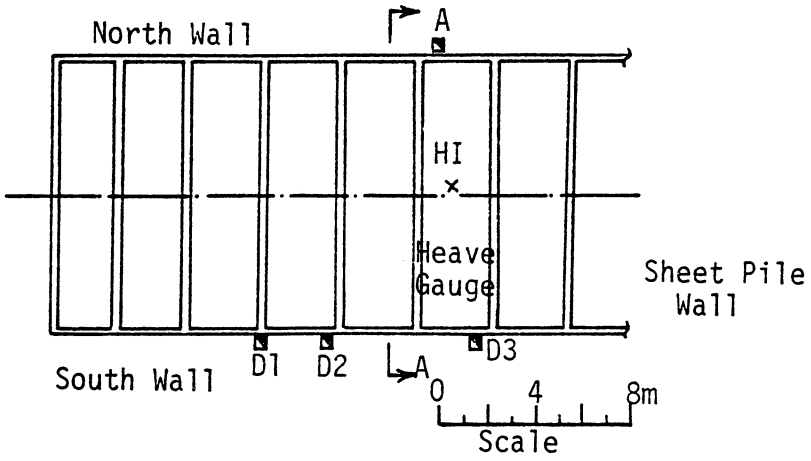

Plan View

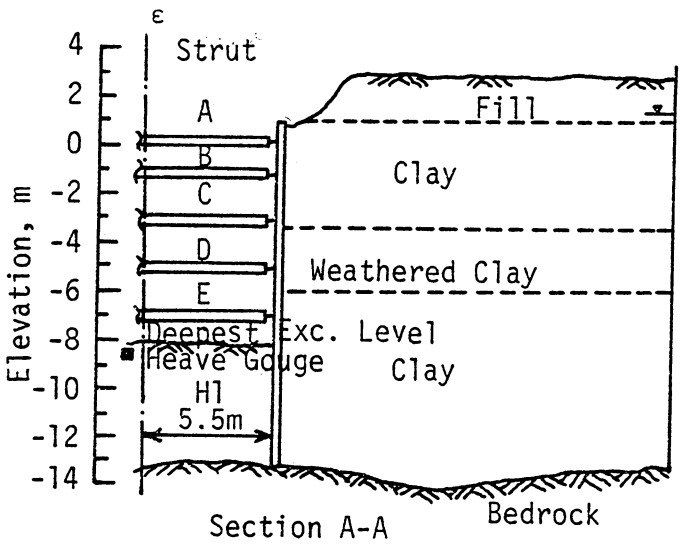

Section A-A

Figure 6.1 Vaterland 1, Site and the Soil Profile [40]

Table 6.1

Soil Properties

Material Number	E (t/m^2)	ν	C (t/m^2)	ϕ	γ (t/m^3)	K_o
1	560.0	0.4933	2.80	0	1.95	0.65
2	500.0	0.4933	2.50	0	1.95	0.65
3	620.0	0.4933	3.10	0	1.95	0.65
4	320.0	0.4967	3.20	0	1.95	0.65
5	220.0	0.4967	2.20	0	1.95	0.65
6	368.0	0.30	1.42	0	1.95	0.65

Wall properties $E = 2.76 \times 10^6 t/m^2$ $\nu = 0.33$

Interface Properties $E = 450.0\ t/m^2$ $\nu = 0.33$ $G = 10.0\ t/m^2$

Struts Properties A,D $K_n = 1600.0\ t/m/m$

B,C,E $K_n = 800.0\ t/m/m$

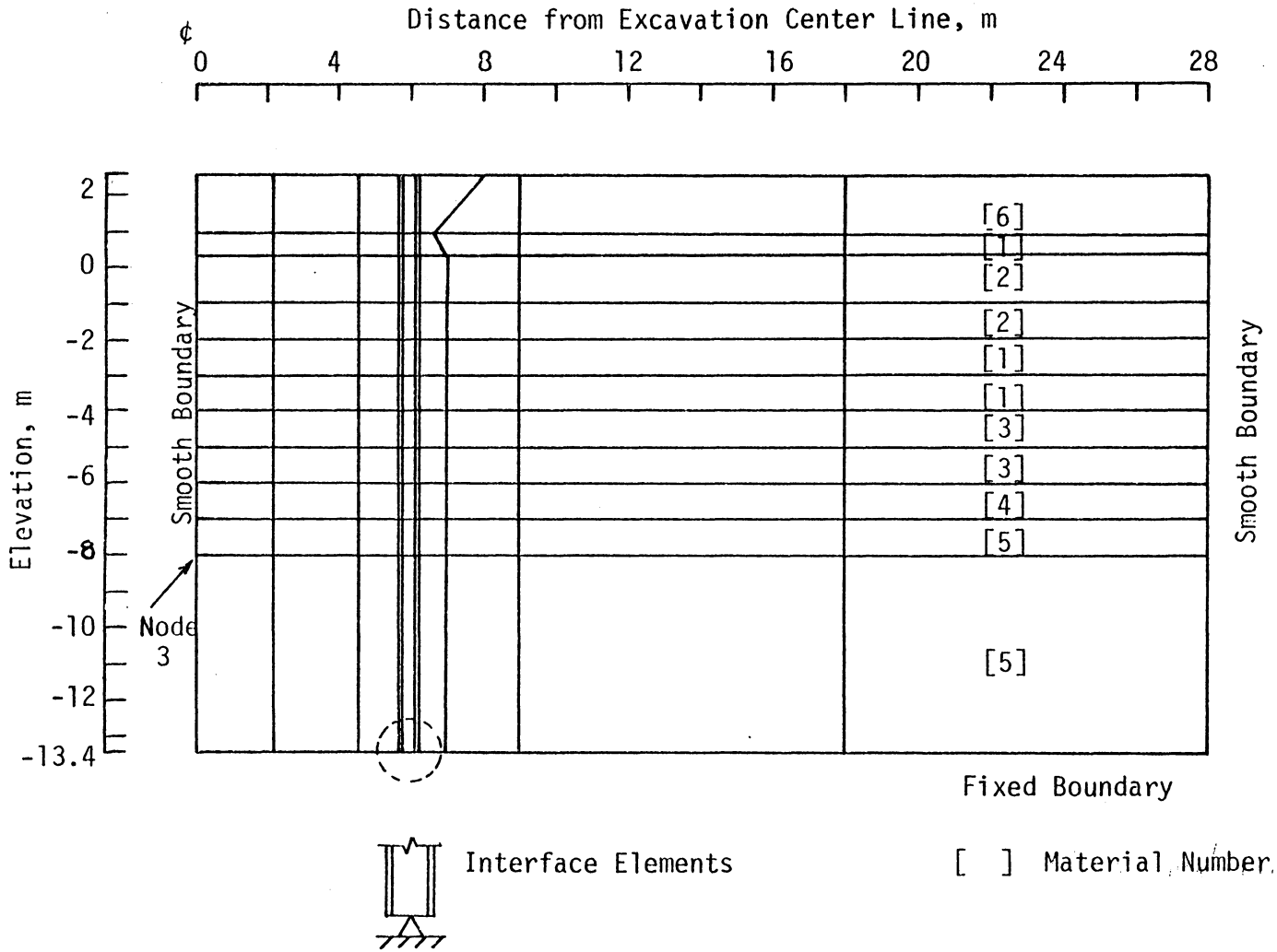

Figure 6.2 Finite Element Model for Vaterland 1 Excavation

The soil behavior is simulated as elastic-plastic by employing the Drucker-Prager model. The sheet pile is assumed to behave as linear elastic throughout the analysis. Interface elements are used where the soil is in contact with the sheet pile. Since the contact surface is assumed to be smooth, a small value for shear modulus for the interface elements is assigned, Table (6.1). One dimensional bar elements are used to simulate the structures. It has been assumed that the interface elements and the bar elements behave as linear elasticity during the analysis.

Sequences of Construction

In this investigation, the same order of construction sequences as in Ref. [40] is followed. In the first stage, the insitu stresses are computed using linear elastic properties of material, then the sheet pile elements are added and excavation is carried up to +0.2 m. The strut A is installed and then excavation is continued to -2.0 m in the second stage.

After the analysis is carried out up to the foregoing level, strut B is installed, and the excavation is carried up to elevation of -3.0 m, in the third stage. In the next stage of simulation, struct C is installed and excavation is carried up to -4.0 m. In the subsequent stage, only excavation is extended up to -5.0 m.

Similarly, in the sixth stage of operational sequences, the strut D is installed and the excavation is made up to an elevation of -6.0 m. Then, excavation is carried out up to a level of -7.0 m in

the following stage. In the next stage, being the last stage, struct E is installed and the excavation is carried up to -8.0 m.

Prediction and Analysis

In this section, only the behavior of sheet pile, soil, and strut is given for which the field observation is available [40].

Soil and Sheet Pile Deformation

Figure (6.3), (6.4), (6.5), and (6.6) show the sheet pile and the soil deformation in various stages of excavation. It has been demonstrated that the predicted results by the present model are relatively closer to the field observation than the displacement method [40]. In the second stage, the sheet pile deflection is overestimated and also the deformed shape of sheet pile is not similar to the field observation. This may be due to the incorrect simulation of the connection between the pile and bedrock which is laying under the soil deposits and the sheet pile was driven into it. It is interesting to point out that the settlement at the surface of the soil behind the sheet pile is almost the same as the observed data; this could be due to the use of improved interface elements in this study.

It should be mentioned that the finite element analysis is performed based on the assumption of undrained conditions. But most of the field measurements were taken after a period of time. During this time,the results may have been affected by such factors

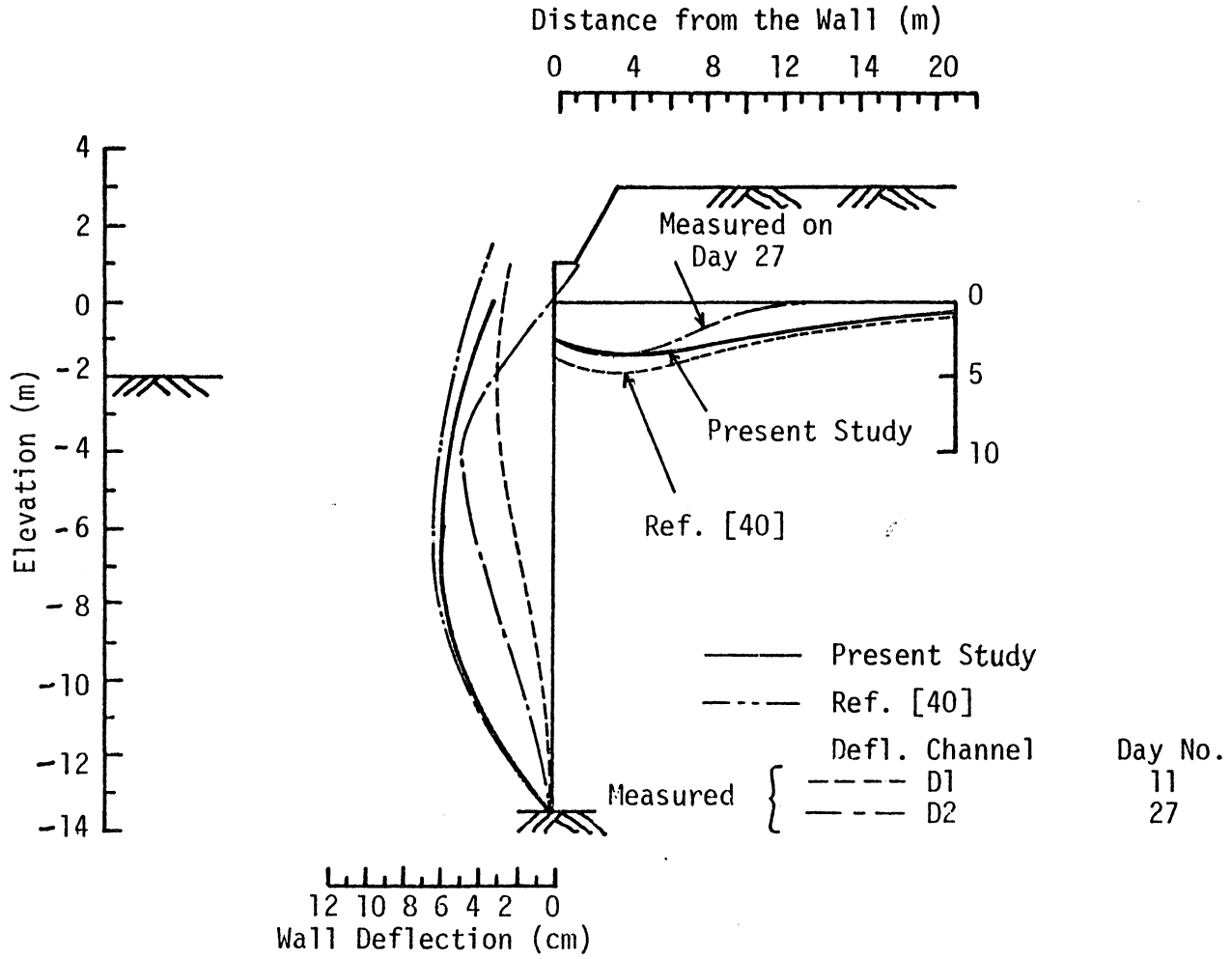

Figure 6.3 Wall and the Soil Deformation (Stage 2)

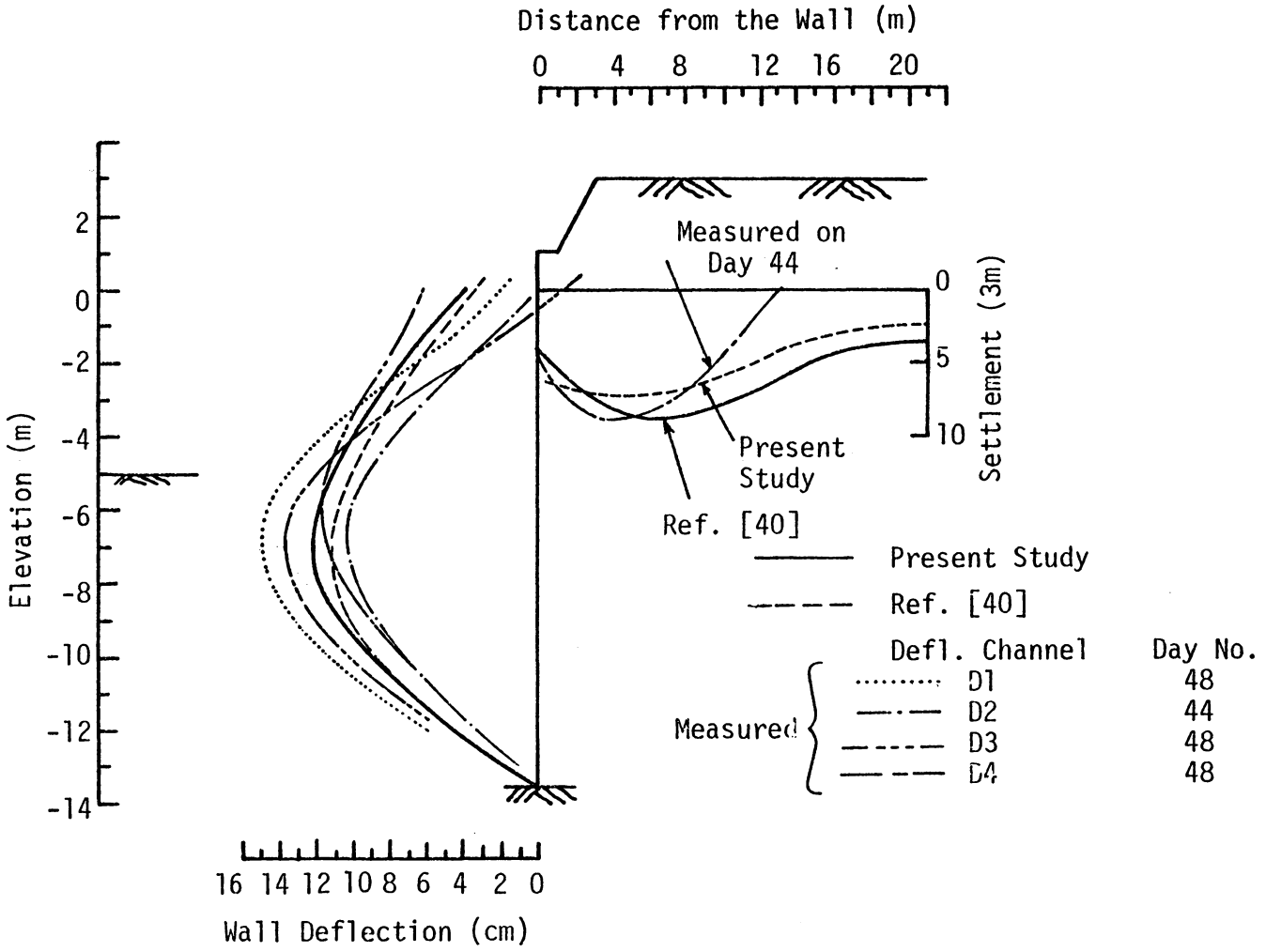

Figure 6.4 Wall and the Soil Deformation (Stage 5)

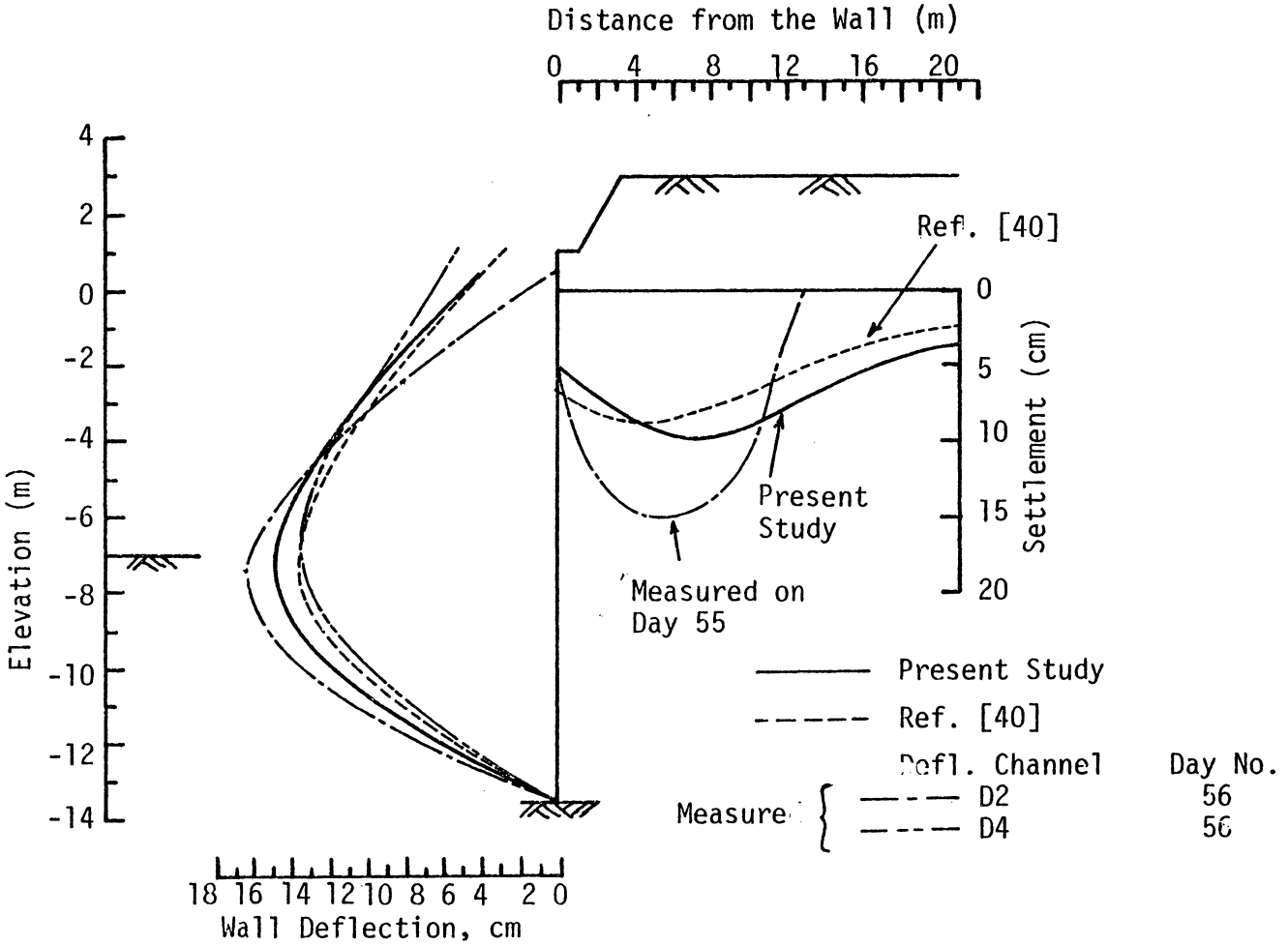

Figure 6.5 Wall and Soil Deformation (Stage 7)

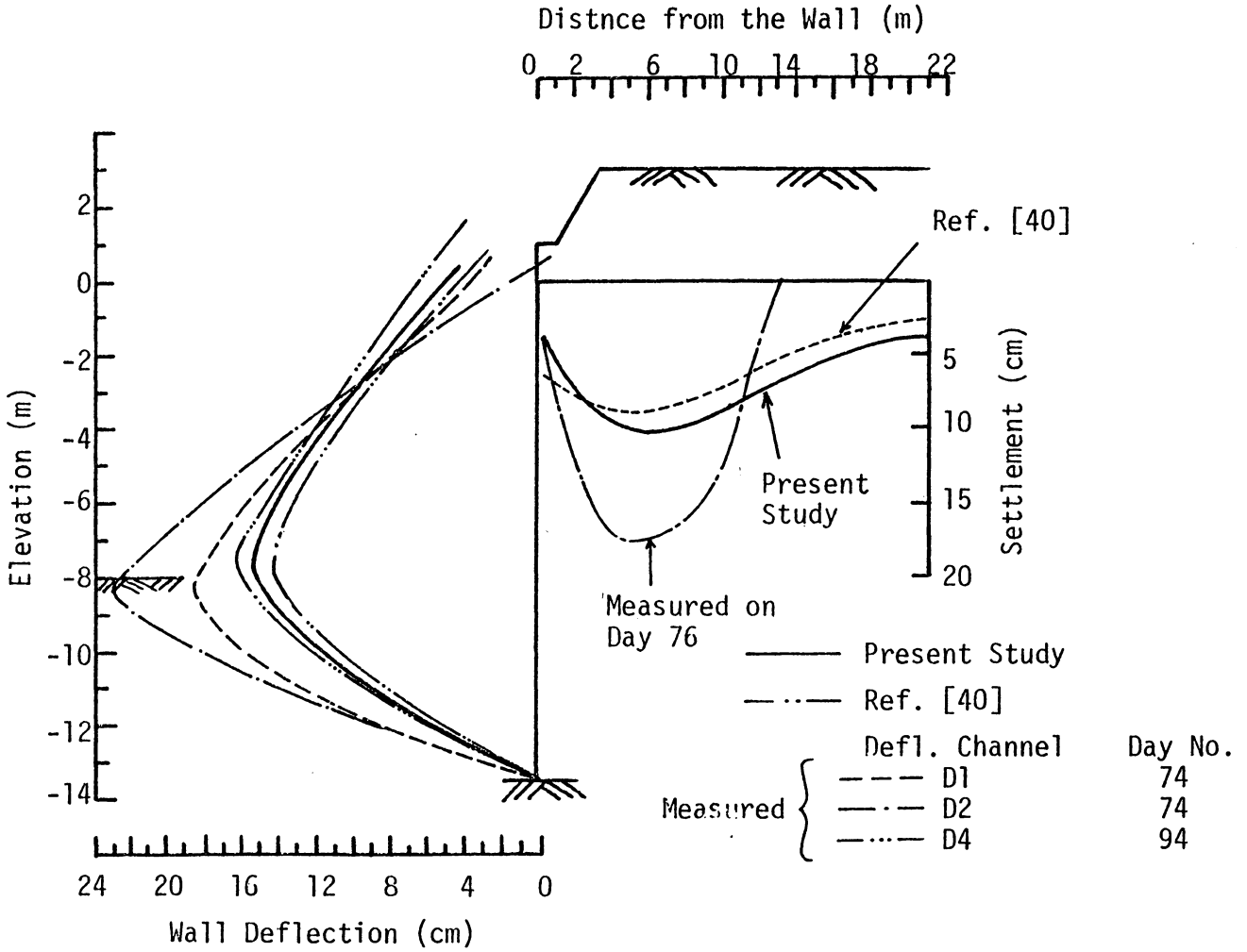

Figure 6.6 Wall and Soil Deformation (Stage 8)

as consolidation and creep and also the strength of clay adjacent to the excavated surface may decrease with time [44]. This could be the reason for underestimation of the deformation of sheet pile and of the soil. Figure (6.7) shows the maximum sheet pile deflection in each stage of excavation level.

The settlement of the soil at elevation +0.2 m is shown in Fig. (6.8). Figure (6.9) shows the heave of the soil at node number 3 (see Fig. (6.2). The current model yields improved predictions compared to the displacement model. This is due to the fact that the hybrid stress model predicts the stress distribution with greater accuracy on the surface of excavation. This phenomenon has been illustrated in the previous chapter.

Strut Load

The axial force in each strut is shown in Figs (6.10) and (6.11). The results using the present model show slight improvement compared to the displacement method. The total axial force of the struts in each stage of excavation is illustrated in Fig. (6.12). The computed values by using the finite element method seems to be within the range of the observed values.

Earth Pressure

In the past, the earth pressures are reported based on horizontal stresses in the elements adjacent to the wall. The earth pressure computations at the interface element are usually so reported because

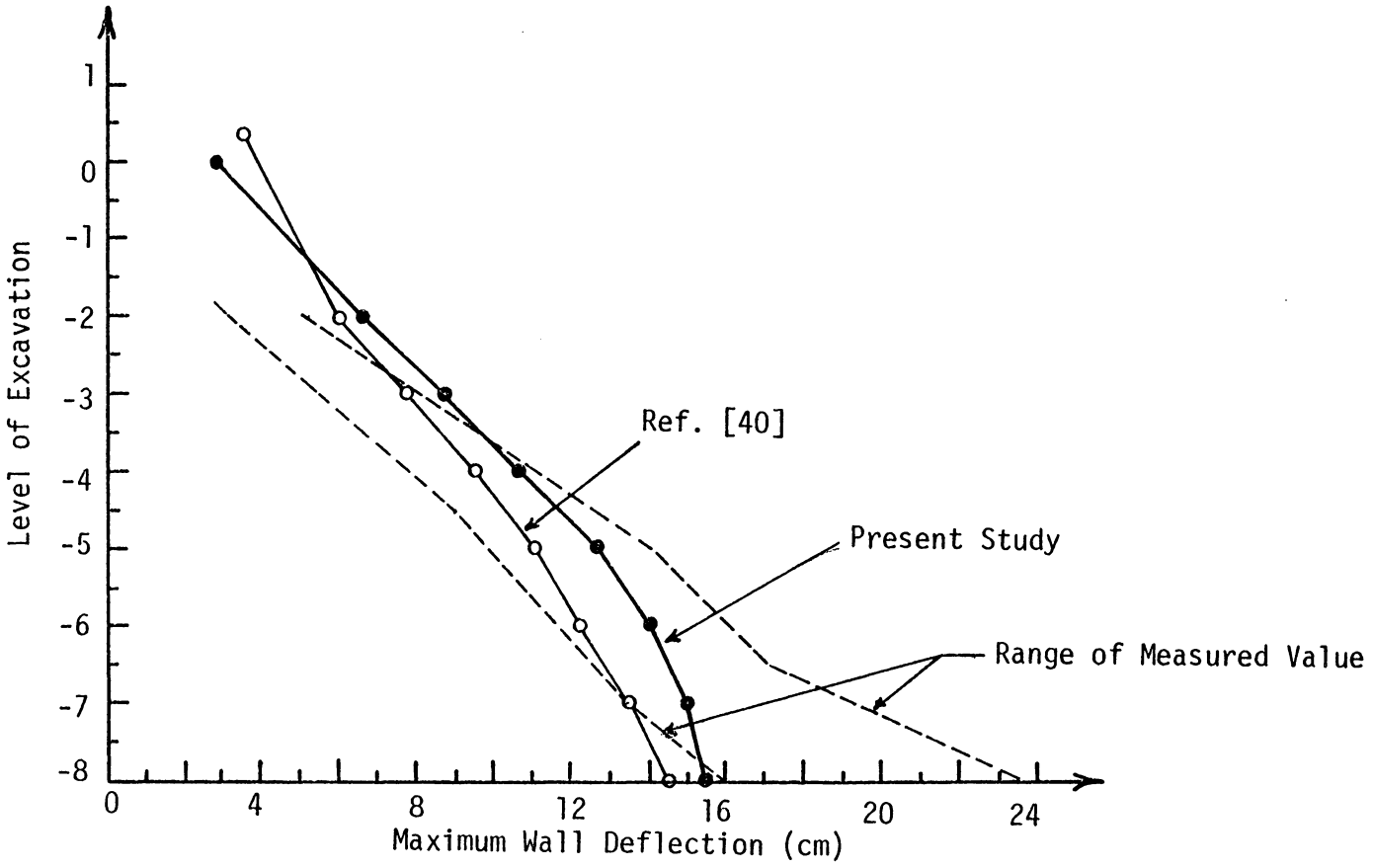

Figure 6.7 Wall Deflection

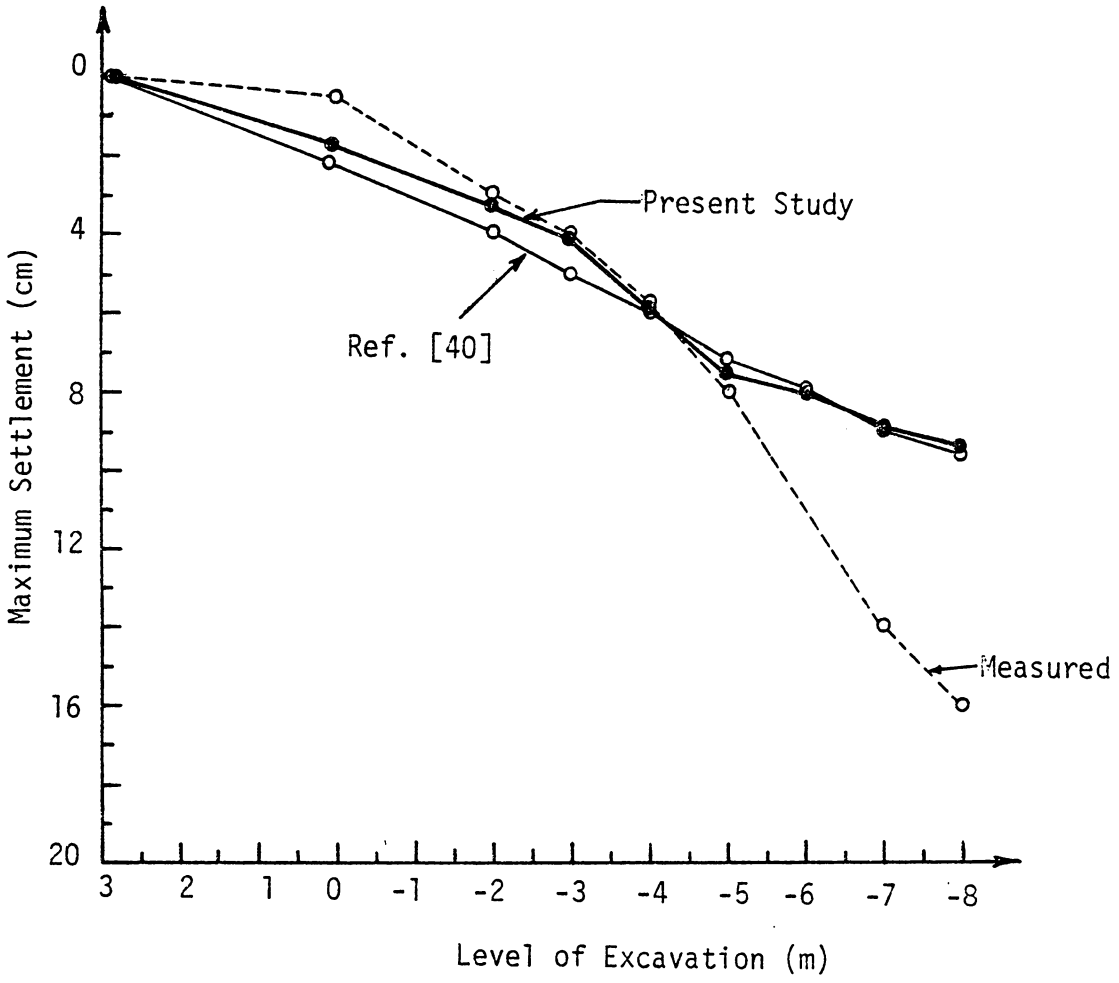

Figure 6.8 Settlement at Elevation +0.2 m

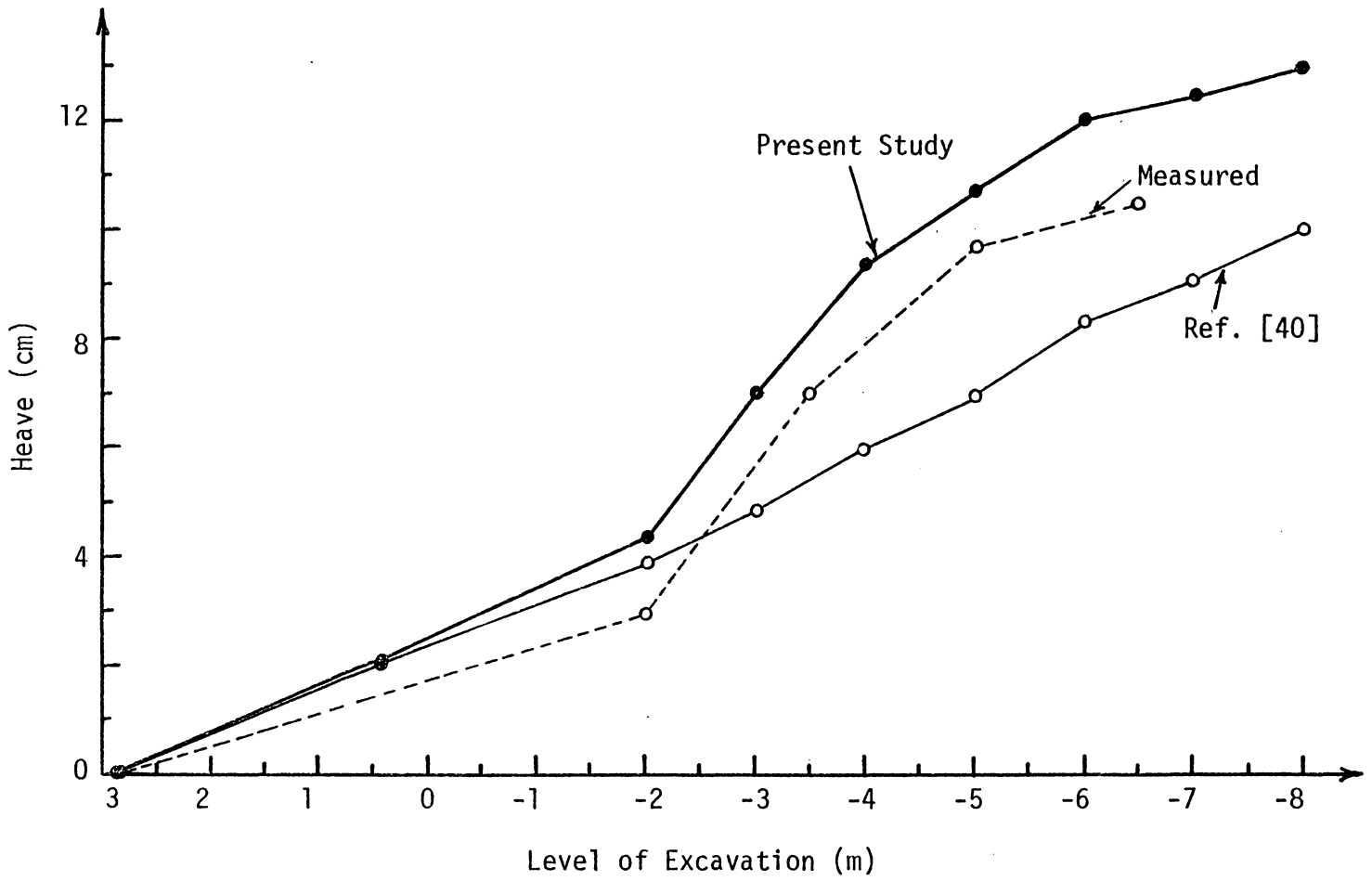

Figure 6.9 Heave at Node 3

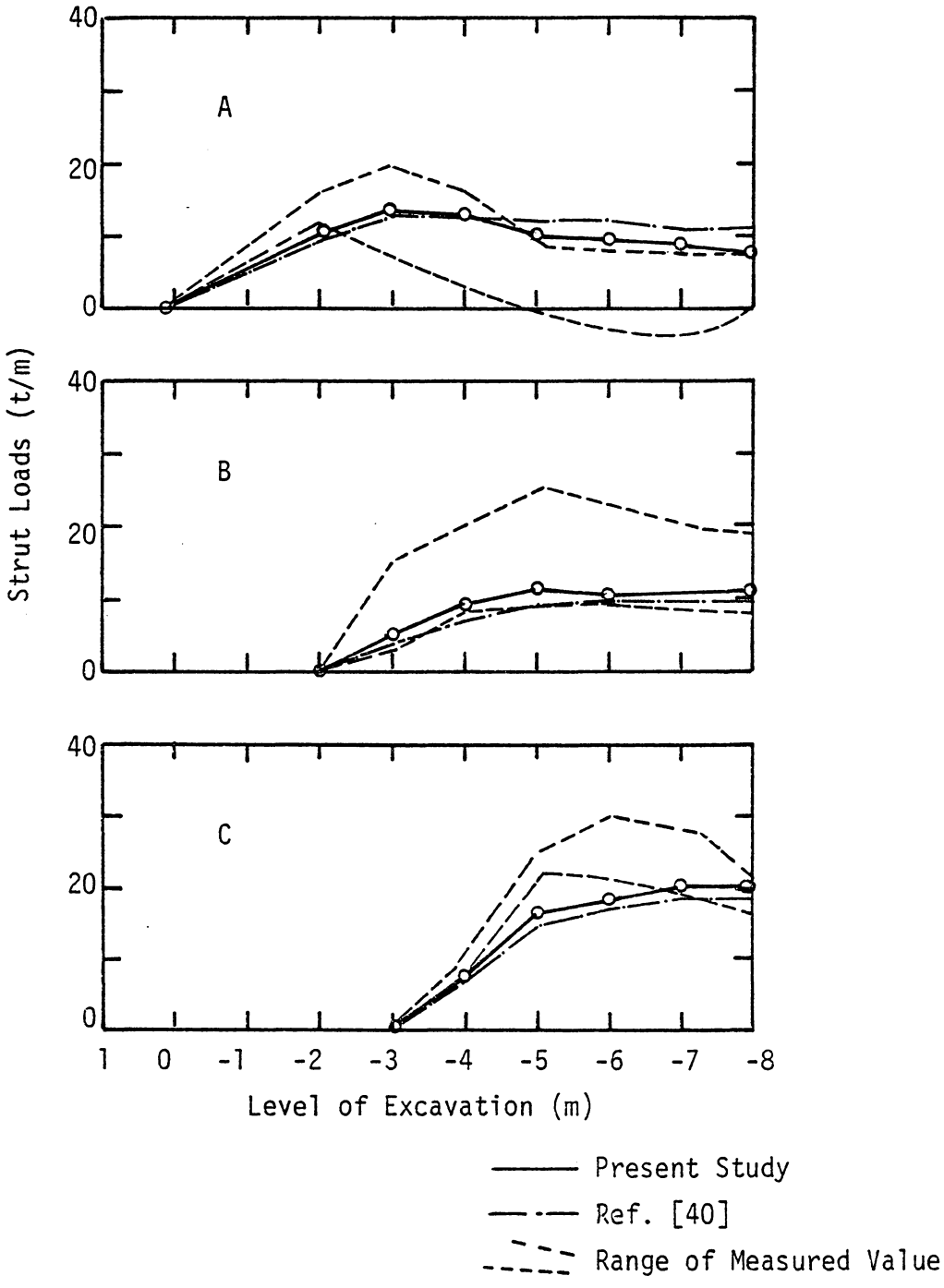

Figure 6.10 Strut Loads

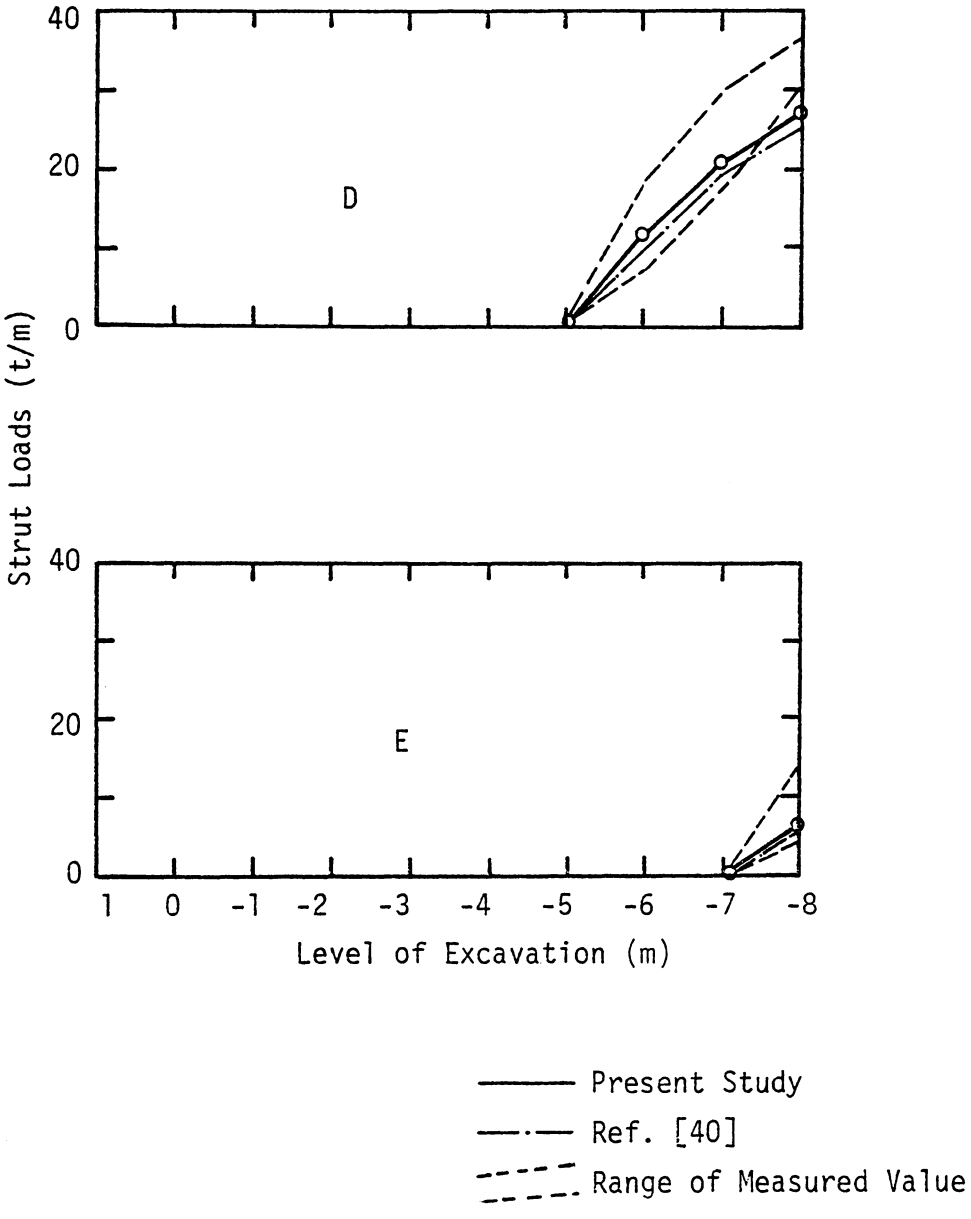

Figure 6.11 Strut Loads

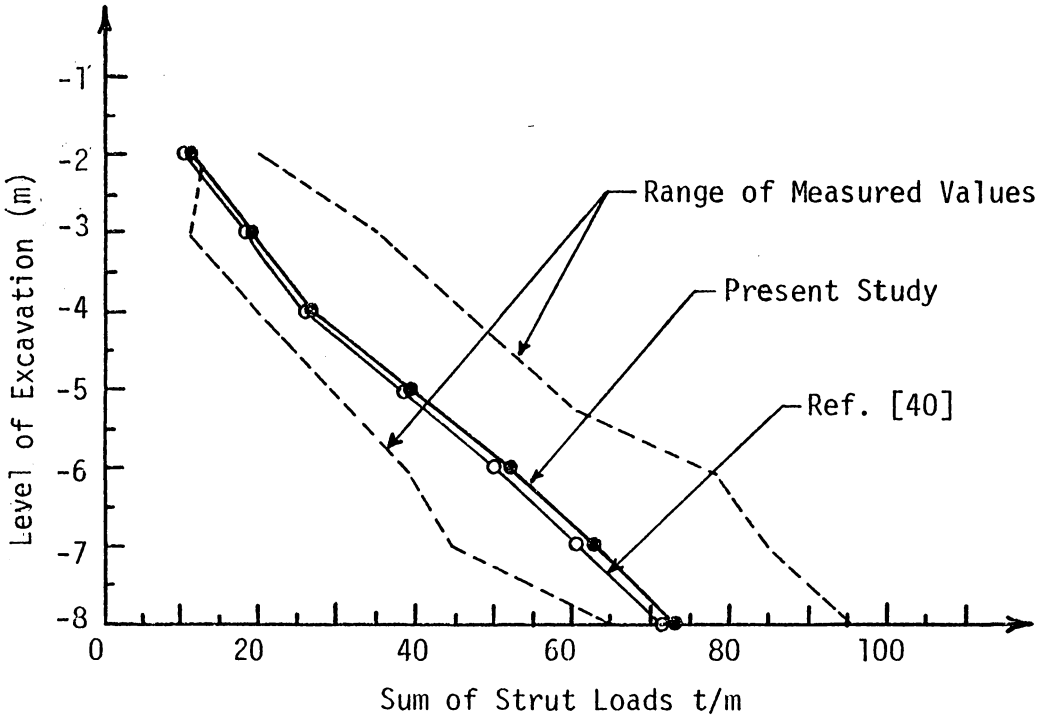

Figure 6.12 Measured and Computed Sum of Strut Loads

the conventional interface element often shows instability, particularly for flexible walls. In this investigation, modified interface elements are used and the earth pressure in these elements are computed in addition to those in the element adjacent to the wall. It is observed that there is nonuniformity in earth pressure distribution within interface elements as shown in Figs. (6.13) and (6.14). When the average earth pressure is computed for each interface element and plotted along with the pressure observed, it has been seen that both the earth pressures at adjacent elements and interface elements are close to each other and they have good correlation with the field observed data as illustrated in Figs. (6.15) to (6.18). It may be noted that with the conventional interface elements it is difficult to obtain even such nonuniform distribution. Hence, the results in Fig. (6.13) and (6.14) are considered to be an improvement although additional research will be needed for further improvements.

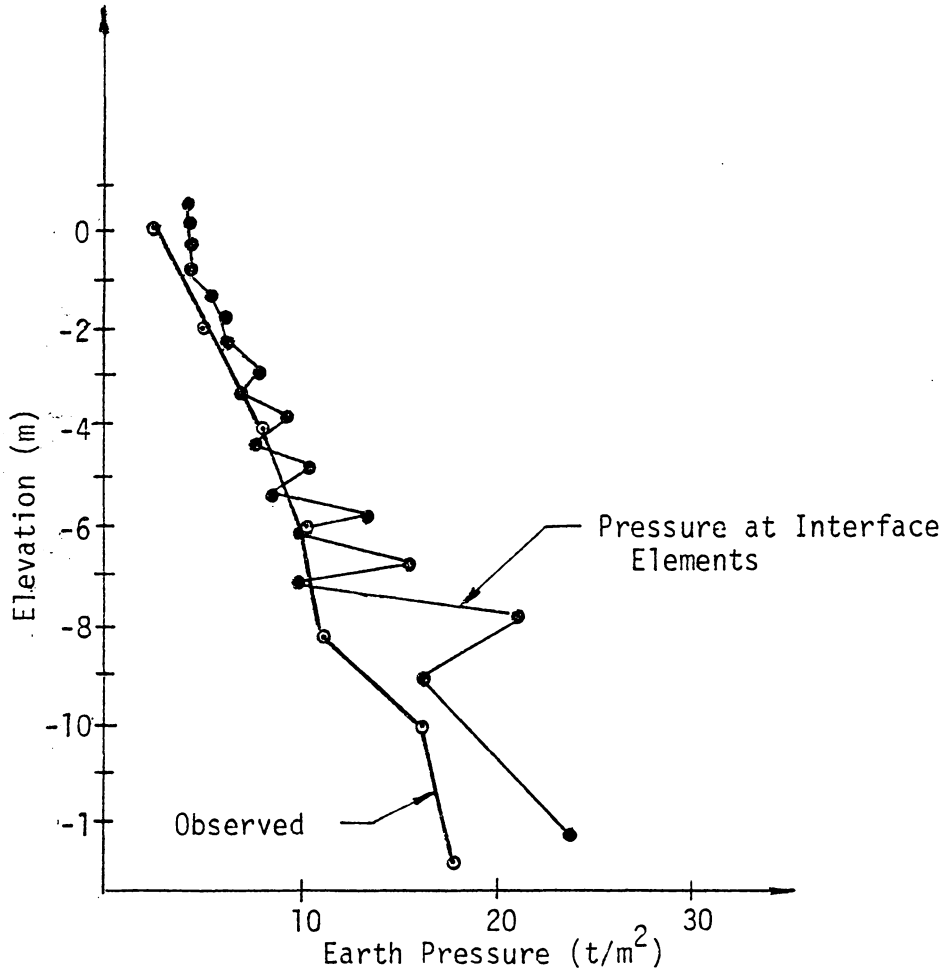

Figure 6.13 Earth Pressure (Stage 2)

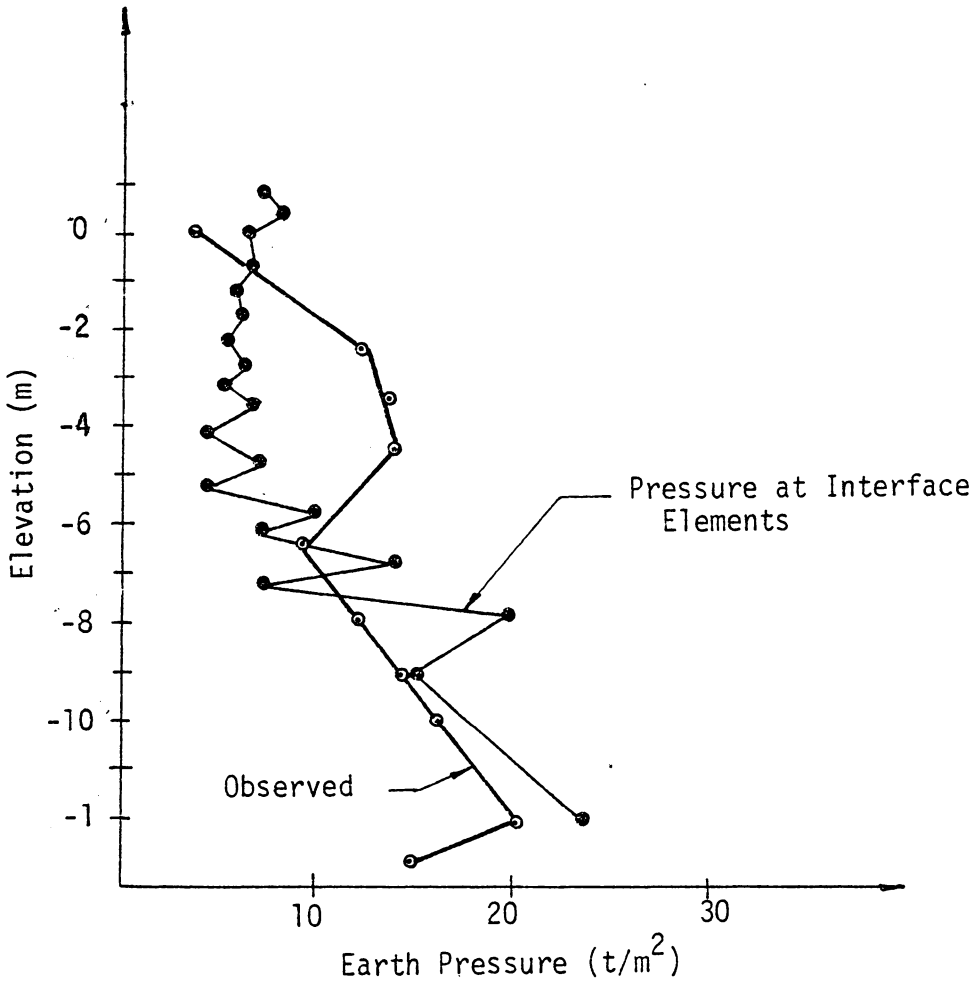

Figure 6.14 Earth Pressure (Stage 5)

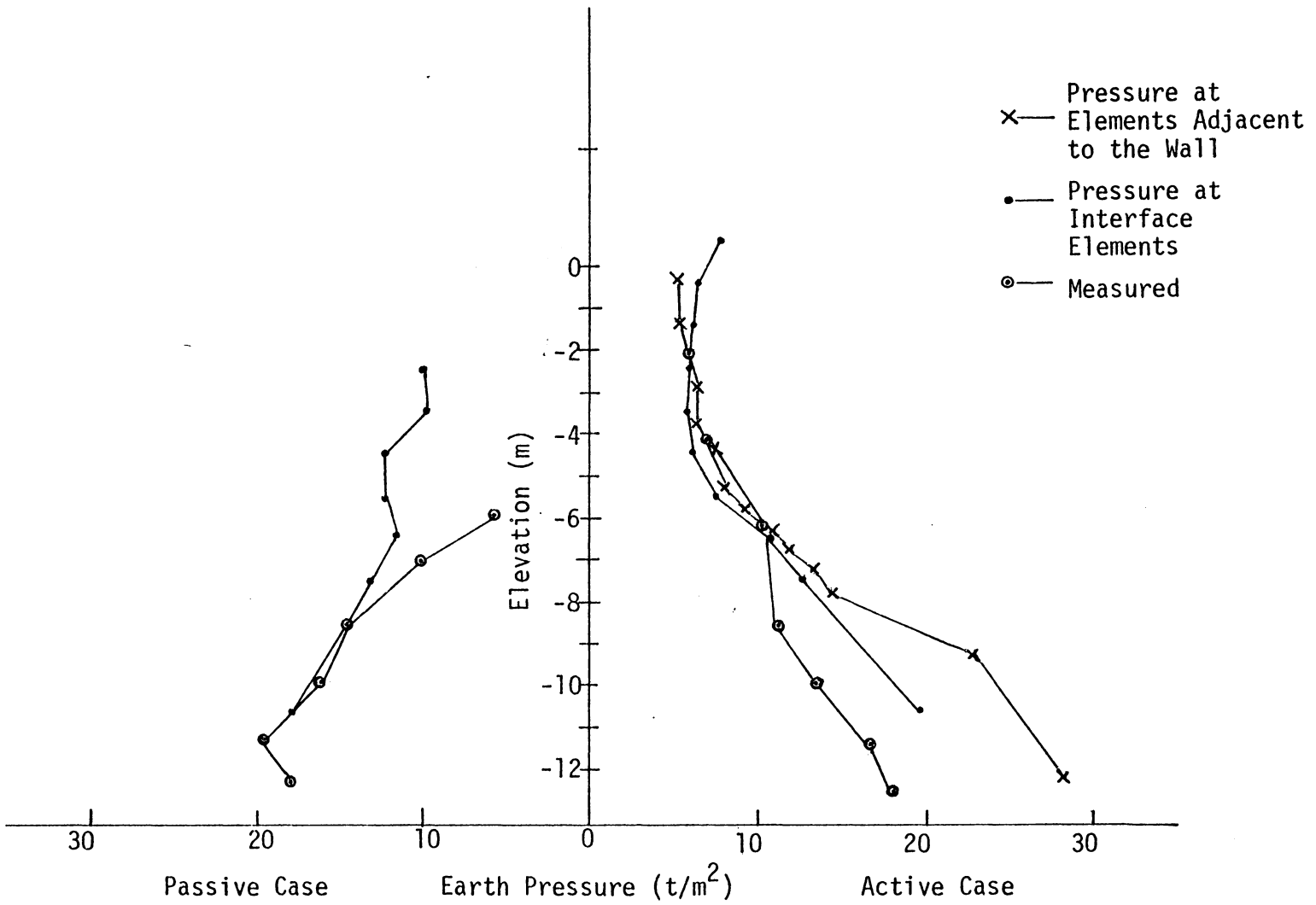

Figure 6.15 Earth Pressure (Stage 2)

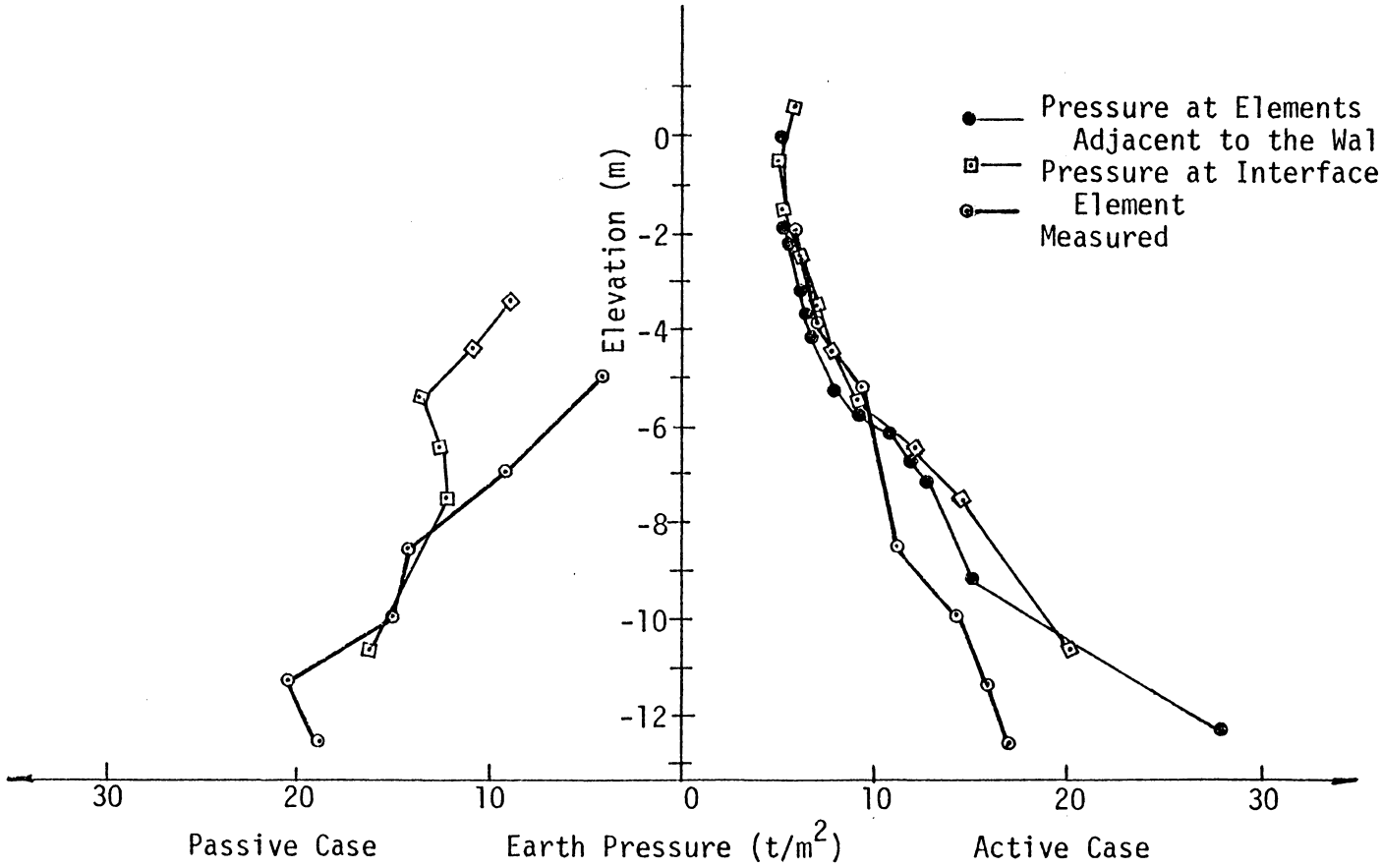

Figure 6.16 Earth Pressure (Stage 3)

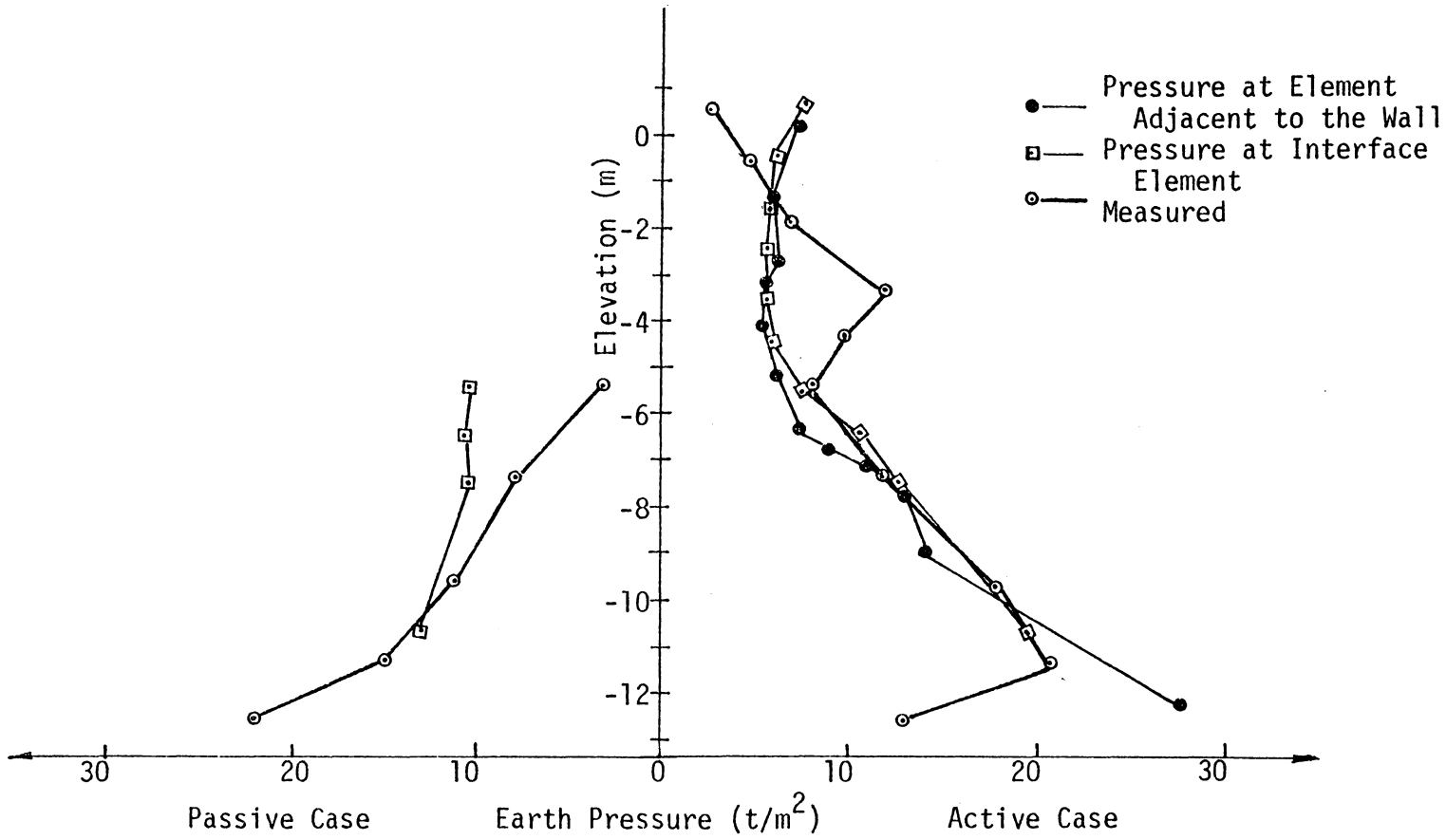

Figure 6.17 Earth Pressure (Stage 5)

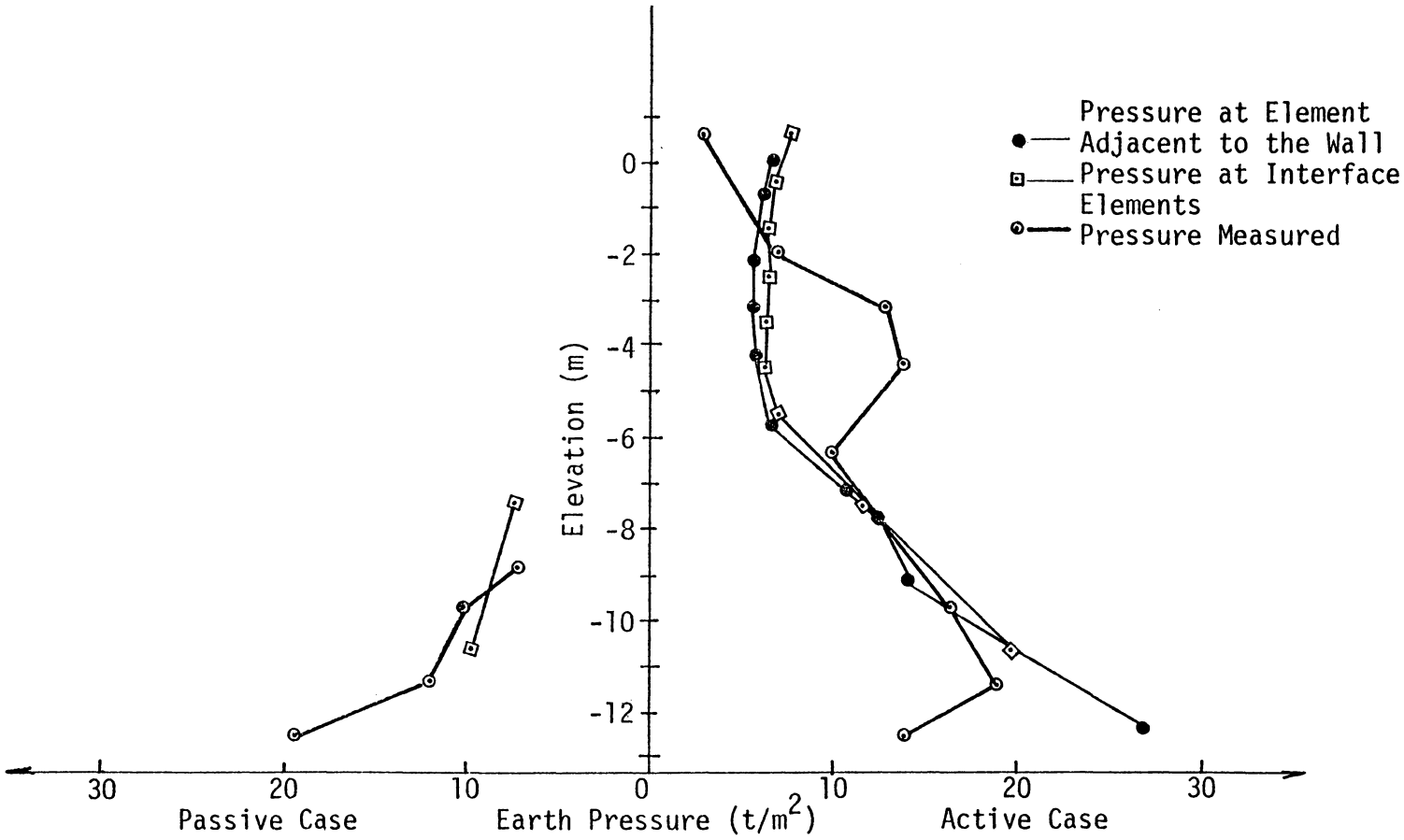

Figure 6.18 Earth Pressure (Stage 7)

6.3 Subway Tunnel

Here an attempt is made to analyze the twin running tunnels and the research chamber in hard rock at the MARTA Peachtree Center (Corn Street) station in Atlanta, Georgia. Finite element analyses using the displacement method were performed by Tudor Engineering Company [45] and Kulhawy [46].

This study is intended to make a comparison between the results from the hybrid stress model and from the displacement method and also perform a parametric study.

Figure (6.19) shows the section (near sta 20+52) which is used for analysis. Some material properties as Refs [45,46] are chosen in Table (6.2). The finite element mesh which is designed for this study is shown in Fig. (6.20).

In this analysis, the excavation sequence is adopted from Ref. [45] and is shown in Fig. (6.21). The problem is solved using linear elastic properties, and it is assumed that the plane strain condition is applicable in this case. The linear elastic assumption is made because the material, granite-gneiss, under the loading-unloading behaves essentially as linear elastic.

Analysis

First the tunnel problem is solved by the hybrid stress model employing eight node isoparametric elements, then using the same finite element mesh and material properties (reduced modulus) the tunnel is analyzed by using the eight-node isoparametric elements

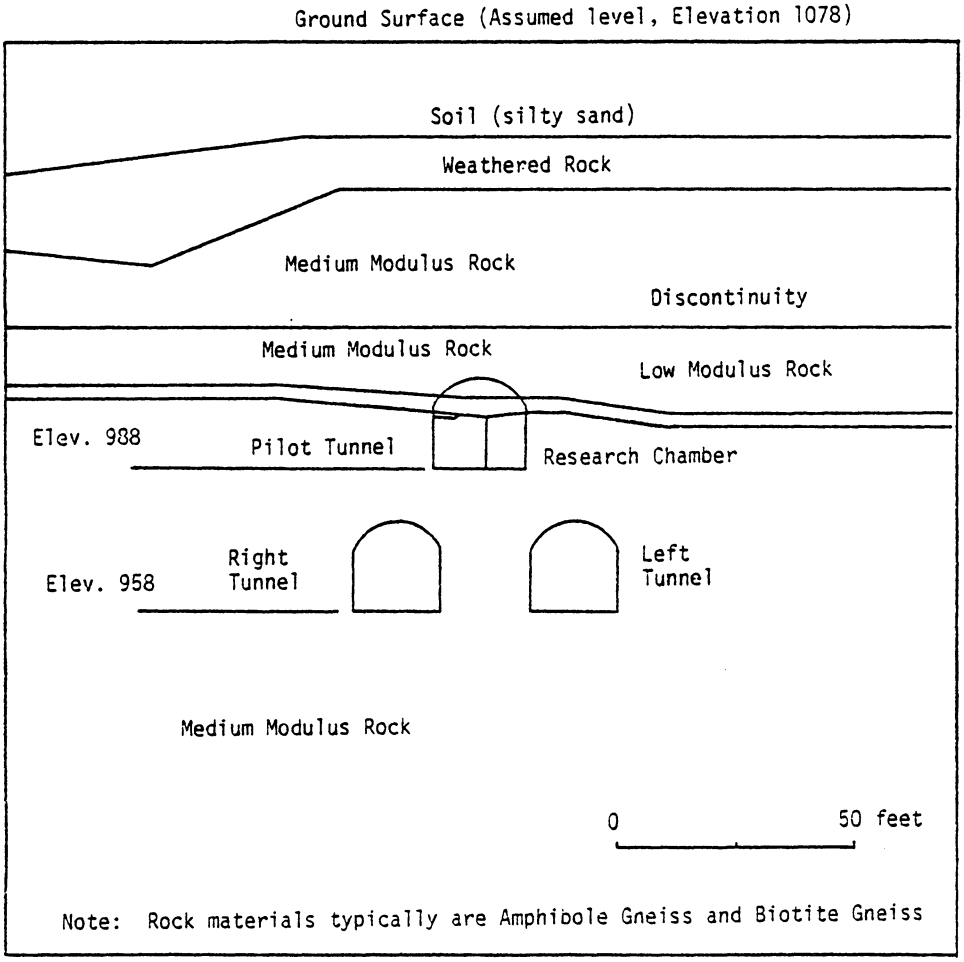

Figure 6.19 Generalized Geologic Section for Analysis, Looking South [45]

Table 6.2

Properties Used in Analyses [45]
(K_o=1.0)

	Unit Weight (pcf)	Intact Modulus	Reduced Modulus	Poisson's Ratio
Soil Overburden	105	5,880 psi (947 ksf)	5,880 psi (847 ksf)	0.40
Weathered Rock	162	1×10^6 psi (144,000 ksf)	0.15×10^6 psi (21,600 ksf)	0.14
Low Modulus Rock	180	3×10^6 psi (432,000 ksf)	0.45×10^6 psi (64,800 ksf)	0.10
Medium Modulus Rock	180	5×10^6 psi (720,000 ksf)	0.75×10^6 psi (108,000 ksf)	0.17
Discontinuity	Normal Stiffness = 31,830 ksf/ft Shear Stiffness = 6,366 ksf/ft			

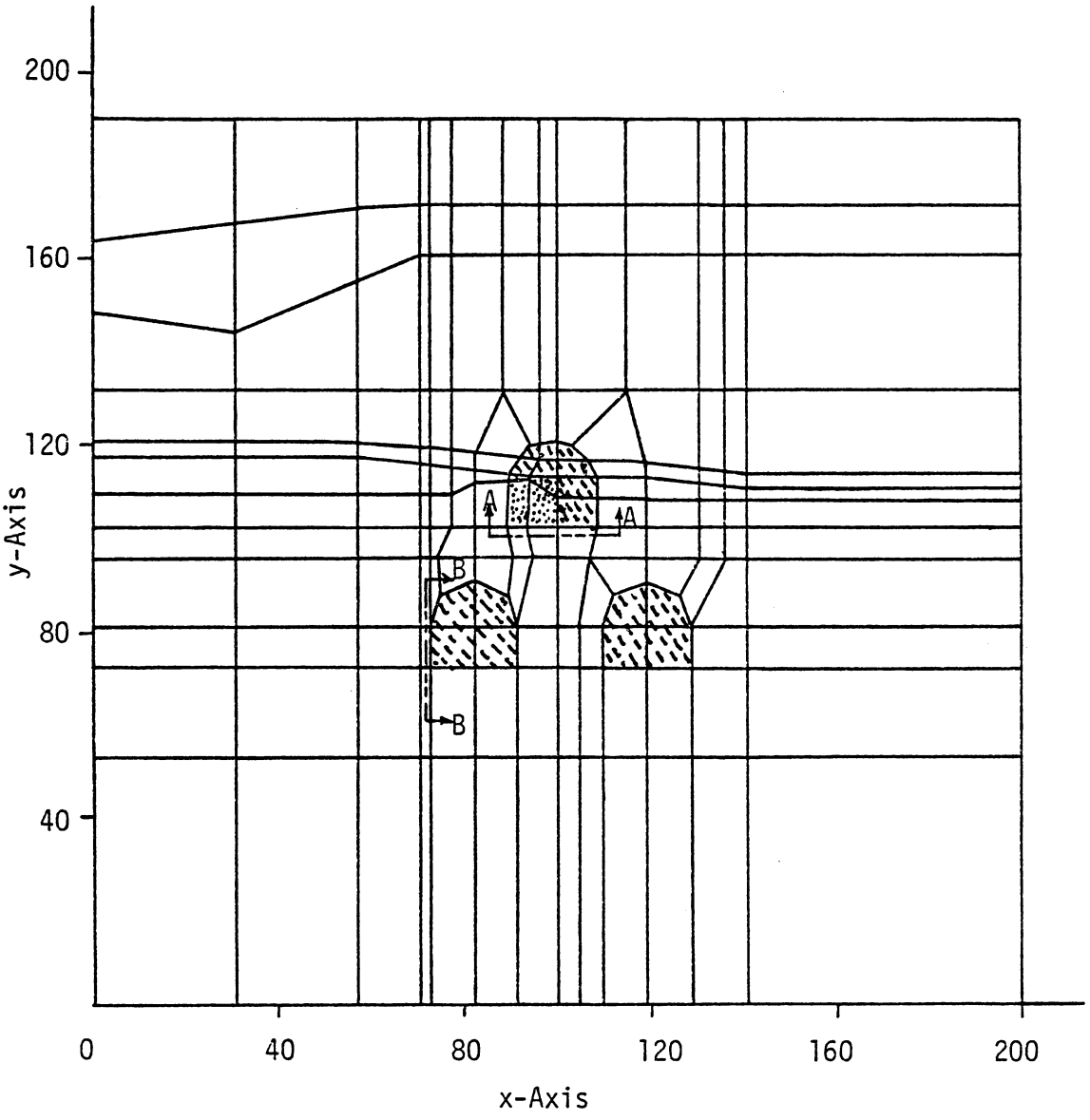

Figure 6.20 Finite Element Mesh

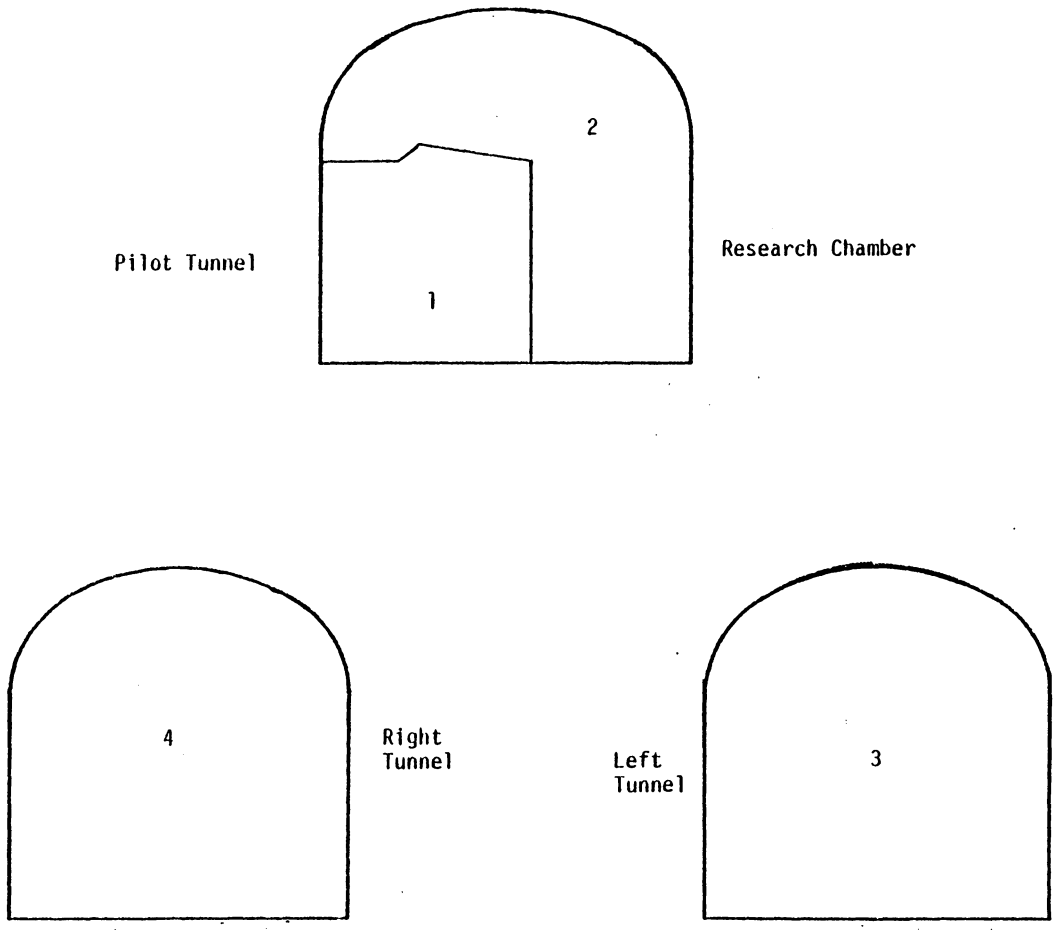

Figure 6.21 Sequence of Excavation [45]

based on the displacement method [41]. The values of computed displacements from the hybrid stress analysis for all the four stages of excavation are shown in Figs. (6.22) to (6.25). There is a slight difference between the values of displacement which are obtained by the hybrid stress model and by the displacement method in the first and second stages of excavation. But there are greater difference in the values of the displacement on the surface of left and right tunnels, Table (6.3).

The principal stresses σ_1 and σ_3 at Section A-A and B-B (see Fig. (6.20)) for the first and third stages of excavation as shown in Figs. (6.26) to (6.33). It can be seen that the hybrid model predicts higher values for the stresses near the corners.

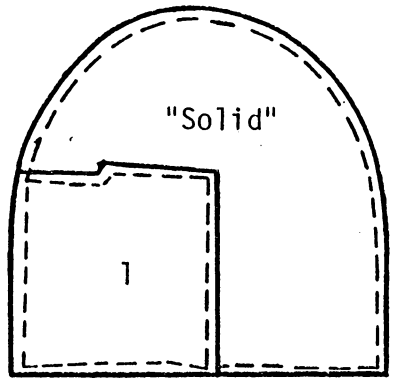

Scale

1 in = 2.54×10^{-2} ft

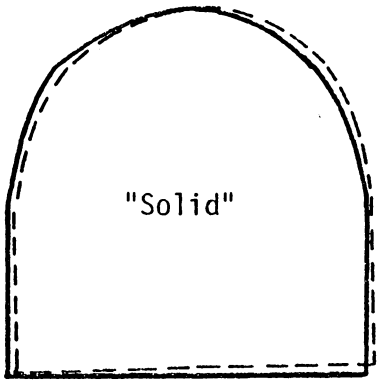

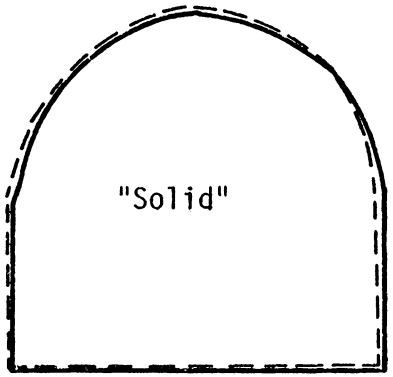

Figure 6.22 Displacement Patterns Step 1

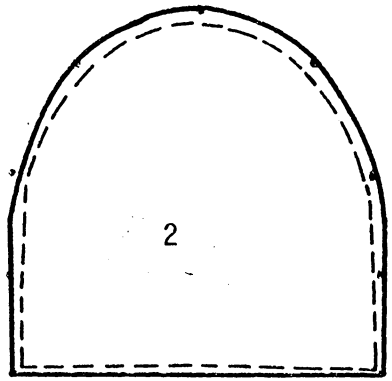

Scale

$1" = 2.54 \times 10^{-2}$ ft

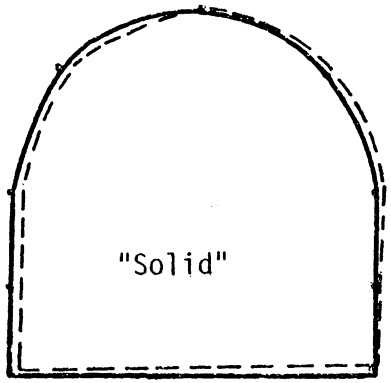

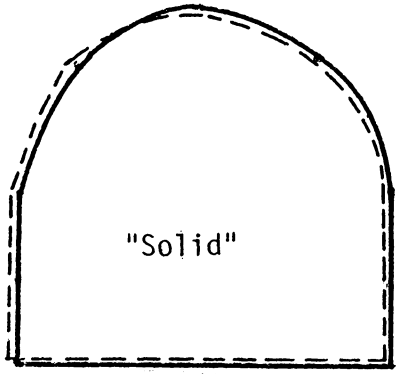

Figure 6.23 Displacement Patterns, Step 2

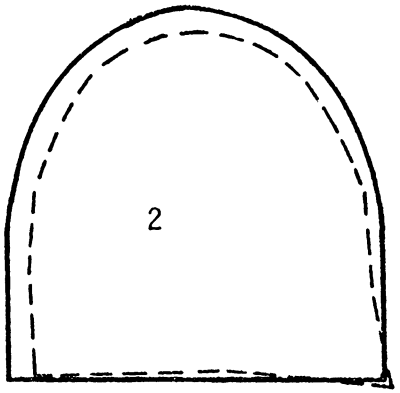

Scale
1 in = 2.54×10^{-2} ft

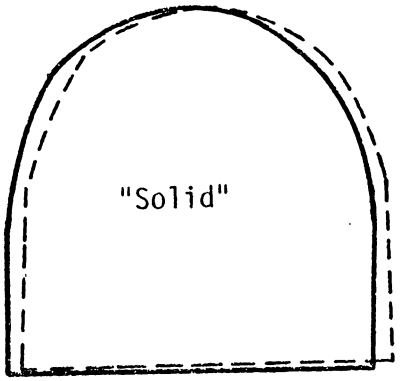

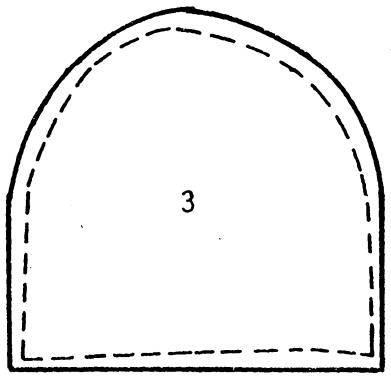

Figure 6.24 Displacement Patterns, Step 3

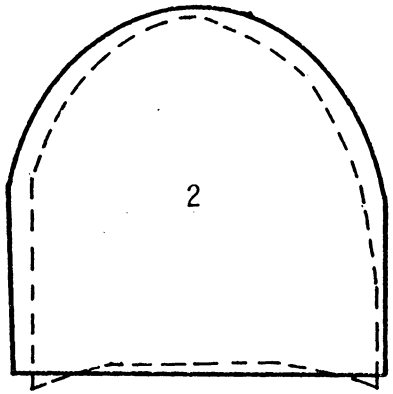

Scale
1 in = 2.54×10^{-2}

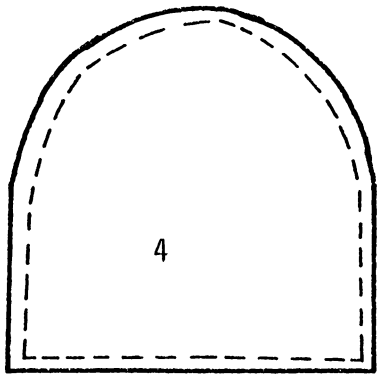

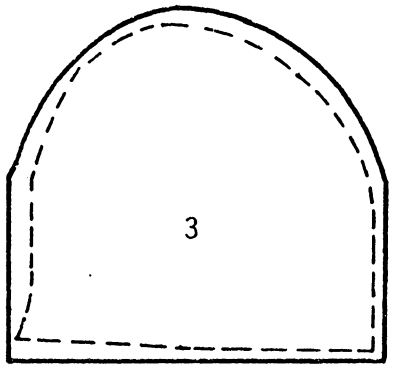

Figure 6.25 Displacement Patterns, Step 4

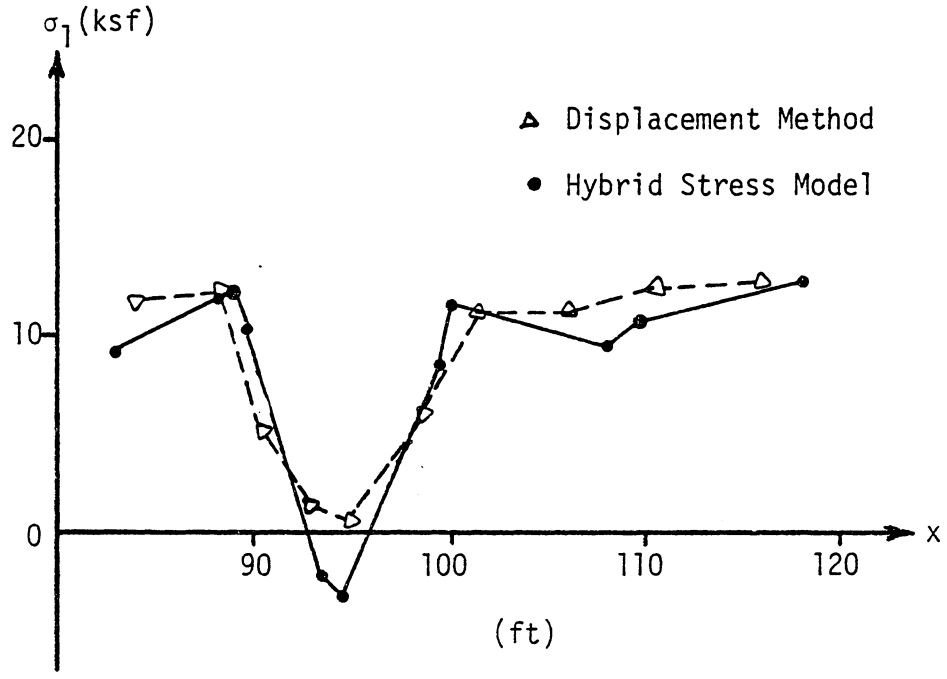

Figure 6.26 Comparison of Principal Stresses
(Step 1, Section A-A)

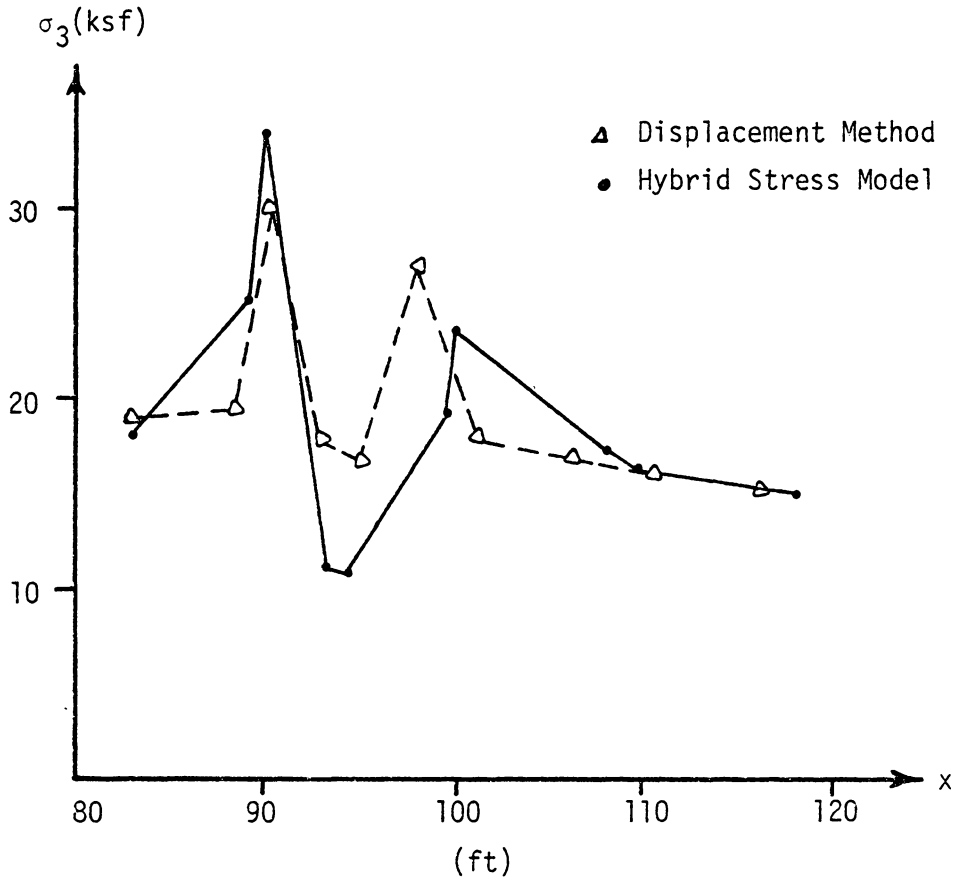

Figure 6.27 Comparison of Principal Stresses
(Step 1, Section A-A)

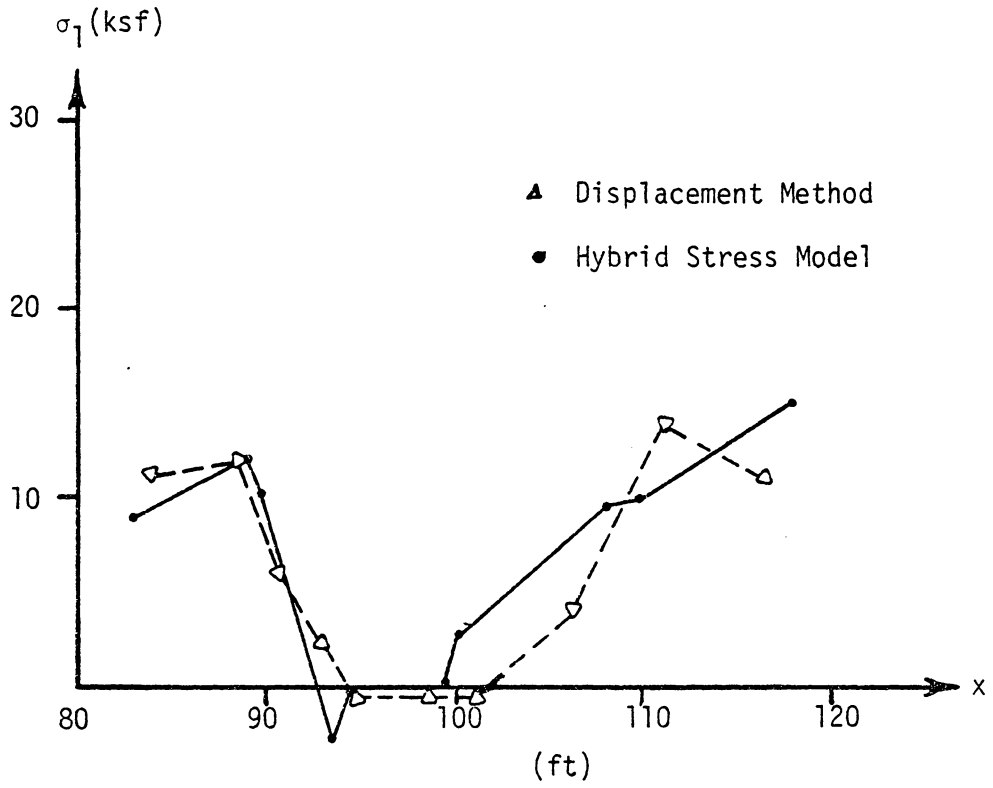

Figure 6.28 Comparison of Principal Stresses
(Step 3, Section A-A)

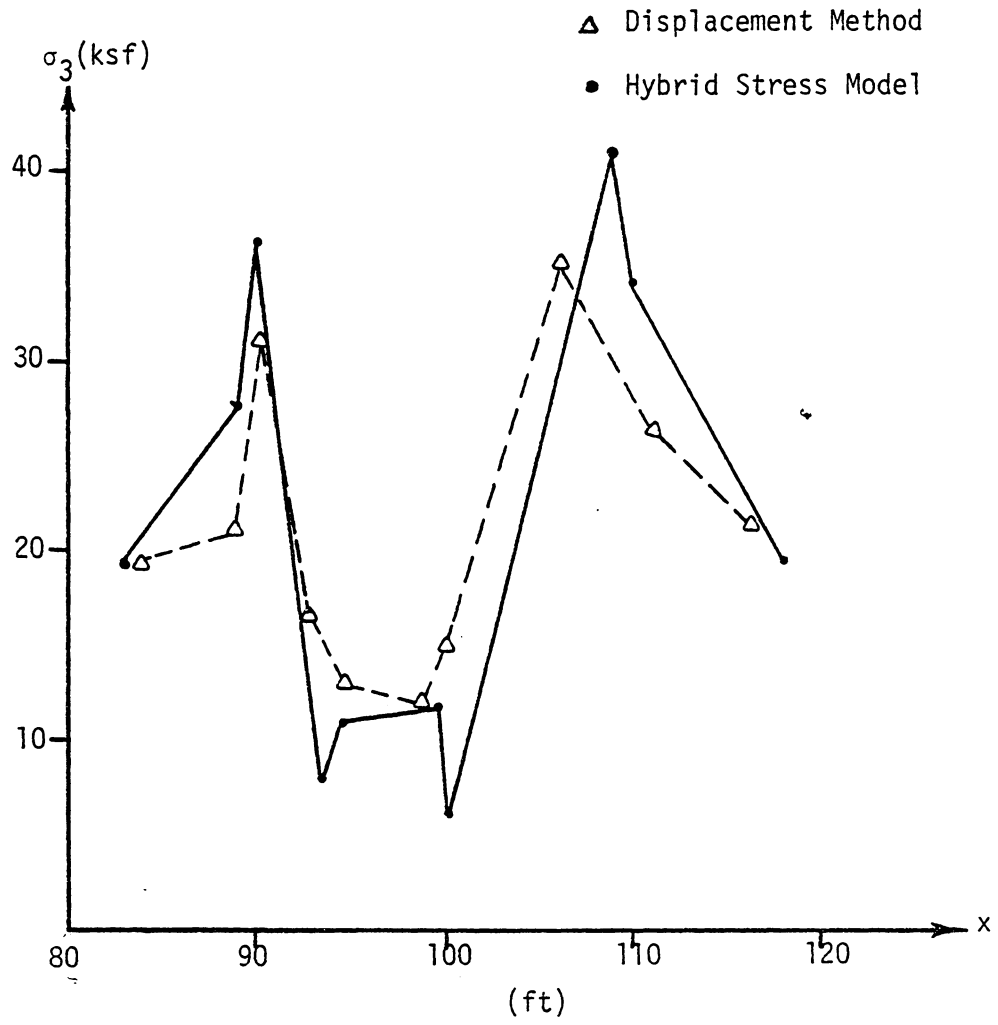

Figure 6.29 Comparison of Principal Stresses
(Step 3, Section A-A)

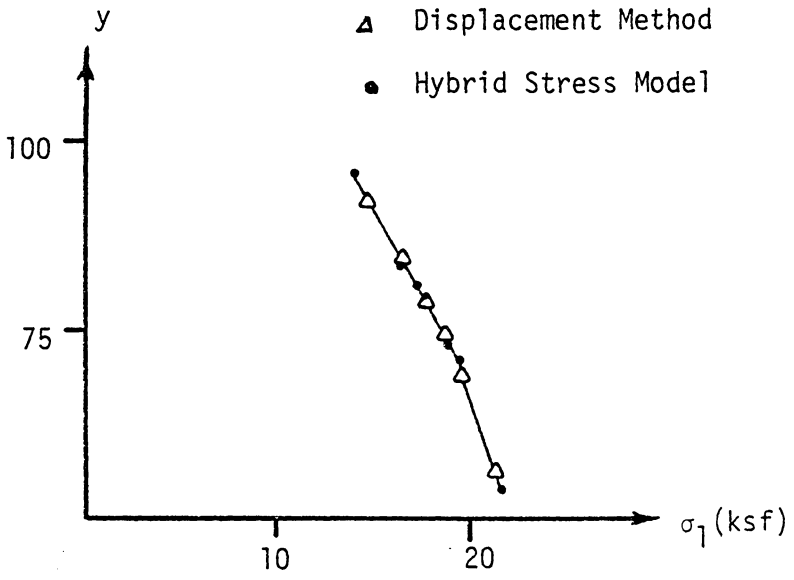

Figure 6.30 Comparison of Principal Stresses (Step 1, Section B-B)

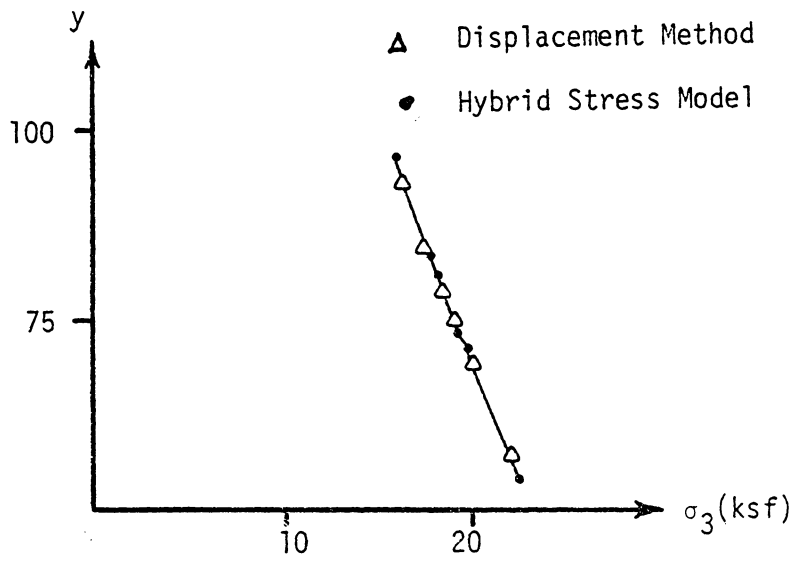

Figure 6.31 Comparison of Principal Stresses (Step 1, Section B-B)

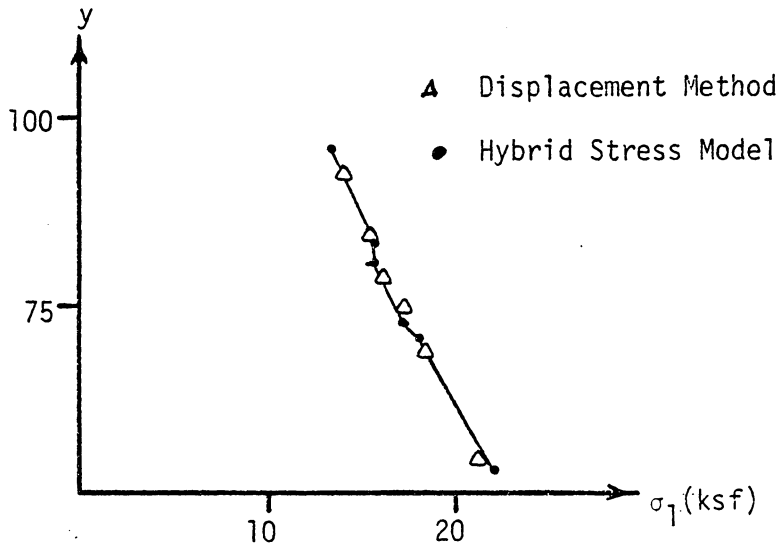

Figure 6.32 Comparison of Principal Stresses
(Step 3, Section B-B)

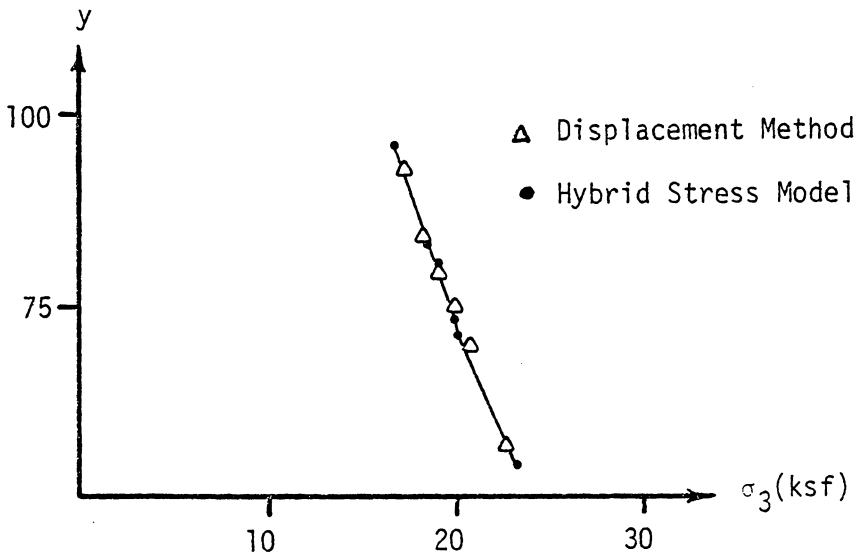

Figure 6.33 Comparison of Principal Stresses
(Step 3, Section B-B)

Table 6.3

Comparison of Displacements (Stage 4)

Node Number	x	y	Hybrid Stress Model (ft x 10^{-3}) u	Hybrid Stress Model (ft x 10^{-3}) v	Displacement Method (ft x 10^{-3}) u	Displacement Method (ft x 10^{-3}) v
91	72.58	72.45	.767	.681	.625	.929
92	77.52	72.59	- .339	2.85	- .279	2.60
93	82.46	72.73	.107	3.62	.035	3.32
94	86.95	72.74	.537	3.17	- .108	2.904
95	91.43	72.74	- .227	1.56	- .251	1.69
114	72.67	77.07	2.38	- .599	2.35	- .462
116	91.5	77.20	-1.28	.597	- .119	.855
132	72.77	81.69	2.67	- .795	2.46	- .738
136	91.56	81.66	-1.26	.183	-1.18	.178
156	73.77	84.91	2.42	-1.16	2.37	-1.24
158	90.53	84.74	- .932	- .197	- .881	- .317
167	74.77	88.14	1.91	-1.66	2.07	-1.63
168	78.56	89.81	1.62	-2.19	1.66	-2.10
169	82.35	91.48	.915	-1.87	.941	-1.86
170	85.93	89.66	.223	-1.71	.199	-1.58
171	89.51	87.83	- .196	- .831	- .379	- .819
101	109.5	72.73	.104	1.56	.01	1.65
102	114.2	72.76	- .622	3.22	- .09	2.95
103	119.0	72.79	- .191	3.65	- .199	3.34
104	123.8	72.76	.309	2.86	- .516	2.55
105	128.7	72.72	- .765	.634	- .908	.881
119	109.6	77.25	1.16	.512	1.15	.688
121	128.6	77.27	-2.29	- .606	-2.06	- .070
142	109.7	81.78	1.04	.061	.917	.100
146	128.6	81.82	-2.50	- .964	-2.34	- .877
161	110.8	85.11	.879	- .395	.833	- .543
163	127.3	85.00	-2.41	-1.31	-2.26	-1.35
172	112.0	88.44	.008	- .998	.196	-1.05
173	115.4	89.83	- .435	-2.00	- .249	-1.77
174	118.8	91.21	- .935	-2.10	- .938	-1.92
175	122.5	89.70	-1.42	-2.35	-1.61	-2.21
176	126.1	88.18	-1.80	-1.77	-1.73	-1.74

CHAPTER 7

CONCLUDING REMARKS

7.1 Summary and Conclusions

A number of geomechanic problems has been solved by the hybrid stress model. The comparison of the results for the hybrid stress model with the displacement method shows that the hybrid stress model provides improved predictions of stresses and displacements.

Excavation is a complex problem in geomechanics and in the past the displacement method has been used to simulate the excavation process despite some of its limitations, such as inability to predict accurate stress distribution in a region where the high stress gradients exist. In this study a new procedure for simulation of excavation utilizing the hybrid stress model has been proposed and applied to the field cases. There are some improvements in the results as compared to the displacement method.

For the constitutive law, the Drucker-Prager model has been used, and for the interface discontinuity, a new interface element based on the displacement method has been introduced in the computer programs.

One of the features of the hybrid stress model is that it can be combined with the displacement method without violation of continuity. Thus, the hybrid stress element can be used in the region of the high stress gradients and the displacement element can be used in other regions.

In this investigation, it has been found that in some cases where an element is located far from the origin of the global coordinates (x,y), due to the computational errors, the matrix [H] may not stay positive definite. Thus, it is recommended that stresses be computed from an assumed stress function which is expressed in terms of local coordinates (s,t). Moreover, it has been learned that with the curvilinear boundary, the application of the hybrid stress model must be made carefully. This is because the determination of the direction cosines of the vector which is normal to the boundary of an element is required in the computation of the matrix [G]. If they are computed inaccurately, the final result can be misleading. In other words, the eight-node isoparametric element utilizing the hybrid stress model is sensitive to the geometry.

The potential for use of the hybrid stress model in geomechanics appears to be great. There is need for further work to improve the application of this model in geomechanics. For instance, one can improve the predicted displacements and stresses by enforcing the traction boundary conditions [46,47]. By employing this idea, a more accurate free stress boundary on the surface of the excavation can be created. Further research can be performed to study the effects of other advanced constitutive models such as critical state and cap.

Use of the hybrid method in geomechanics problems is rather new, and the study herein involving nonlinear material behavior, soil-structure interaction and simulation of construction sequences is perhaps the first. It is believed that for such problems requiring accurate stress distributions and ultimate load computation, the method will have a high potential for continued research and application.

REFERENCES

1. Pian, T. H. and Tong, P., "Finite Element Method in Continuum Mechanics", Advances in Applied Mechanics, Vol. 12, Academic Press, Inc., New York, 1976.

2. Desai, C. S., and Christian, J. T., Numerical Methods in Geotechnical Engineering, McGraw-Hill, N.Y., 1977.

3. Pian, T. H. H., "Derivation of Element Stiffness Matrices", AIAAJ. Vol. 2, No. 3, March 1964.

4. Pian, T. H. H. and Tong, P., "Rationalization in Deriving Element Stiffness Matrix by Assumed Stress Approach", Proc. 2nd Conf. on Matrix Methods in Structural Mech., AFFDL-TR 68-150, WPAFB, Ohio, 1968.

5. Tong, P. and Pian, T. H. H., "A Variational Principle and the Convergence of Finite Element Method Based on Assumed Stress Distribution", Int. J. of Solids and Structures, Vol. 5, 1969.

6. Tong, P. and Pian, T. H. H., "Bound to the Influence Coefficient by the Assumed Stress Method", Int. J. of Solids and Structures, Vol. 6, 1970.

7. Ahmad, S. and Irons, B. M., "An Assumed Stress Approach to Refined Isoparametric Finite Element in Three Dimensions," Proc. of the 1974 Inter. Conf. on Finite Element Methods in Engineering, The University of New South Wales, 1974.

8. Rao, A., "An Assumed Stress Hybrid Finite Element Model for the Analysis of an Axisymmetric Thick Walled Pressure Vessel," Proc. of the First Inter. Conf. on Structural Mechanics in Reactor Technology, September 1971.

9. Desai, C. S. and Abel J. F., Introduction to the Finite Element Method, VAN NOSTRAND REINHOLD COMPANY, 1972.

10. Zienkiewicz, O. C., The Finite Element Method, McGraw Hill, London, 1977.

11. Pian, T. H. H., Tong, P., Luk, C. H. and Spilker, R. L., "Elastic-Plastic Analysis by Assumed Stress Hybrid Model," Proc. of the 1974 Inter. Conf. on Finite Element Methods in Engineering, The University of New South Wales, 1974.

12. Horrigmoe, G., and Eidsheim, O. H., "Hybrid Stress Finite Element Model for Elastic-Plastic Analysis", Inter. Conf. on Finite Elements in Nonlinear Solid and Structural Mechanics, Geilo, Norway, Vol. 1, 1977.

13. Barnard, A. J., and Sharman, P. W., "Elasto-Plastic Analysis Using Hybrid-Stress Finite Elements", Inter. Conf. on Finite Elements in Nonlinear Solid and Structural Mechanics, Geilo, Norway, Vol. 1, 1977.

14. Spilker, R. L., "Elastic-Plastic Analysis by the Hybrid Stress Model and the Initial-Stress Approach", ASRL TR 172-1, MIT, September, 1973.

15. International Mathematical and Statistical Libraries, Inc., 1980.

16. E. Hinton and D. R. J. Owen, Finite Element Programming, Academic Press, London, 1977.

17. Goodman, R. E., Taylor, R. L., and Brekke, T. L., "A Model for Mechanics Jointed Rock", J. of Soil Mechanics and Foundations Division, ASCE, Vol. 94, No. SM5, 1968.

18. Goodman, R. E., and Christopher, J., "Finite Element Analysis for Discontinuous Rocks", Numerical Methods in Geotechnical Engineering, Desai, C. S. and Christian, J. T., eds., McGraw-Hill, N.Y., 1977.

19. Ghaboussi, J., Wilson, E. L., and Isenberg, J., "Finite Element for Rock Joints and Interfaces", J. of Soil Mech. and Found. Engg., SM10, ASCE, October, 1973.

20. Herrman, L. R., "Finite Element Analysis of Contact Problems", J. of E. M. Division, ASCE, Vol. 104, No. EM5, 1978.

21. Desai, C. S., Personal Communication.

22. Lightner, J. G., Personal Communication.

23. Siriwardane, H. J., "Nonlinear Soil-Structure Interaction Analysis of One-, Two-, and Three- Dimensional Problems Using Finite Element Method", Ph.D. Dissertation, VPI & SU, Blacksburg, VA, November 1980.

24. Frederick, D. and Chang, T. S., Continuum Mechanics, Scientific Publishers, Inc., Boston, 1972.

25. Washizu, K., Variational Methods in Elasticity and Plasticity, Pergamon Press, 1975.

26. Hill, R., The Mathematical Theory of Plasticity, Oxford University Press, 1950.

27. Drucker, D. C., and Prager, W., "Soil Mechanics and Plastic Analysis of Limit Design," Gluart, Appl. Math., Vol. 10, No. 2, July 1952.

28. Shieh, W. Y. J., and R. S. Sandhu, "Application of Elasto-Plastic Analysis in Earth Structures", Proc. Nat. Mech. Water Resources Eng., ASCE, Memphis, Tenn., January 1970.

29. Timoshenko, S., and Goodier, J. N., Theory of Elasticity, New York, McGraw-Hill Book Co., 1951.

30. Lambe, T. W. and Whitman, R. V., Soil Mechanics, John Wiley & Sons, Inc., 1969.

31. Boonlualohr, P., Valliappan, S., and Lee, I. K., "Elastic-Plastic Analysis of Shallow Foundations", Proc. of the 1974 Inter. Conf. on Finite Element Methods in Engineering, The University of New South Wales, 1974.

32. Christian, J. T., Hagmann, A. J., and Marr, Jr., W. A., "Incremental Plasticity Analysis of Frictional Soils", Inter. J. for Numerical and Analytical Methods in Geomechanics, Vol. 1, 1977.

33. Taylor, D. W., Fundamentals of Soil Mechanics, J. Wiley & Sons, New York, 1948.

34. Goodman, R. E., and Brown, C. B., "Dead Load Stresses and the Instability of Slopes," J. of Soil Mechanics and Foundations Division, proc. ASCE, Vol. 89, SM 3, May 1963.

35. Clough, G. W. and Duncan, J. W., Finite Element Analysis of Port Allen and Old River Locks, Report No. TE 69-3 to U.S. Army Engineers Waterways Experiment Station, September, 1969.

36. Clough, G. W., and Manna, A. I., "Lessons Learned in Finite Element Analysis of Temporary Excavations", Int. Conf. on Numerical Methods in Geomechanics, Virginia Polytechnic Institute and State University, Blacksburg, Va., June, 1976.

37. Christian, J. T., and Wong, I. H., "Errors in Simulation Excavations in Elastic Media by Finite Elements", Soils and Foundations, Japanese Society of Soil Mechanics and Foundation Engineering, Vol. 13, No. 1, March, 1973.

38. Desai, C. S., Johnson, L. D., and Hargett, C. M., "Analysis of Pile-Supported Gravity Lock", J. of the Geotechnical Engineering Division, ASCE, Vol. 100, No. GT9, September, 1974.

39. Desai, C. S., "Soil-Structure Interaction and Simulation Problem", A Term Paper, Proc. International Symposium on Numerical Methods in Soil Mechanics and Rock Mechanics, University of Karlsruhe, West Germany, September, 1975.

40. Mana, A. I., "Finite-Element Analyses of Deep Excavation Behavior in Soft Clay", Ph.D. Dissertation, Stanford University, March, 1978.

41. Lightner, J. G., "Improved Numerical Procedures for Soil-Structure Interaction Including Simulation of Construction Sequences", M.S. Thesis, VPI & SU, Blacksburg, Va., September 1979.

42. Desai, C. S., A FE Code for Earth-Structure Interaction and Pile Foundations", Report No. VPI-E-78-28, Department of Civil Engineering, Virginia Tech, 1975.

43. Lightner, J. G., and Desai, C. S., "Improved Finite Element Procedures for Soil-Structure Interaction Including Construction Sequences", Session on Soil-Structure Interaction, ASCE Convention, Portland, Oregon, 1980.

44. Lambe, T. W., and Turner, E. K., "Braced Excavations", Special Conf. of Lateral Stresses in the Ground, ASCE, 1970.

45. Chen, W. C.,"Finite Element Analysis of Twin Running Tunnels and Research Chamber at Peachtree Center Station, Atlanta, Georgia," Tudor Engineering Company, Consulting Engineers and Planners, Dec., 1977.

46. Kulhawy, F. H., "Finite Element Analyses of Twin Running Tunnels and Research Chamber at Marta Cain Street Station, Atlanta, Georgia," Report Prepared for Parsons, Brinkerhoff, Quade & Douglas, Inc./Tudor Engineering Company, 1977.

47. Rose, D. C., "The Atlanta Research Chamber Applied Research Monographs", U.S. Dept. of Transp., Report No. UMTA-GA-06-0007-79-1, Oct., 1979.

The vita has been removed from the scanned document

A HYBRID FINITE ELEMENT PROCEDURE FOR SOIL-STRUCTURE INTERACTION INCLUDING CONSTRUCTION SEQUENCES

by

Shad Muhammad Sargand

(ABSTRACT)

An alternative to the displacement finite element method, the hybrid stress model, is applied to problems in geomechanics. A two-dimensional finite element procedure based on the hybrid stress model is developed for simulation of construction sequences including underground and surface excavations. In this procedure, an eight-node isoparametric element is employed. In the analysis, the effect of soil-structure interaction is incorporated by using a special interface element for behavior at the contact between two different materials.

In the elastic-plastic analysis, the Drucker-Prager model is used as a constitutive law. In order to verify the computer program and to examine the accuracy of the hybrid stress model, several problems such as a beam, a plate with circular hole, and footings are analyzed, and the results are compared with those from the displacement method and closed-form solutions.

The proposed procedure for simulation of excavation is verified by performing an excavation in linear elastic material. Finally,

two field cases of excavation are solved and the results are compared with the displacement method and the field observations.

It is believed that the proposed (stress) hybrid method can have significant potential of application for various problems in geomechanics, and it can be particularly appropriate for situation where computation of stresses is important.